European Commission
H2020 Programme for Research & Innovation

Advanced monitoring, simulation and control of tidal devices in unsteady, highly turbulent realistic tide environments

Grant Agreement number: 727689

Project Acronym: RealTide

Project Title: Advanced monitoring, simulation and control of tidal devices in unsteady, highly turbulent realistic tide environments

WP3 Realistic Simulation of Tidal Turbine

Deliverable 3.2

Blade resolved CFD modelling of tidal turbines

WP Leader: The University of Edinburgh (UEDIN)

Authors: Bureau Veritas Solutions (BVS)

Dissemination level: Public

Summary: This report presents the work carried out in the context in T3.2 of RealTide third work package which aims at developing realistic simulations of tidal turbines. It focuses on the development of a blade resolved CFD model of the turbine. The work presented is based on STAR-CCM+ software and uses D12 Sabella's turbine and UEDIN 3-bladed generic turbine as reference tidal turbine geometry.

First, a simplified model is created. Based on the axi-symmetry of the turbines it models only a 1/N slice– N being the number of blades – of the geometry in an ideal cylindrical domain with uniform inflow. This model is used to conduct the performance analysis of the turbines and provide pressure loads applied on the blades for structural analysis. Then, a more complex blade resolved CFD model is developed. It aims at including realistic environmental conditions to simulate the turbine operating in its environment. This is done using a step-by-step approach enabling successively to:

- Take into account a full turbine geometry instead of a 1/N slice
- Switch from RFM rotation method to RBM method, more relevant
- Integrate the seabed and vertical velocity profile's inflow, along with simplified free surface
- Integrate simplified wave modelling

The resulting models are used to conduct various case studies enabling to quantify the influence of these realistic conditions on the turbine loads and performance. The development of the models discussed above is presented in this document along with the different results obtained in the simulations.

Objectives:

Develop a blade-resolved CFD model of the tidal turbines integrating realistic operating conditions. It will enable an accurate modelling of the hydrodynamics around the turbine and analysis of the loads applying on the blades depending on the environmental conditions modelled.

Table of Contents

Advanced monitoring, simulation and control of tidal devices in unsteady, highly turbulent realistic tide environments........ 2
Abbreviations & Definitions........ 10
References........ 11
Distribution List........ 12
1 Introduction........ 13
1.1. Scope of work........ 13
1.2. Work performed........ 13
1.1.1 Simplified model 3D model........ 14
1.1.2 Realistic 3D model........ 14
2 Tidal turbine theory and structures........ 16
2.1 Introduction of the numerical model theory........ 16
2.2 Notations and conventions........ 17
2.3 Geometries........ 19
2.3.1 Sabella's D12 tidal turbine........ 19
2.3.2 Generic 3-bladed horizontal axis........ 20
3 Performance assessment of two tidal turbines – Simplified model........ 22
3.1 Simulation features........ 22
3.1.1 Domain definition........ 22
3.1.2 Mesh description........ 23
3.1.3 Simulation parameters........ 25
3.2 Sensitivity studies on the preliminary results........ 26
3.2.1 Time step interval influence........ 26
3.2.2 Time convergence........ 27
3.2.3 Stability of the results........ 27
3.2.4 Sensitivity to the Reynolds number........ 28
3.2.5 Mesh sensitivity analysis........ 29
3.2.6 Conclusion on sensitivity analysis carried out on the model........ 30
3.3 D10 simulation and comparison with experiment results........ 31
3.3.1 Presentation of the experimental results and CFD model settings........ 32
3.3.2 CFD simulations results presentation and analysis........ 33
3.4 Final performance assessment........ 33
3.4.1 Final performance assessment of D12 and 3-bladed generic tidal turbines........ 33
3.4.2 Analysis of the flow hydrodynamics around the blades........ 36
3.5 Structural analysis of the D12 blade........ 37
3.6 Conclusion on the development of the model........ 38
4 Integration of realistic conditions in the model........ 39
4.1 Literature review on turbulence modelling........ 39
4.1.1 CFD models characterisation applied to turbulence........ 39
4.1.2 Turbulence generation methods and related data needed for implementation........ 42
4.2 Analysis of UEDIN data tide measurements from Orkney........ 44

4.2.1 Description of the key turbulence parameters 45
4.2.2 Analysis of turbulence data from UEDIN datasets 46
4.3 Development of a complex model integrating realistic environmental conditions 48
4.3.1 Turbine fully modelled and modification of the rotation method 48
4.3.2 Integration of the seabed and free surface 51
4.3.3 Integration of the turbine's structure 54
4.4 Conclusion of the work carried out to integrate realistic conditions in the model 55
5 influence of realistic environmental conditions on the tidal turbine behaviour 57
5.1.1 Influence of a vertical velocity profile on the turbine without structure 60
5.1.2 Influence of the turbine's structure 64
5.1.3 Comparison of influence of two speed profiles 67
5.2 Influence of oscillating inflow due to waves 70
5.2.1 Preliminary study on ideal cylinder 70
5.2.2 Waves and U70 coupled 71
5.3 Critical operating condition – Forced stop after freewheel rotation 76
5.4 Influence of the inflow incidence 81
5.4.1 Influence of inflow incidence at flood tide 82
5.4.2 Influence of inflow incidence at ebb tide 85
6 Conclusions 90
7 Discussion and opportunities 92

List of Figures

Figure 2-1: Forces induced by the interaction between the current and the turbine rotation 18
Figure 2-2: Velocity perceived by the blade profile and resulting angle of attack 19
Figure 2-3: 3D CAD view of Sabella's D12 tidal turbine 19
Figure 2-4: Sabella D12 turbine positioned on its structure 20
Figure 2-5: Layout of the turbine baseplate 20
Figure 2-6: 3D CAD views of Alstom/GE generic tidal turbine 21
Figure 3-1: Development of the simplified model - Workflow 22
Figure 3-2: Simulation domain type for the Sabella D12 and generic turbines (illustration on 3-bladed generic turbine here) 23
Figure 3-3: Mesh views of M0 simulation 24
Figure 3-4: Wall Y+ - wall distance on the turbines 25
Figure 3-5: Standard deviation in sliding 100 time steps series along Cp time series 27
Figure 3-6: Relative difference between min and max values in sliding 100 time steps intervals along Cp time series. 28
Figure 3-7: Influence of Reynolds number on the power coefficient Cp 29
Figure 3-8: Visual comparison of meshes used for sensitivity study for D12 performance assessment 30
Figure 3-9: Sabella's D10 tidal turbine CAD representation 31
Figure 3-10: Wall Y+ value on D10 turbine slice 32
Figure 3-11: Final performance assessment on the D12 Sabella's tidal turbine - Power coefficient, Cp - Torque coefficient, Cq - Thrust coefficient, Ct 34
Figure 3-12: Final performance assessment on the 3-bladed generic tidal turbine - Power coefficient, Cp - Torque coefficient, Cq - Thrust coefficient, Ct 35
Figure 3-13: Side view of a D12 blade, position of the plane Z=3m 36
Figure 3-14: Velocity profiles around D12 blade at Z=3m for TSR = 2, 2.5 and 3 36
Figure 3-15: Pressure coefficient and turbulent kinetic energy (in blue) generated by D12 blade at TSR = 2.5.......... 37
Figure 3-16: Illustration of the 108 patches division of the D12 blade 38
Figure 3-17: Pressure field on the D12 blade 38
Figure 4-1: Energy characteristics of turbulent structures based on size 40
Figure 4-2: Idealized view of DES zonal repartition of calculation methods.. 41
Figure 4-3 : Turbulence intensity depending on the turbulence length scale – 1^{st} part of flood 46
Figure 4-4 : Turbulence intensity depending on the turbulence length scale – 2^{nd} part of flood 46
Figure 4-5 : Linear regression of turbulence intensity depending on the 1^{st} part of flood 47
Figure 4-6 : Linear regression of turbulence intensity depending on the 2^{nd} part of flood 47
Figure 4-7: Presentation of the model setup used for RBM in the cylinder 49
Figure 4-8: Mesh view of the RBM model applied in a cylinder domain 50
Figure 4-9: Outer grid – Stationary domain 51
Figure 4-10: Inner grid – Rotating domain and interface with outer domain 52
Figure 4-11: Velocity on the XZ plane (length x width) – Pressure outlet (left) vs. symmetry plane (right) applied on the sides 52
Figure 4-12: Velocity along the width of the domain – Width of 92m 53
Figure 4-13: Velocity along the width of the domain – Width of 184m 53
Figure 4-14: Presentation of the model using RBM method and integrating seabed 54
Figure 4-15: Outer grid – Domain with tripod integrated 55
Figure 4-16: Inner grid – Domain with tripod integrated 55
Figure 5-1: Speed profiles from different tidal coefficients 58
Figure 5-2: Blade sections and reference coordinate system at blade root 59
Figure 5-3: U70 inflow - Difference of velocity on the rotational plane induced by the current front 60
Figure 5-4: U70 inflow – Turbine alone – Axial forces acting on blades 62
Figure 5-5: U70 inflow – Turbine alone – Tangential forces acting on the blades 62
Figure 5-6: U70 inflow - Turbine alone - Radial forces acting on the blade 62
Figure 5-7: U70 inflow – Turbine alone – Pressure loads applied on the blade sections depending on the time 63
Figure 5-8: U70 inflow – Turbine inflow – Dimensionless velocity along the length of the domain 64
Figure 5-9: U70 inflow – Turbine with structure – Axial forces acting on the blades 65
Figure 5-10: U70 inflow – Turbine with structure – Tangential forces acting on the blades 65
Figure 5-11: U70 inflow – Turbine with structure – Radial forces acting on the blades 65

Figure 5-12: U70 inflow – Turbine with structure vs. Turbine alone – Cp over one period of rotation 66
Figure 5-13: U70 inflow - Turbine with structure - Velocity field from a long distance view 66
Figure 5-14: U70 inflow - Turbine with structure - Velocity field from a close view 67
Figure 5-15: U70 vs. U120 inflow – Difference of velocity on the limits of the rotation plane 67
Figure 5-16: Turbine with structure – U70 vs. U120 inflow - Axial forces acting on the blades 68
Figure 5-17: Turbine with structure – U70 vs. U120 inflow- Tangential forces acting on the blades 68
Figure 5-18: Turbine with structure – U70 vs. U120 inflow- Radial forces acting on the blades 68
Figure 5-19: Velocity field on turbine rotation axis – U70 (left) vs. U120 (right) – Side view on top and top view at bottom 69
Figure 5-20: Ideal cylinder – Oscillating inflow - Temporal evolution of power coefficient and TSR........................ 70
Figure 5-21: Ideal cylinder – Oscillating inflow - Power coefficient evolution depending on the TSR...................... 71
Figure 5-22: Variation of the wave horizontal velocity with the depth 72
Figure 5-23: Envelope of the time varying horizontal inflow based on U70 velocity profile 72
Figure 5-24: Turbine with structure – U70 oscillating inflow – V0 measured at hub level 20 m ahead of the turbine used as reference in the following analysis 73
Figure 5-25: Turbine with structure – U70 oscillating inflow - Temporal evolution of power coefficient and TSR . 74
Figure 5-26: Turbine with structure – U70 oscillating inflow – Axial loads acting on the blades 75
Figure 5-27: Turbine with structure – U70 oscillating inflow – Tangential loads acting on the blades 75
Figure 5-28: Turbine with structure – U70 oscillating inflow – Radial loads acting on the blades 75
Figure 5-29: Turbine with structure – U70 oscillating inflow – Wake induced by the turbine at low TSR................ 76
Figure 5-30: Turbine with structure – U70 oscillating inflow – Wake induced by the turbine at high TSR 76
Figure 5-31: U120 inflow – Turbine with structure – Temporal evolution of the TSR during the critical operating behaviour modelling.. 77
Figure 5-32: U120 inflow – Turbine with structure – Temporal evolution of performance coefficients during the critical operating behaviour modelling 77
Figure 5-33: U120 inflow – Turbine with structure – Axial forces evolution during rotation rate increase 78
Figure 5-34: U120 inflow – Turbine with structure – Tangential forces evolution during rotation rate increase .. 78
Figure 5-35: U120 inflow – Turbine with structure – Radial forces evolution during rotation rate increase 78
Figure 5-36: U120 inflow – Turbine with structure – Axial forces evolution during emergency stop...................... 80
Figure 5-37: U120 inflow – Turbine with structure – Tangential forces evolution during the emergency stop 80
Figure 5-38: U120 inflow – Turbine with structure – Radial forces evolution during the emergency stop 80
Figure 5-39: Flood and Ebb tides – Definition of the convention - Flow at different incident angle 81
Figure 5-40 U70 inflow – Flood tide – Turbine with structure – -10° vs. 0° vs. 10° – Axial forces acting on a blade 83
Figure 5-41: U70 inflow – Flood tide – Turbine with structure – -10° vs. 0° vs. 10° – Tangential forces acting on a blade 83
Figure 5-42: U70 inflow – Flood tide – Turbine with structure – -10° vs. 0° vs. 10° – Radial forces acting on a blade 83
Figure 5-43: Comparison of dimensionless velocity around the structure for speed profiles for different angle of incidence – 10° (left) and -10° (right).. 84
Figure 5-44: Comparison of dimensionless velocity around the structure for speed profiles for different angle of incidence – 10degrees (left) vs. -10° (right) 85
Figure 5-45: U70 inflow – Ebb tide – Turbine with structure – -10° vs. 0° vs. 10° – Axial forces acting on a blade ... 87
Figure 5-46: U70 inflow – Ebb tide – Turbine with structure – -10° vs. 0° vs. 10° – Tangential forces acting on a blade 87
Figure 5-47: U70 inflow – Ebb tide – Turbine with structure – -10° vs. 0° vs. 10° – Radial forces acting on a blade . 87
Figure 5-48: Comparison of dimensionless velocity around the structure for speed profiles for different angle of incidence – 10° (left) vs. -10° (right) 88
Figure 5-49: Comparison of dimensionless velocity around the structure for speed profiles for different angle of incidence – 10° (left) vs.-10° (right) 88

List of Tables

TABLE 3-1: SIMULATIONS PARAMETERS USED FOR THE SIMPLIFIED MODEL 25
TABLE 3-2: SENSITIVITY OF RESULTS TO TIME STEP INTERVAL AND ASSOCIATED RELATIVE ERROR........ 26
TABLE 3-3: INFLUENCE OF SIMULATION DURATION ON RESULTS CONVERGENCE AND ASSOCIATED RELATIVE ERROR 27
TABLE 3-4 MESH SENSITIVITY ANALYSIS ON RESULTS AND ASSOCIATED RELATIVE ERROR 30
TABLE 3-5: COMPARISON BETWEEN CFD AND EXPERIMENTAL RESULTS ON CP FOR D10 TURBINE 33
TABLE 4-1: NECESSARY INPUTS FOR TURBULENCE MODELLING METHOD........ 44
TABLE 5-1: LIST OF CONSIDERED CASE STUDIES 57
TABLE 5-2: U70 INFLOW - TURBINE ALONE - POWER COEFFICIENTS........ 61
TABLE 5-3: U70 INFLOW - TURBINE ALONE - BLADE LOADS SUMMARY........ 63
TABLE 5-4: U70 INFLOW – TURBINE WITH STRUCTURE – BLADE LOADS SUMMARY 64
TABLE 5-5: U70 INFLOW - TURBINE WITH STRUCTURE VS. TURBINE ALONE - POWER COEFFICIENTS........ 66
TABLE 5-6: U70 VS. U120 INFLOW - TURBINE WITH STRUCTURE – LOADS COMPARISON BETWEEN BOTH INFLOWS 69
TABLE 5-7: U70 AND U120 INFLOW - TURBINE WITH STRUCTURE – PERFORMANCE COEFFICIENT COMPARISON 69
TABLE 5-8: U70 INFLOW – FLOOD TIDE – TURBINE WITH STRUCTURE – LOADS COMPARISON BETWEEN DIFFERENT FLOW INCIDENCES 84
TABLE 5-9: U70 INFLOW – - FLOOD TIDE – TURBINE WITH STRUCTURE– INFLUENCE OF THE INFLOW INCIDENCE ON THE POWER COEFFICIENT 85
TABLE 5-10: U70 INFLOW – TURBINE WITH STRUCTURE - EBB TIDE – LOADS COMPARISON BETWEEN DIFFERENT FLOW INCIDENCES 88
TABLE 5-11: U70 INFLOW – TURBINE WITH STRUCTURE - EBB TIDE – INFLUENCE OF THE INFLOW INCIDENCE ON THE POWER COEFFICIENT 89
TABLE 5-12: U70 INFLOW – TURBINE WITH STRUCTURE – EBB VS. FLOOD TIDE – COMPARISON OF POWER COEFFICIENT VALUES 89

Abbreviations & Definitions

(D)DES	(Delayed) Detached Eddy Simulation
1-T	1-Tech
BEMT	Blade Element Momentum Theory
BV	Bureau Veritas
BV M&O	Bureau Veritas Marine & Offshore
BVS	Bureau Veritas Solutions
CAD	Computer Aided Design
CFD	Computational Fluid Dynamics
CPU	Central Processing Unit
DNS	Direct Numerical Simulation
DNV GL	Det Norske Veritas and Germanischer Lloyd
DOF	Degree Of Freedom
EO	EnerOcean
GA	Grant Agreement
GE	General Electric
IEC	International Electrotechnical Commission
IFR	Ifremer (Institut Français pour la Recherche et l'Exploitation de la Mer)
ISSA	Ingeteam Power Technology
LES	Large Eddy Simulation
MRF	Moving Reference Frame
NREL	National Renewable Energy Laboratory
NS	Navier-Stokes
PMP	Project Management Plan
RANSE	Reynolds Average Navier Stokes Equations
RBM	Rigid Body Motion
RFM	Reference Frame Motion
RSM	Reynolds-Stresses Model
RST	Reynolds Stresses Tensor
SAB	Sabella
SEM	Synthetic Eddy Method
SST	Shear Stress Transport
T	Task
TI	Turbulence Intensity
TSR	Tip Speed Ratio
TSR	Tip Speed Ratio
UEDIN	University of Edinburgh
UK	United Kingdom
WP	Work Package

References

[1] "Grant Agreement n° 727689 RealTide - RealTide Consortium & European Commission - December, 2017," December 2017.

[2] T. Ebdon, D. O'Doherty, Mason-Jones and A., "Simulating marine current turbine wakes using advanced turbulence models," School of Engineering, Cardiff University and University of South Wales, Cardiff, United Kingdom.

[3] T. S. R. M. G. S. Payne, "Design and manufacture of a bed supported tidal turbine model for blade and shaft load measurement in turbulent flow and waves," Edinburgh, Manchester, 2017.

[4] N. Dhamankar and al., "An overview of turbulent inflow boundary conditions for large eddy simulations (LES)," in *22nd AIAA Computational Fluid Dynamics Conference*, June 2015.

[5] N. Jarrin, "A synthetic eddy method for generating inflow conditions for large eddy simulations," *International Journal of Heat and Fluid FLow 27 ,* pp. 585-593, August 2006.

[6] NREL - Jonkman, B., "TurbSim User's Guide: Version 1.50," [Online]. Available: https://nwtc.nrel.gov/TurbSim.

[7] DNV GL Energy, "Tidal Bladed theory manual," May 2014. [Online]. Available: https://www.dnvgl.com/services/tidalbladed-3799.

[8] J. Thomson, B. Polagye and M. Richmond, "Measurements of turbulence at two tidal power sites in Pujet Sound, WA (USA)," *Journal of Oceanic Engineering,* 2012.

[9] A. A., A. Elshaer and al., "Consistent inflow turbulence generator for LES evaluation of wind-induced responses for tall buildings," *Journal of wind engineering and industrial aerodynamics, Vol. 142,* pp. 198-216, 2015.

[10] S. Gant and T. Stallard, "Modelling tidal turbine in unsteady flow," School of Mechanical, Aerospace and Civil Engineering, University of Manchester, Manchester, 2008.

[11] C. Carlier, G. Pinon and A. Fur, "A synthetic eddy method to represent the ambient turbulence in numerical computations of marine current turbines," in *15èmes Journées de l'Hydrodynamique*, Brest, France, 2016.

[12] B. Sellar, D. Ingram and G. Wakelam, "Characterisation of tidal flows at the European marine energy centre in the absence of ocean waves," School of Engineering, Institute for Energy Systems, University of Edinburg, Edinburg, United Kingdom, 2018.

[13] "CFD Online - Turbulence Intensity," 2018. [Online]. Available: https://www.cfd-online.com/Wiki/Turbulence_intensity. [Accessed April 2019].

[14] R. A. L. H. M. M. R. S. B. v. W. B. Andersson, "Computational Fluid Dynamics for Engineers," Cambridge, 2012, pp. pp 70-75.

[15] W. M. J. B. A. S. B. T. Blackmore, "Influence of turbulence on the wake of a marine current turbine simulator," *The Royal Society,* 2014.

[16] "CFD Online - Turbulence length scale," 2012. [Online]. Available: https://www.cfd-online.com/Wiki/Turbulence_length_scale. [Accessed April 2019].

[17] "Turbulent Time, Length, and Velocity Scales," 2019. [Online]. Available: file:///C:/Program%20Files/CD-adapco/13.06.012/STAR-CCM+13.06.012/doc/en/online/index.html#page/STARCCMP%2FGUID-3BB06169-ED12-486D-9802-6D0889D8AA3F%3Den%3D.html. [Accessed 2019].

[18] J. Keylock and Tokyav, "A method for characterising the sensitivity of turbulent flow to the structure of inlet turbulence," *Journal of tubulence - Vol.12,* pp. 45-.., 2011.

[19] "Consortium Agreement Rev3 FINAL – RealTide Consortium – November, 2017".

[20] "Document Numbering Procedure – RLT-WP6-1-PRO-000-00 22nd January 2018".

Distribution List

This Document is a RealTide Internal Document and is classified as an Internal Report. It is for distribution solely within the RealTide Consortium.
It can be distributed if all Beneficiaries, represented by the General Assembly, give approval.

1 INTRODUCTION

In the context of RealTide European project, the following document presents the work carried out in T3.2 of WP3. The aim of RealTide third work package is the "Realistic Simulation of Tidal Turbines" [1]. The work presented hereafter focuses on the development of a blade resolved CFD modelling of the turbines. It is conducted by Bureau Veritas Solutions Marine & Offshore (BVS), specialized in computational fluid dynamics (CFD) with the help of UEDIN and Sabella. The model developed will enable to determine hydrodynamic loads as well as turbine wake quite accurately and be of use for structural and performance analysis.

In parallel, a BEMT tool and a BEMT-CFD model are presented in D3.1 and D3.3 respectively. A paper comparing the different methods and experimental data will be produced later in the project in the context of D3.4.

1.1. Scope of work

The hydrodynamic study of tidal turbines focuses on four main points of interest:

- The hydrodynamic loads applied on the turbine

  An accurate knowledge of the hydrodynamic loads is essential to ensure a suitable and reliable design of the turbine in accordance with the site specifications. From these loads, it is possible to determine the power coefficients (Cp, Cq, Ct) and assess the potential energy conversion capacity of the turbine.
- Wake around the turbine

  The presence of the turbine in the water creates a perturbation of the flow which leads to the apparition of a wake behind it. It can be of great interest to predict this wake accurately when studying possible array configurations for tidal turbines farms. It is a key parameter to determine the appropriate turbine positions.
- The flow environment

  The surrounding environmental conditions generate effects directly impacting the flow around turbine. Wind interaction at the surface leads to wave generation and bottom effect modifies the initial velocity profile of the flow. Moreover, tides also have an evident impact on the flow. These elements generate an unsteady flow in terms of velocity, direction or turbulence. It highly influences the hydrodynamic loads and the wake of the turbine [2].

The aim of BVS contribution is to define and study an accurate and realistic CFD model of the tidal turbine including the points listed above. To do so, input data from other partners are needed, especially:

- The tidal turbine geometries – from Sabella (D12 Sabella's tidal turbine used as reference) and UEDIN (3-bladed generic tidal turbine)
- The flow environment data – from Sabella and UEDIN

1.2. Work performed

Based on the objectives of the project presented above, BVS contribution will be divided into key steps necessary to fill the defined goal:

- Assessment of the hydrodynamic loads and power performance of the tidal turbine in simplified steady unidirectional flow
- Development of the realistic flow model (inclusion of vertical velocity profiles, turbulence and waves' horizontal components in particular)
- Assessment of hydrodynamic loads and performance in real conditions enabling to quantify the influence of these conditions on the turbine

The tidal turbine used as reference for the CFD model is the Sabella D12 turbine. Moreover, for dissemination purposes a 3-bladed generic turbine provided by UEDIN will also be studied in the simplified model.

The CFD models and calculations carried out in this project will be done using STAR-CCM+® developed by Siemens™. It is a powerful software commonly used for computational fluid dynamics. The simulations will be running on a cluster (DATARMOR provided by IFREMER and LIGER provided by Centrale Nantes) to reduce the computation time. The simulations will be Reynolds Averaged Navier-Stokes (RANS) type unless specified otherwise.

1.1.1 Simplified model 3D model

The first step of the project is the definition of a first simplified – yet satisfying – CFD model of the tidal turbine. This model only considers ideal conditions such as uniformity of the flow, no ground nor surface interactions. It will allow to conduct a preliminary study on the key parameters of the simulation such as mesh refinement and get preliminary results of power performance useful for Sabella.

In this model, the flow environment is supposed ideal. It has a steady and unidirectional velocity profile in the direction of the turbine rotation axis. Moreover, seabed and surface are not modelled as their effects are neglected. To reduce computational cost and based on the axi-symmetry of the tidal turbine and the flow, only 1/N – N being the number of blades – of the turbine is modelled. A sensitivity analysis will be carried out on mesh, time and steadiness of the results. Finally, an assessment of the turbine performance will be presented.

1.1.2 Realistic 3D model

The second part of the project is the modelling of a realistic turbulent flow environment on STAR-CCM+. This implies to rethink the established simplified model through the integration of seabed, waves, turbulences and non-linear velocity profile based on on-site observation data. The resulting model will not have a symmetry axis, consequently the entire tidal turbine will be modelled.

A literature review is necessary to assess the existing methods to build this model but also to identify the main associated difficulties. The first observations are:

- Different methods have been developed to add a turbulence profile to a flow environment based on the turbulence intensity and scale length. Von Karman spectral approach and Synthetic Eddy method are the most used ones
- The use of RANS simulations is satisfying to get averaged loads as it is done in the simplified model. However only averaged turbulence intensity can be considered as turbulence fluctuations tend to be erased by the averaging resolution method
- LES or DES (and Delayed DES) methods may be of great interest to study turbulence in the flow environment (inflow and tidal turbine wake) as it resolves more accurately turbulent

fluctuations and the associated flow interactions. However the computation cost linked to these simulations is higher than RANS methods and may lead to excessively long computations.

Therefore, different simulation settings are available depending on the desired objectives. An assessment of the most suitable and feasible calculation methods will be done depending on the different objectives, namely:

- Integration of realistic flow conditions
- Hydrodynamic loads and performance assessment

2 TIDAL TURBINE THEORY AND STRUCTURES

2.1 Introduction of the numerical model theory

The objective of the work package WP3 is to provide a better understanding of the interaction of the real tidal current with the tidal devices through numerical and experimental modelling. The numerical modelling includes a model based on the BEMT method developed by BV (see D3.1), a BEMT-CFD coupled numerical model developed by UEDIN (see D3.3) and finally a blade resolved CFD model developed by BVS presented in this report.

These various models developed in the context of RealTide are complementary. Depending on the theory used, the complexity of the model and the information obtained vary:

- The BEMT model provides a fast and easy to use tool enabling to conduct a performance assessment of the turbine. However, hydrodynamics are largely simplified and no visualization of the flow is available.

- On the other hand, the BEMT-CFD coupled model enables a good understanding of the flow surrounding the turbine thanks to CFD by taking into account the loads calculated by BEMT method in an actuator disk. It provides an interesting tool to simulate the influence of the inflow on the wake and overall performance of the turbine with reasonable computational cost.

- The blade resolved CFD model enables the most accurate resolution of the hydrodynamics around the turbine. The whole turbine geometry is taken into account which enables detailed calculation of the pressure field and loads applied on the blades. It provides a great tool to quantify the influence of the inflow on the structure. However, the computational cost to execute the model is very high.

The CFD blade resolved model is the only one that takes into account an accurate description of the geometry. A mesh is used to discretize the 3D CAD and implement it in the numerical model. Thanks to this, the turbine rotation is resolved accurately enabling a good capture of the hydrodynamics. It enables to quantify the efficiency of the turbine in various inflow conditions. However, this model also asks for a fine mesh of the domain to integrate the inflow conditions and the wake resolution. These specificities generate a very high computational costs necessary to run it. As such, long simulations are difficult to carry out. Therefore, it could be more relevant to use the BEMT-CFD coupled model to simulate long time varying inflows in some cases.

As presented above, each of the models considered in the project have their pros and cons. The most adapted one should be selected depending on the objective of the study. This report presents the development of the blade resolved CFD numerical model. It will be developed using STAR-CCM+ software. It is commonly used for hydrodynamic analysis. A presentation of the tool is available in Appendix.

2.2 Notations and conventions

The rotation rate of the turbine is an essential factor to consider as it directly influences the inflow encountered by the turbine. This aspect can be controlled by the generator inside the turbine. It is very important to identify the best rotation rate compared to the inflow characteristics to optimise the turbine efficiency. The rotation rate has to be considered with regard to the inflow velocity as they both have an effect on the relative flow characteristics at the blade. Therefore, a normalized velocity integrating both of these parameters is defined as follows:

$$TSR = \frac{\omega R}{U_{infinity}}$$

With
$U_{infinity}$ – Uniform mean inflow speed velocity in m/s
R – Tidal turbine radius in m
ω – Rotation rate of the tidal turbine in rad/s

In these studies, different TSR are simulated in order to determine for each of them the corresponding efficiency and hydrodynamic loads. It allows to find the best operating point which corresponds to the optimal efficiency. To assess the tidal turbine efficiency three significant performance coefficients are defined from the loads: the power coefficient Cp, torque coefficient Cq, and thrust coefficient Ct. They are defined as follows:

$$C_p = \frac{Power\ absorbed\ by\ tidal\ turbine}{Theoretical\ incident\ flow\ developed\ power} = \frac{M_x.\omega}{\frac{1}{2}\rho U_{infinity}^3 \pi R^2}$$

$$C_q = \frac{Induced\ torque\ on\ tidal\ turbine}{Theoretical\ incident\ flow\ developed\ torque} = \frac{M_x}{\frac{1}{2}\rho U_{infinity}^2 \pi R^3}$$

$$C_t = \frac{Induced\ drag\ on\ tidal\ turbine}{Theoretical\ incident\ flow\ developed\ thrust} = \frac{F_x}{\frac{1}{2}\rho U_{infinity}^2 \pi R^2}$$

With
M_x – Moment on the rotor axis generated by the effect of the inflow on the blades in N.m
F_x – Load on the rotor axis generated by the effect of the inflow on the blades in N
ω – Rotation rate of the tidal turbine in rad/s
$U_{infinity}$ – Uniform mean inflow speed velocity in m/s
R – Tidal turbine radius in m

The blades of a horizontal axi-symmetric tidal turbine are facing an inflow velocity composed of two key components (cf. Figure 2-1):

- The current inflow velocity
- The rotation velocity of the rotor

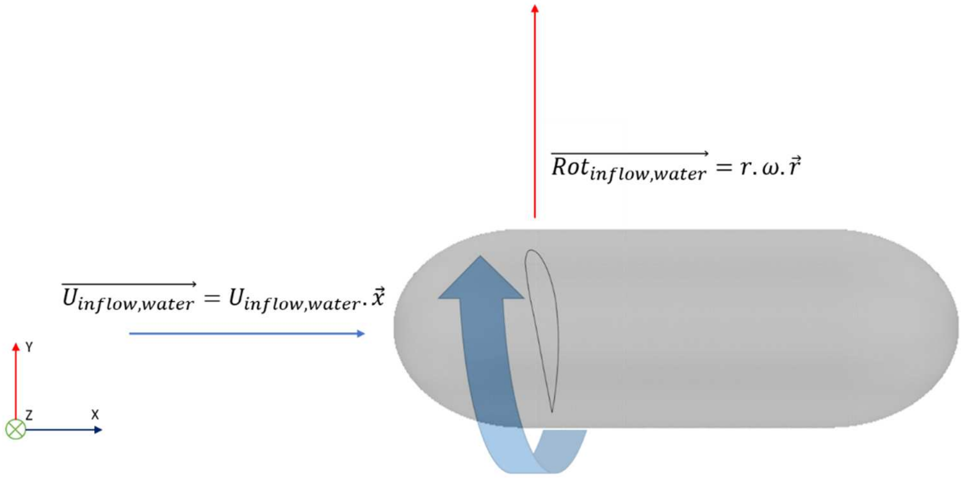
$\overrightarrow{Rot_{inflow,water}} = r.\omega.\vec{r}$
$\overrightarrow{U_{inflow,water}} = U_{inflow,water}.\vec{x}$
Y
Z
X

Figure 2-1: Forces induced by the interaction between the current and the turbine rotation

A blade cut at r height is considered. If the tidal turbine has an angular velocity of ω (rad/s), then at a r height, the tangential velocity of the blade due to the rotation is:

$$\overrightarrow{Rot_{inflow,\,water}} = r.\omega.\vec{r} = n.(2.\pi.r).\vec{r}$$

n being the rotation speed (Hz or Turn/s)

Relative velocity acting on the blades of the tidal turbine is obtained from the coupling of the inflow velocity and the tangential velocity (cf. Figure 2-2). Norm of the relative velocity represents the real flow velocity acting on the blade profile.

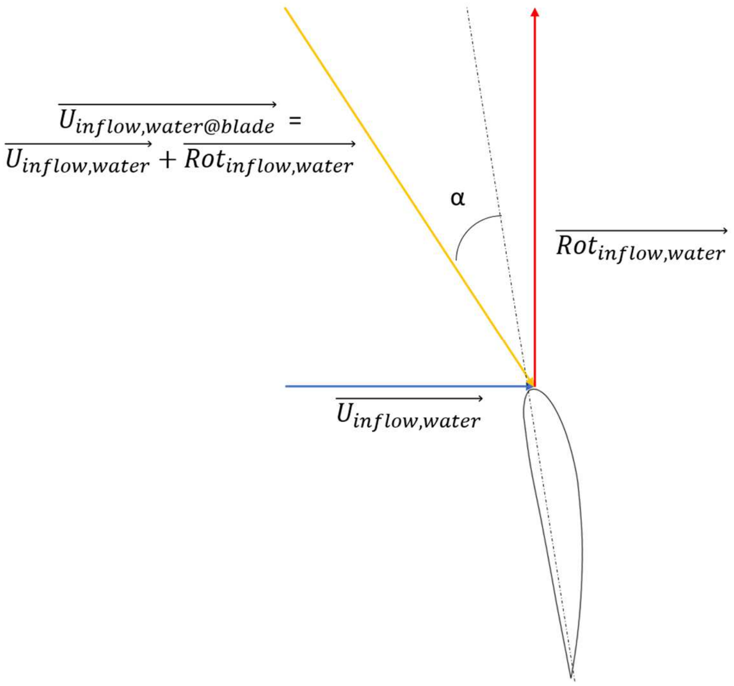
$\overrightarrow{U_{inflow,water@blade}} = \overrightarrow{U_{inflow,water}} + \overrightarrow{Rot_{inflow,water}}$
α
$\overrightarrow{Rot_{inflow,water}}$
$\overrightarrow{U_{inflow,water}}$

Figure 2-2: Velocity perceived by the blade profile and resulting angle of attack

This relative velocity acts on the blade with an angle of attack α, formed by the intersection between relative velocity vector and chord of the blade. The value of this angle depends on the norm of the inflow velocity vector and the rotation velocity vector. Angle of attack changes are proportional to the inflow velocity changes and inversely related with rotation velocity.

2.3 Geometries

2.3.1 Sabella's D12 tidal turbine

Sabella's D12 tidal turbine is a 5 bladed turbine. This turbine with winglets at each blade tip has a diameter of 12m and a blade size of 4m. The rotation axis is located at 12.5m above ground level. CAD representations in Figure 2-3 give an overview of the turbine geometry.

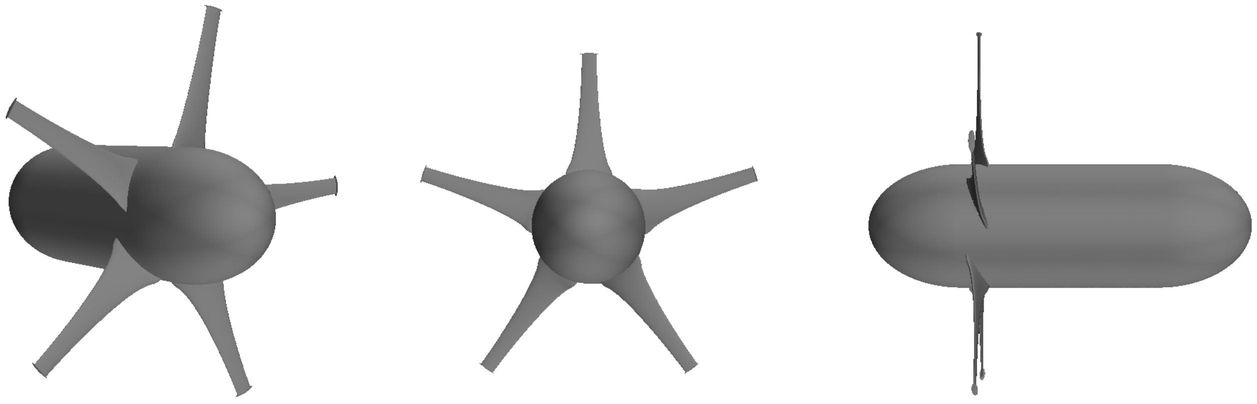

Figure 2-3: 3D CAD view of Sabella's D12 tidal turbine

The structure of the turbine will surely influence the tidal turbine performance. It will be studied in the work presented hereafter. This structure is a tripod connected to the D12 hub 3.9m behind the rotating plane (cf. Figure 2-4). Figure 2-5 gives a representation of the way the tripod is positioned. In order to run fluid dynamic computation, a simplification has been made on this tripod. Each leg is composed of two smooth pipes and a truncated cylinder.

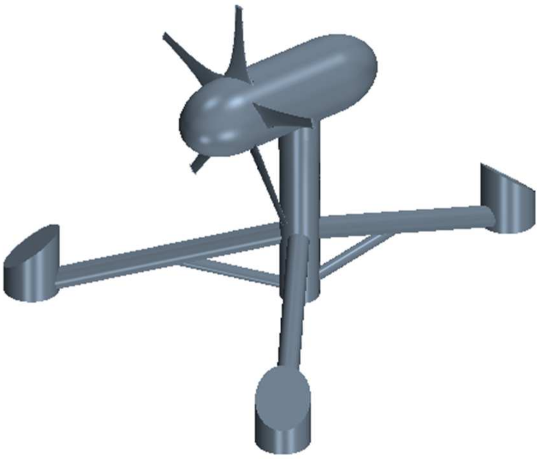

Figure 2-4: Sabella D12 turbine positioned on its structure

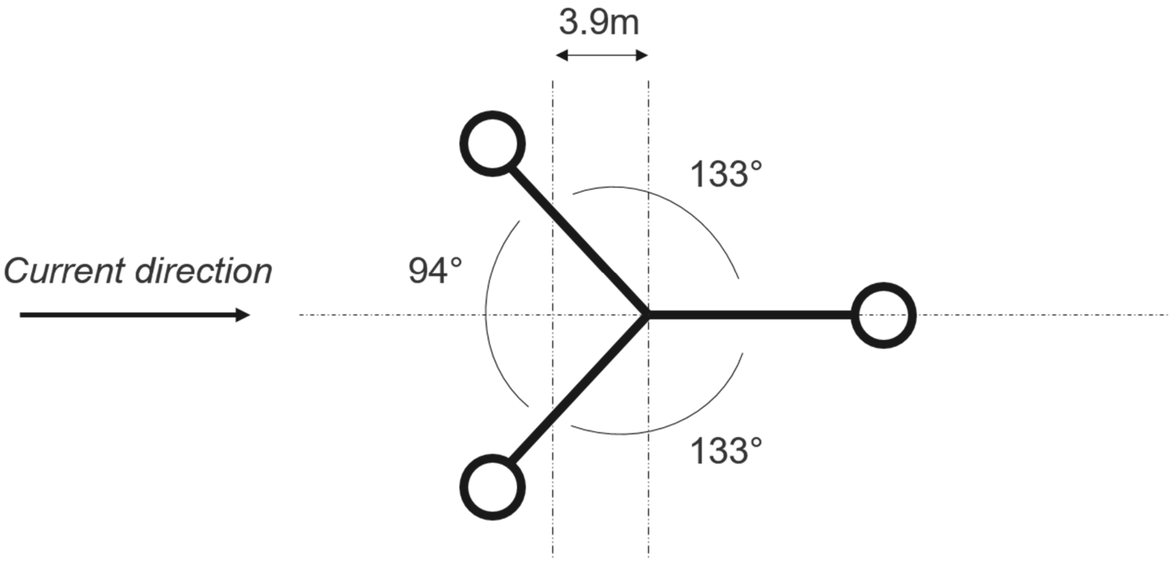

Figure 2-5: Layout of the turbine baseplate

2.3.2 Generic 3-bladed horizontal axis

The generic tidal turbine is a 3-bladed tidal turbine [3]. This Alstom/GE turbine has a diameter (called *2R*) of 18m for a blade length of 8.1m. The hub measures 15.45m (called *L*). The blades are based on the NACA 63-8XX profile and do not have winglet. The blade chord dimension ranges from 0.66m to 1m. Besides, rotation axis of the turbine is located at 15m above ground. Figure 2-6 gives CAD representations of this 3-bladed tidal turbine.

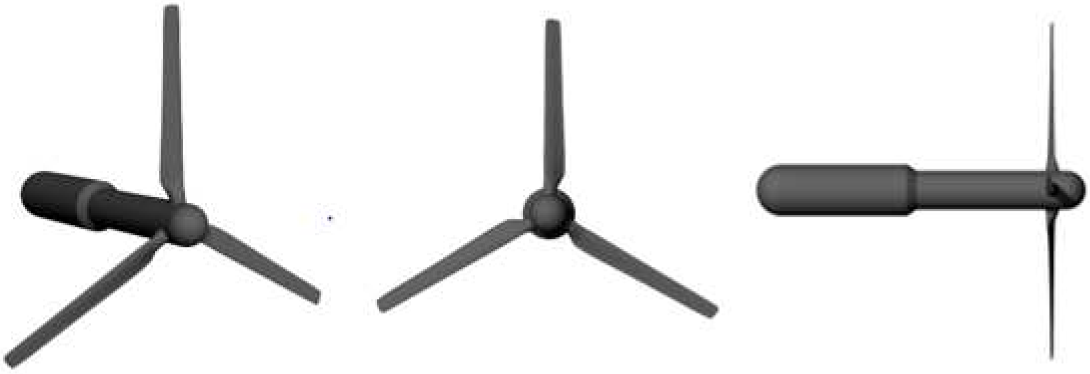

Figure 2-6: 3D CAD views of Alstom/GE generic tidal turbine

3 PERFORMANCE ASSESSMENT OF TWO TIDAL TURBINES – SIMPLIFIED MODEL

The objective of this model is to develop a first simplified model of the tidal turbines enabling to assess “ideal” performance of the geometry. As such, the turbine is considered as operating in an ideal flow without seabed nor free surface influence. The numerical setup takes advantage of the axi-symmetry of the turbine designs by considering only a “one blade slice” with symmetric conditions applied on the sides.

The simulation considers a uniform and steady velocity input. It focuses on the calculation of the mean hydrodynamic loads applying on key parts of the turbine (blades, winglet, and hub). Sensitivity analysis including mesh and time sensitivity study are carried on the D12 tidal turbine to ensure reliable results.

The model setup is used on the D10 tidal turbine to compare the CFD results to experimental data and validate the model setup. Once the model setup is validated, it is used to determine the performance curves of the Sabella’s D12 and generic 3-balded tidal turbine.

The applied workflow is presented hereafter in Figure 3-1.

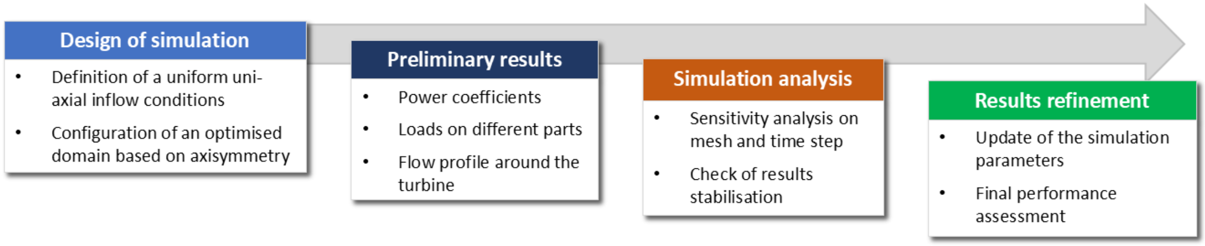
Design of simulation
• Definition of a uniform uni-axial inflow conditions
• Configuration of an optimised domain based on axisymmetry
Preliminary results
• Power coefficients
• Loads on different parts
• Flow profile around the turbine
Simulation analysis
• Sensitivity analysis on mesh and time step
• Check of results stabilisation
Results refinement
• Update of the simulation parameters
• Final performance assessment

Figure 3-1: Development of the simplified model - Workflow

3.1 Simulation features

3.1.1 Domain definition

As introduced above, the numerical model developed does not model seabed and sea surface. Moreover as the turbines are N bladed and axi-symmetric, only 1/N of the geometry is considered with periodic conditions on the side limits of the simulation domain

To avoid wall effects on the domain limits, large distances are used as diameter (about 10 to 15 turbine diameters) and length (around 16 to 24 turbine lengths). The resulting simulation domain is illustrated in Figure 3-2.

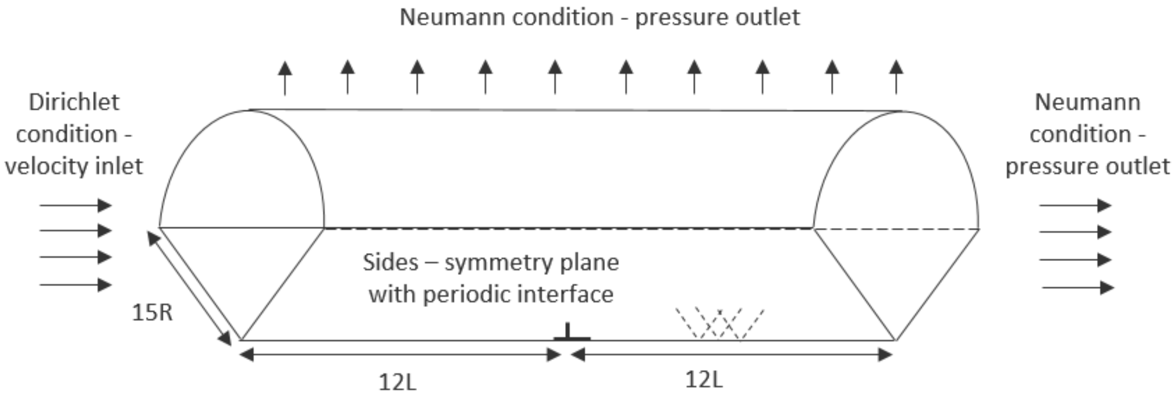
Neumann condition - pressure outlet
Dirichlet condition - velocity inlet
Neumann condition - pressure outlet
Sides – symmetry plane with periodic interface
15R
12L
12L

Figure 3-2: Simulation domain type for the Sabella D12 and generic turbines (illustration on 3-bladed generic turbine here)

3.1.2 Mesh description

To ensure a good capture of the flow behaviour around the tidal turbine, a refined mesh is defined on the key areas. The cells are polyhedral. It enables a more flexible mesh than hexahedral cells for a better capture of the turbine geometry.

The initial generated mesh with about 10 millions of cells is presented in Figure 3-3.

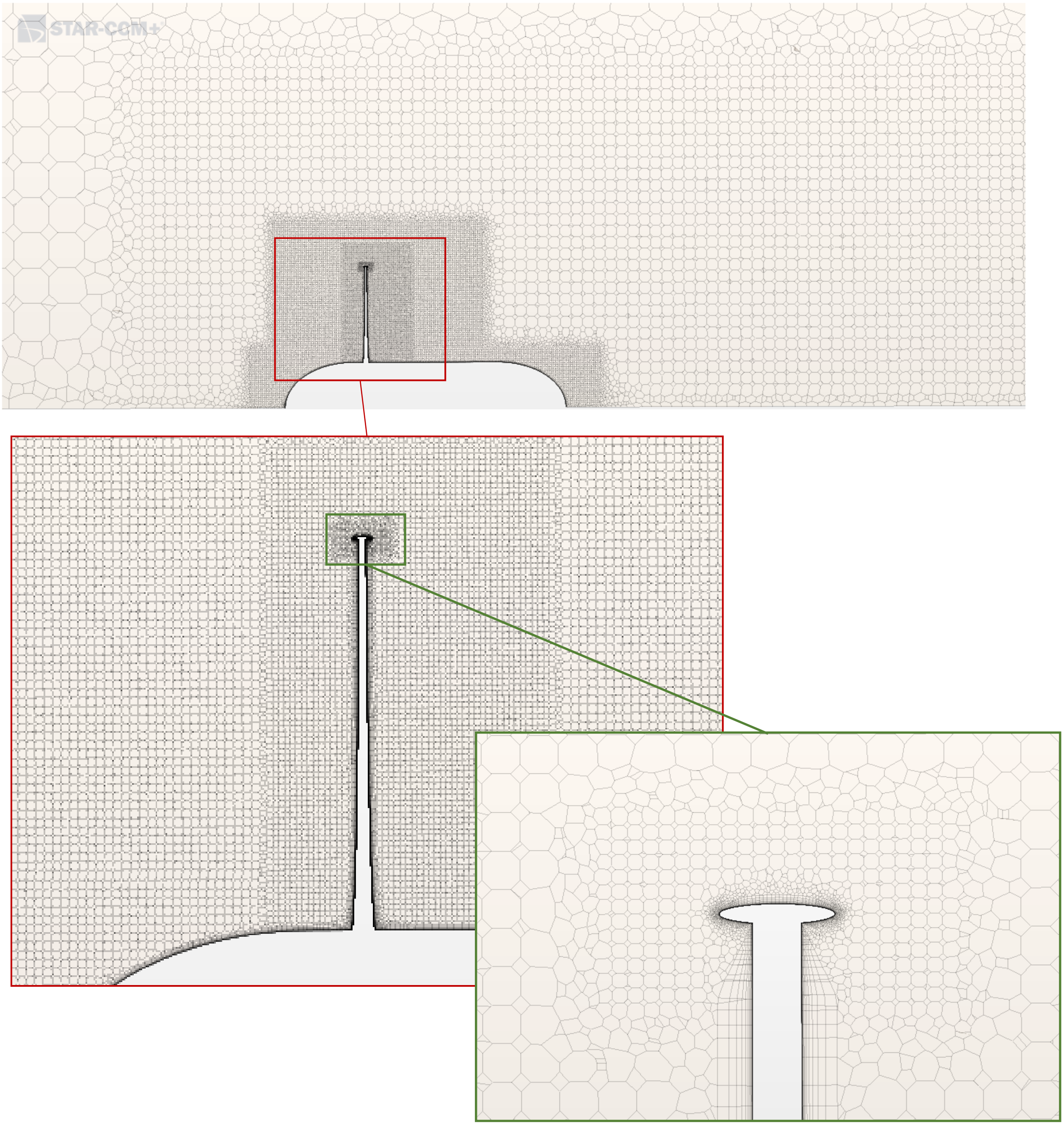

Figure 3-3: Mesh views of M0 simulation

A boundary layer is also added on the entire body such as:

- Y+ < 1 on the blade and winglet (set to ensure a resolution of fluid dynamic equations at viscous layer)
- Y+ > 60 on the hub (set to activate a model viscous layer model – Area between 1 and 60 avoided as it corresponds to the buffer zone)

The resulting wall Y+ values on the turbines are shown in Figure 3-4.

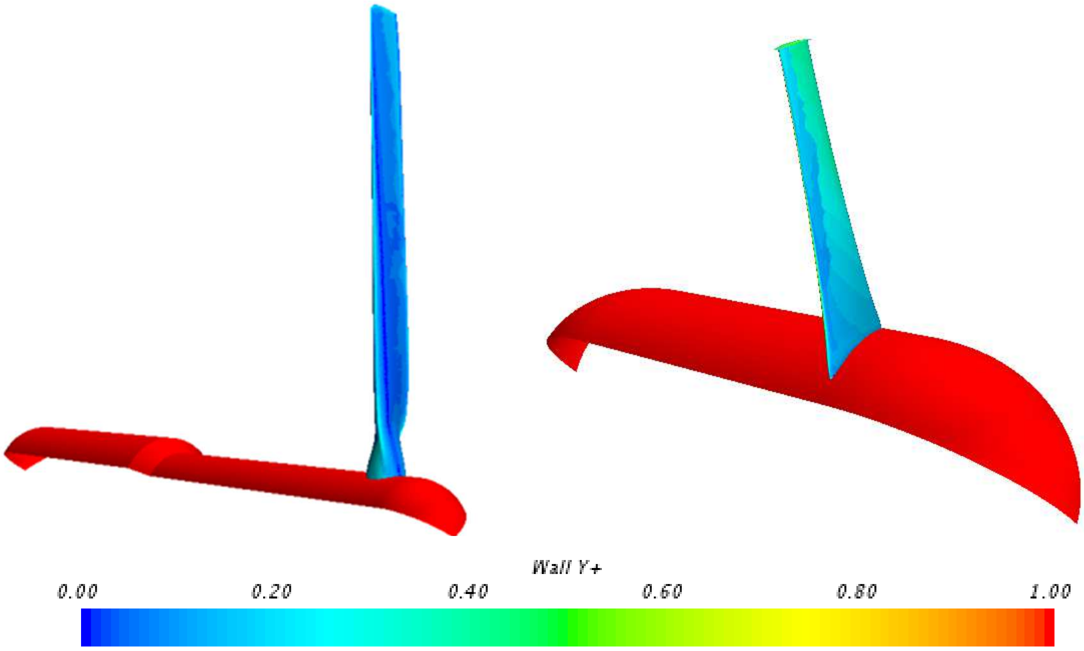

Figure 3-4: Wall Y+ - wall distance on the turbines

These parameters allow an appropriate wall treatment based on the aimed accuracy and avoid buffer layer zone which can lead to uncertainties.

3.1.3 Simulation parameters

Simulation Parameters	Models
Type	CFD - RANS
	Three dimensional
	Implicit Unsteady
Flow	Constant density
	Segregated flow
	Turbulent
Turbulence	Gamma transition
	SST (Menter) k-ω
	k-ω Turbulence
Calculation	All y+ Wall Treatment
	Cell Quality Remediation
	Gradients

Table 3-1: Simulations parameters used for the simplified model

The simulations are based on a RANS calculation method. The turbulence model used in the simulations is the k-ω SST turbulence model which mixes the advantage of the k-ω model next to the walls (turbine faces) and the less sensitive k-ε model in the far field. It tends to add stability in the turbulence resolution.

The simulation duration is set to 1800 time steps with a rotation rate of 2°/time step. It corresponds to 10 complete turbine rotations. The 2°/time step is selected based on BVS best practices for the analysis of propellers. It was applied in that case given the strong similarities between turbines and propellers. The uniform and steady inflow velocity is $\vec{U}_{infinity}$ =2.75$\vec{x}$ (m/s).

3.2 Sensitivity studies on the preliminary results

To ensure trustworthy results, a sensitivity analysis on numerical settings is necessary. This is done on D12 turbine model. A first assessment of the tidal turbine performance is carried out using M1 mesh and simulation parameters presented above. Based on the preliminary results, TSR = 4.5 was identified as the most performant operating point. The following sensitivity analysis are run on the simulation with at this particular TSR value.

The studied parameters are listed hereafter by order of consideration:

- Time step interval
- Duration of the calculation
- Steadiness of the results
- Mesh

3.2.1 Time step interval influence

The definition of the time step interval has an impact on the reliability of the results obtained at the end of the simulation. As a matter of fact it defines the capacity of the simulation to capture flow variations. A large time step will reduce the simulation computational cost but will surely miss some of the flow behaviour. On the other hand, a small time step will capture the flow behaviour more accurately but the computational cost will be higher. It is important to find the appropriate time step to reach a compromise between the expected accuracy and a reasonable computational time.

So far the simulation at TSR = 4.5 was set with a time step interval of Δ= 2°/time step on 1800 time steps. It corresponds to 10 complete rotations of the tidal turbine. In this study, Δ=1 and 8 °/time steps are simulated. To compare equivalent situations, the simulations are all set such as the turbine reaches 10 complete rotations at the end. It leads to an adjustment of the number of time steps depending on the time step interval: 3600 time steps for Δ=1°/time step and 450 time steps for Δ=8°/time step. The results obtained are presented in Table 3-2. This analysis is based on the 25 million cell mesh, see section 3.2.5.

$U_{infinity}$	TSR	°/t.s.	Cp,Cq,Ct	Run time (280cores)	Number of time steps
2.75	4.5	**1**	Ref.	18h	3 600
		2	0.12%	9h	1 800
		8	1.03%	2.25h	450

Table 3-2: Sensitivity of results to time step interval and associated relative error

The time step interval Δ= 1°/time step is defined as reference as it generates the most accurate results. The relative error between the reference and the two other simulations is the same for (Cp, Ct, and Cq) it only depends on the time step interval refinement.

For Δ=2°/time step, the error compared to reference is very small and almost negligible (0.12%). It becomes slightly higher with Δ= 8°/time step reaching about 1% but remains low. Therefore, the choice of Δ=2°/time step is reasonable when considering the computation time gains (about 50%) and the negligible reduction in accuracy.

3.2.2 Time convergence

The time step is now validated. The simulation duration is another important parameter which can lead to poorly converged power, thrust and torque predictions despite apparently steady or stable results being predicted. To ensure a good time convergence of the results over time, the 30 seconds simulation (10 turbine rotations) is continued to 70 seconds (4100 time steps or about 22 turbine rotations). Table 3-3 presents a comparison of the results obtained in both cases.

Iterations	$N_{rotation}$	Time	TSR	Cp	Cq	Ct
1800	10	30s	4.5	0.6%	0.6%	0.4%
4100	**~22**	**70s**		Ref.	Ref.	Ref.

Table 3-3: Influence of simulation duration on results convergence and associated relative error

The relative error of the results obtained from the 1800 time steps simulation compared to the 4100 time steps simulation is not greater than 0.6%. It is very small compared to the computation time cost of a longer simulation (about 20h for 4100 time steps compared to 9h for 1800 time steps). Therefore, even if this error is not completely negligible, it is considered as acceptable. The 1800 time steps simulation is validated and will be used later on.

3.2.3 Stability of the results

In order to ensure a good convergence of the results, a verification on their stability at the end of the simulation is done. To do so, the results data set is decomposed in 100 time steps samples and the standard deviation of each sample is measured. The curve in Figure 3-5 represents the output of this analysis.

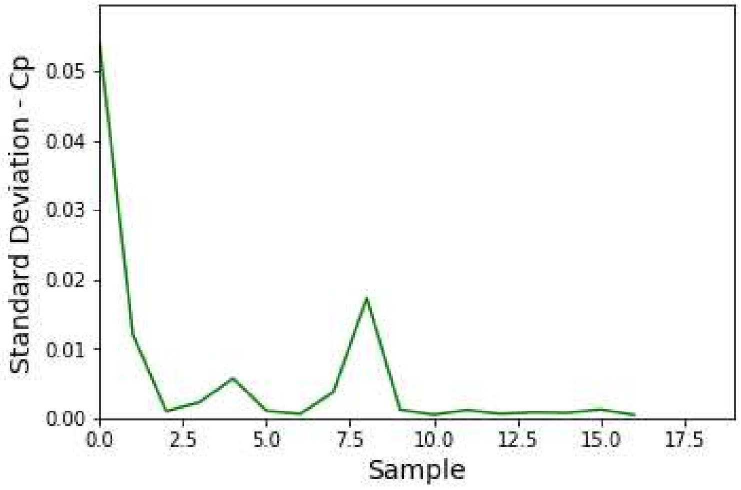

Figure 3-5: Standard deviation in sliding 100 time steps series along Cp time series

It is obvious that standard deviation of the samples decreases drastically as the simulation progresses. It converges quite rapidly to finally reach a standard deviation lower than 0.1% which validates the steadiness of the results at the end of the simulation.

N.B.: This analysis is also carried on the relative variation between the maximum and minimum values of the samples. It leads to the same conclusion as this relative variation converges close to zero. The curve in Figure 3-6 shows the output of this analysis.

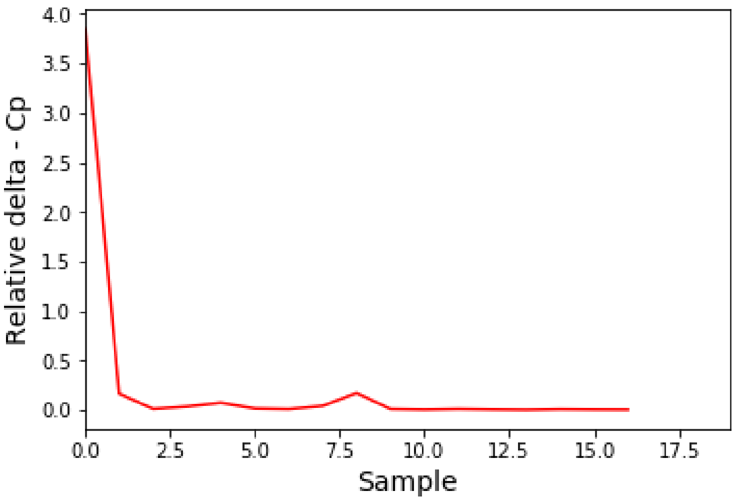

Figure 3-6: Relative difference between min and max values in sliding 100 time steps intervals along Cp time series

3.2.4 Sensitivity to the Reynolds number

The sensitivity of the model to the initial parameters defined as input is also an important aspect to consider before validating the generalisation of the model. So far, the hypothesis was made of a turbine performance only dependant of the TSR. Here, the model sensitivity to the Reynolds number is investigated. The modification of the inflow velocity directly impacts the Reynolds number value. In previous simulations, the inflow velocity has been set to $U_{infinity}$=2.75 m/s. In this analysis, the inflow velocity is successively set to:

$$U_{infinity} = [0.75, 1.75, 2.75, 3.75]\ m.s^{-1}$$

The other parameters are unchanged: TSR=4.5, Δ= 2°/time step, $N_{time\ step}$=1800.

The resulting effect of the inflow velocity variation on the turbine efficiency is a direct increase of the Reynolds number. The associated impact on the performance results is represented in Figure 3-7.

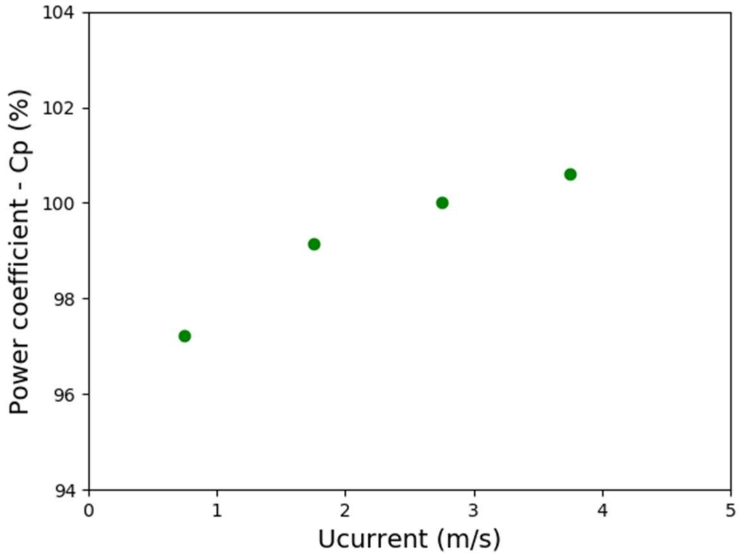

Figure 3-7: Influence of Reynolds number on the power coefficient Cp

The inflow velocity increase generates an increase of the power coefficient. It would be necessary to consider a larger set of inflow velocities to evaluate the value at which the efficiency reaches a converged value to estimate the theoretical maximum reachable efficiency. However, in real conditions, such inflow velocities are rarely reached. Therefore, it would not have a real physical meaning except for very particular areas.

These results show the possible dependence between the power coefficient value and the Reynolds number of the inflow. However, the calculations used for this sensitivity analysis have been run on the same model without any modification of the viscous layer mesh with respect to the inflow value. Therefore, deeper analysis should be carried out to validate this preliminary conclusion.

3.2.5 Mesh sensitivity analysis

The mesh parameters used to generate the first mesh are appropriate for preliminary stage of the performance assessment. However, it may need to be refined to reach converged results as refinement directly impacts the accuracy of the computation. The mesh sensitivity study is a key part of every computational fluid dynamic (CFD) model validity assessment.

The preliminary mesh (M1) is composed of 10 million cells. A second mesh (M2) of 25 million cells is generated with an increased refinement around the blade and winglet which are key hydrodynamic elements of the tidal turbine. The main interest of this study is to define a mesh capable of capturing as accurately as possible the flow behaviour on these elements. Finally, a third mesh (M3) of 40 million cells is generated by refining the zones of interest even more than done in M2. The results obtained with these two meshes are compared at identical simulation parameters: TSR=4.5, Δ= 2°/time step, $N_{time\ step}$=1800, $U_{infinity}$=2.75 m/s.

Figure 3-8 presents the different meshes under the same perspective and allows a visual comparison.

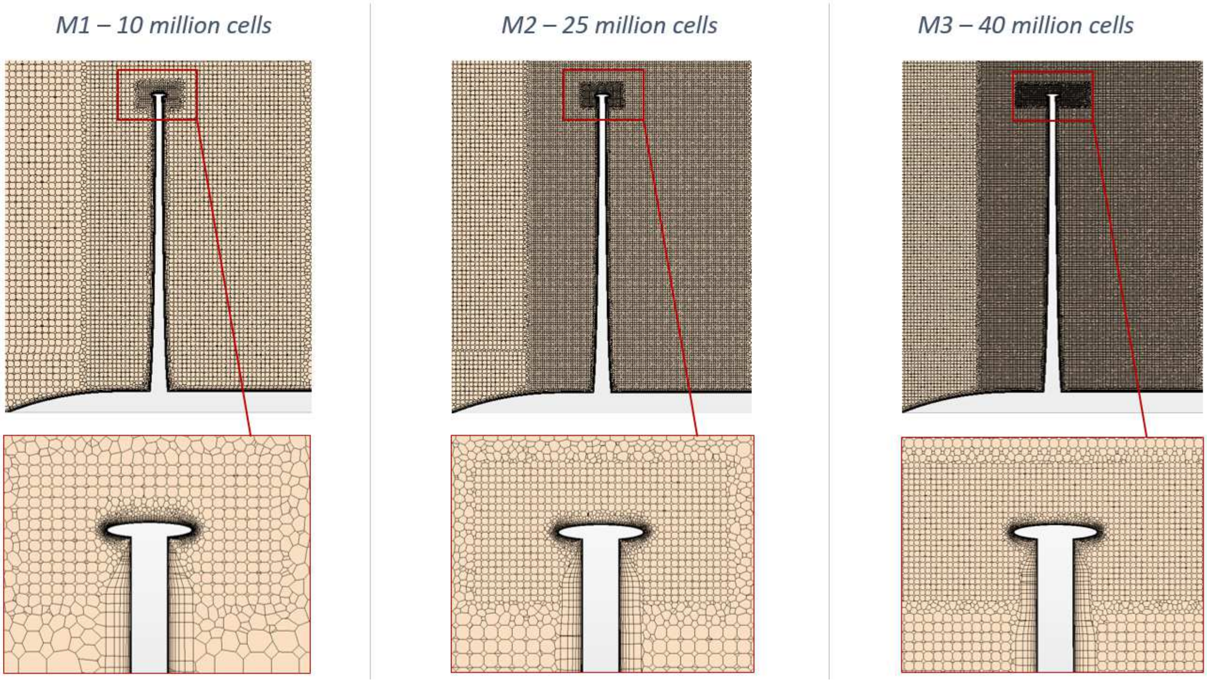

Figure 3-8: Visual comparison of meshes used for sensitivity study for D12 performance assessment

The results obtained for the different meshes are summarized in Table 3-4.

Mesh	Cells	TSR	$U_{infinity}$	$N_{time\ step}$	°/t.s.	Cp	Cq	Ct
M1	10M	4.5	2.75	1800	2	1.70%	1.70%	1.18%
M2	25M					0.67%	0.67%	0.33%
M3	**40M**					**Ref.**	**Ref.**	**Ref.**

Table 3-4 Mesh sensitivity analysis on results and associated relative error

The coarse mesh tends to overestimate the results. As presented in the chart above, this overestimation is reasonable (about 1.7%) which gives credit to the results obtained using the preliminary mesh M1. However, to ensure accurate and mesh independent results, it is necessary to recalculate the hydrodynamic loads of the tidal turbine using the refined mesh M2. The results obtained from M2 and M3 are very close with less than 0.7% error. Given the computational time necessary to run M3, it has been decided to use M2 as reference for further calculation as it allows a good compromise between computational time and accuracy.

3.2.6 Conclusion on sensitivity analysis carried out on the model

The analysis of the preliminary results enabled to obtain a first good approximation of the hydrodynamic loads on the turbine in different conditions. Using these results, it was also possible to locate the best operating point around TSR = 4.5.

However, this sensitivity study also pointed out various sources of uncertainties on the results. A few of those are inherent to the use of CFD models as computation time and cost must stay within feasible limits. On the other hand, some can be reduced in order to increase accuracy on results. Concerning mesh sensitivity analysis, it appears that the second mesh offers a good compromise between accuracy and computation cost.

So far, some simulation parameters can already be validated as their influence appeared to be very small (and even negligible in some cases) compared to their influence in computation time:

- Time step interval : Δ =2°/time step
- Simulation duration in time steps : 1800 (5 complete rotations of the turbine at Δ =2°/time step)
- Results calculated averaging the last 10% of the calculated values to smooth any possible fluctuations and guarantee convergence of the results

N.B.: The refined meshes generate some instabilities in the resolution of the turbulence. The turbulence kinetic energy residual have been skyrocketing in some cases. This is a known numerical instability when using dense meshes in STAR-CCM+. It occurs at the initialisation of the calculation when the inflow velocity is set up. In consequence, the under-relaxation factors used by the turbulence models were reduced in order to increase the computation stability. This method does not modify the final results as the number of inner iterations was sufficient. It is only used to increase robustness of the calculation numerically during the first steps.

3.3 D10 simulation and comparison with experiment results

Sabella uses an “in-house” blade element momentum theory (BEMT) code to estimate the performance of its tidal turbines. This BEMT code was validated on earlier turbine designs tested in experimental trials conducted in tanks. CFD simulations run on the D12 Sabella’s turbine were discussed with Sabella. It came out that the performance calculated using the CFD model were quite different from the performance estimation made using Sabella BEMT code. The CFD simulations appear to give higher results. In order to verify the validity of the model, it is decided to run simulations on the D10 Sabella’s turbine on which experimental data exist and compare the results obtained.

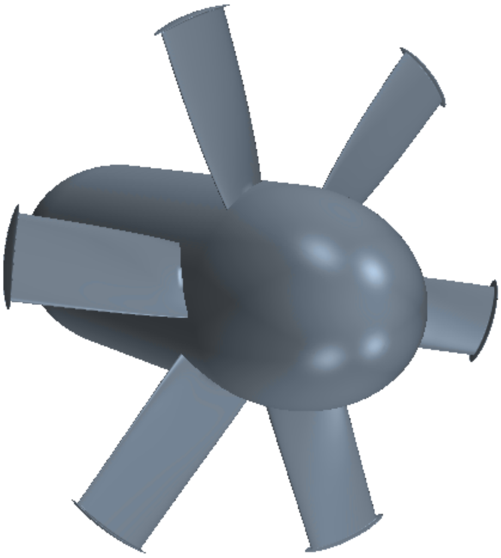

Figure 3-9: Sabella's D10 tidal turbine CAD representation

The D10 Sabella’s turbine is a 6 bladed turbine with larger blades than D12 turbine. It was put into service in 2015. A 3D CAD view is available in Figure 3-9. Some experiment results exist and are used as reference for CFD results validation.

3.3.1 Presentation of the experimental results and CFD model settings

3.3.1.1 **Experimental setting and associated results**

Experimental testing at Reynolds similitude was not achievable due to tank facility limitations. Therefore, a power coefficient curve convergence test was carried out instead by Sabella. To do so, a range of high inflow velocities were generated, and the turbine load response measured. The experiment setting was the following one:

- Towing tank of L = 10m, l = 3.6m, h = 2.5m
- D10 - 1/25 model scale of the turbine (D = 400mm) placed at the centre of the towing tank
- Axial inflow velocities : [0.75, 1.5, 2.25, 2.5, 2.75, 3, 3.25, 3.5] m/s

The results obtained from the experiments are provided by Sabella at each velocity. The performance curve profile reaches an overall converged state for inflow velocities above 2 m/s.

3.3.1.2 **CFD simulations definition**

To work under the same conditions as done for 5 bladed D12 turbine a 1/6th modelling of the turbine in ideal domain is used to create the CFD model of the D10 turbine. It corresponds to a “one blade slice” of the 6-bladed D10 turbine. The D10 turbine modelled in CFD is identical to the one used for experiments.

The inflow velocity U = 2.5 m/s is selected to calculate a power coefficient curve. A point is also computed at U = 0.75 m/s to evaluate results obtained at low inflow speed where convergence has not been reached yet.

To limit the number of simulations key (U_inflow,TSR) points are selected to run simulations:

- P1(0.75, 2.4) – Verification of the results obtained at low inflow speed
- P2(2.5, 1.8), P3(2.5,2.0), P4(2.5, 2.4), P5(2.5, 2.8) – To get a performance curve at an inflow velocity of 2.5 m/s which can be compared to experimental results

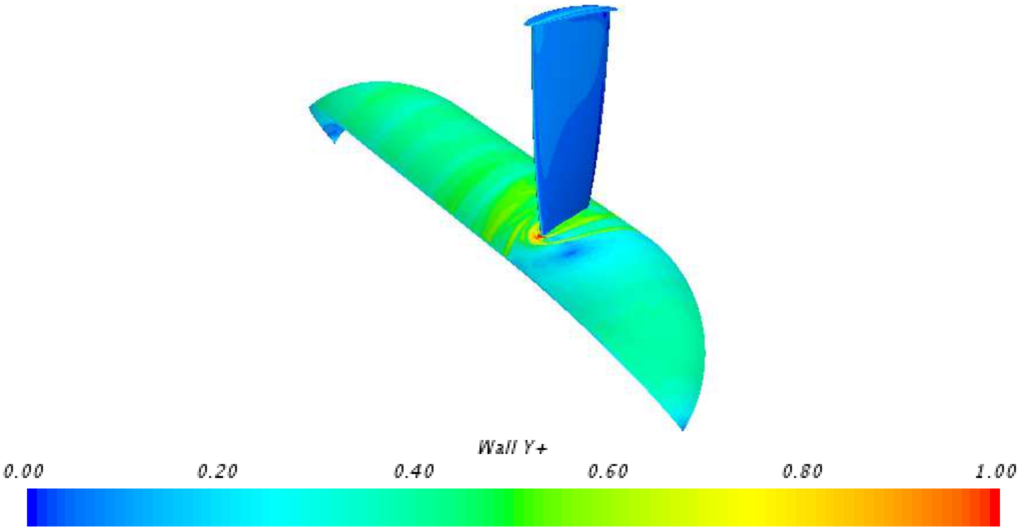

Figure 3-10: Wall Y+ value on D10 turbine slice

For all configurations, the wall function is set to Y+ < 1 on the blade and remains very small on the hub. It enables to capture the flow behaviour on the turbine surface as accurately as possible. Its value on the blade is presented in Figure 3-10.

The noticeable difference with the wall function presented above (cf. Figure 3-4) is due to the scaling of 1/25th carried out on the turbine mesh and domain to meet experimental settings.

3.3.2 CFD simulations results presentation and analysis

The results obtained using CFD are presented in Table 3-5. They are very encouraging. The correlation between experimental and calculated results is good. The overall performance assessment is correct for U = 2.5 m/s. The maximum power coefficient value may be slightly over estimated by CFD but it remains very coherent. However, this comparison points out a big difference in the results for U = 0.75 m/s, confirmed by multiple verifications. After discussing these conclusions with Sabella, it was confirmed that it exists a big uncertainty on the U =0.75 m/s experimental results. A possible cause is a Magnus effect correction applied which may not be adapted to low inflow speeds.

A simulation considering the whole turbine instead of a slice containing a single blade was carried out. It showed very little difference in the results for an excessively higher computational cost. It justifies the use of the slice model.

	P1 (0.75, 2.4)	P2 (2.5, 1.8)	P3 (2.5,2.0)	P4 (2.5,2.4)	P5 (2.5,2.8)
Exp. data	Ref.	Ref.	Ref.	Ref.	Ref.
CFD result	+15.16%	-6.67%	+1.37%	+3.59%	+2.40%

Table 3-5: Comparison between CFD and experimental results on Cp for D10 turbine

The comparison between experimental and CFD results on the D10 turbine enabled to verify the validity of the hypothesis made on the CFD model. It validates the “one blade slice” domain definition used to reduce computational cost. Therefore, this model will be used to run a final hydrodynamic performance assessment on the D12 using the simulation parameters defined above through the sensitivity study carried out.

3.4 Final performance assessment

The conclusions obtained from the sensitivity analysis carried out on D12 tidal turbine are used to define the final model setup.

3.4.1 Final performance assessment of D12 and 3-bladed generic tidal turbines

As presented in the tidal turbine theory, three coefficients are used to assess the turbine performance: the thrust coefficient, the torque coefficient and finally the power coefficient directly representative of the flow energy captured. The results obtained are presented in Figure 3-11 for D12 and Figure 3-12 for the 3-bladed generic turbine.

For each graph, the performance coefficient values are presented as percentage of the highest value reached on the points of interest.

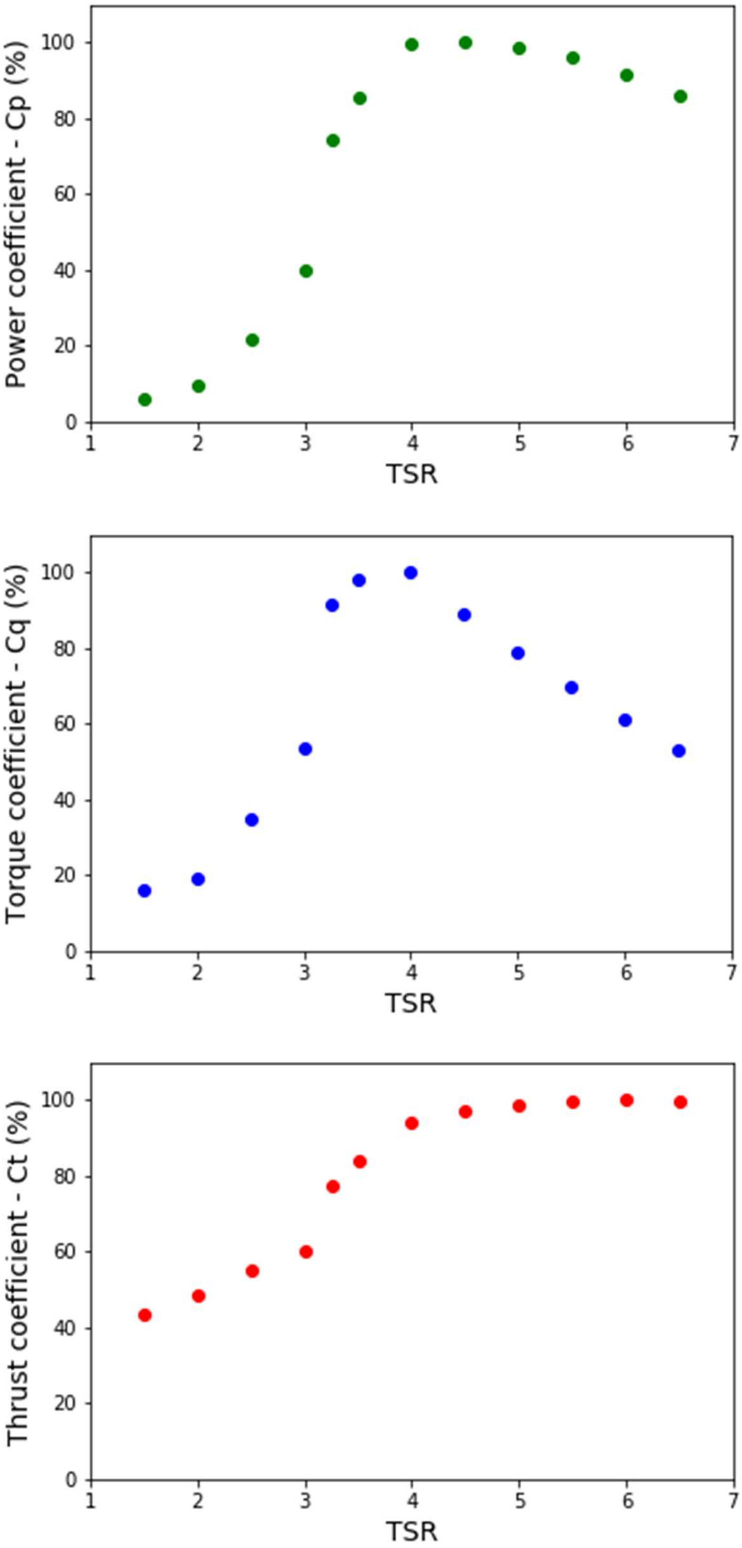

Figure 3-11: Final performance assessment on the D12 Sabella's tidal turbine - Power coefficient, Cp - Torque coefficient, Cq - Thrust coefficient, Ct

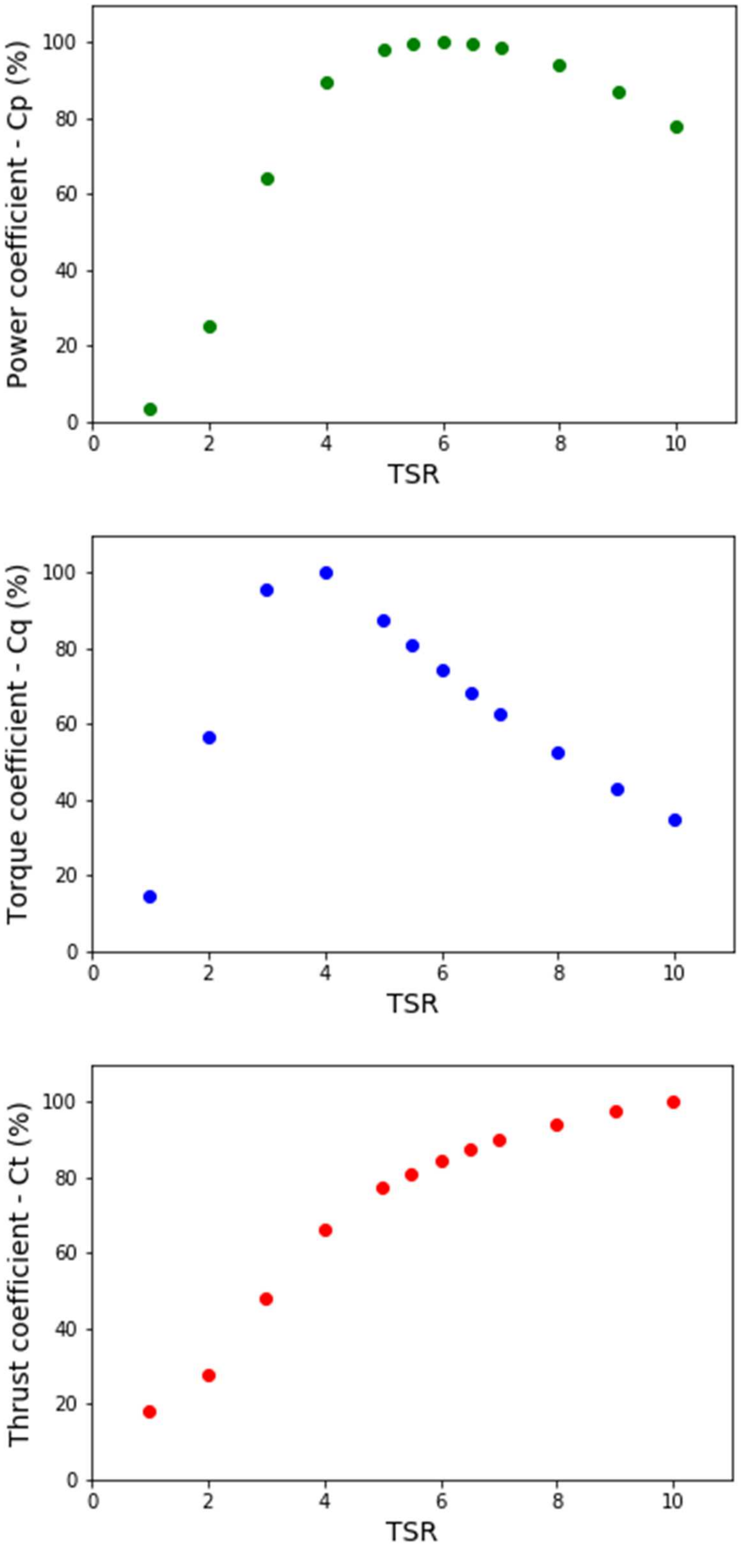

Figure 3-12: Final performance assessment on the 3-bladed generic tidal turbine - Power coefficient, Cp - Torque coefficient, Cq - Thrust coefficient, Ct

3.4.2 Analysis of the flow hydrodynamics around the blades

3.4.2.1 **Velocity profiles analysis (at Z=3m) on D12 blade**

A noticeable inflexion point appears around TSR = 3.5. It is representative of a change in flow behaviour around the blade: as TSR increases, the boundary layer separation diminishes leading to a vortex shedding intensity decrease. The velocity profiles around the blade captured at different TSR (Figure 3-14) illustrate this phenomenon at a particular location on the blade (cf. Figure 3-13).

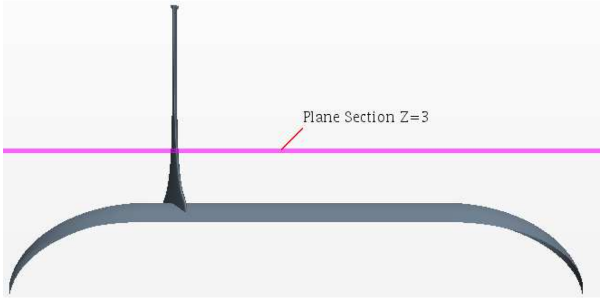

Figure 3-13: Side view of a D12 blade, position of the plane Z=3m

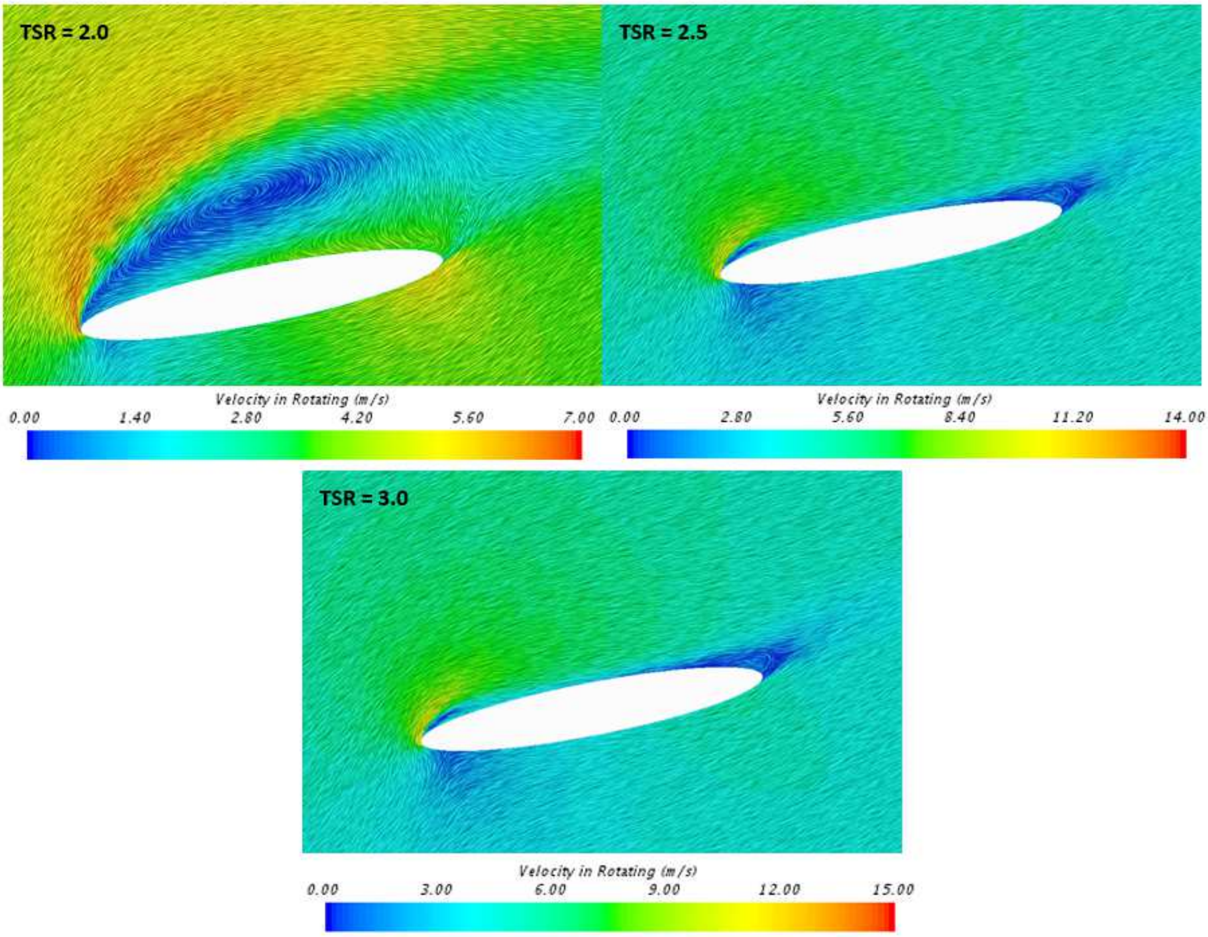

Figure 3-14: Velocity profiles around D12 blade at Z=3m for TSR = 2, 2.5 and 3

The phenomenon observed in Figure 3-14 is explained by the coupling of the flow velocity and the rotation speed of the blades introduced earlier.

The pitch of the blade also has an influence on the flow profile around the blade. As the rotational velocity is dependent of the radial position, a “curvature” of the blade usually enables to compensate this effect. It modifies the angle of attack of the profile depending on the radius. The 3D view of the turbulent kinetic energy of the flow around the blade at TSR =2.5 in Figure 3-15 shows this phenomenon. The root of the blade has a smooth flow profile with low turbulence generation due to the pitch. However, the vortex shedding occurs higher on the blade. It creates turbulence.

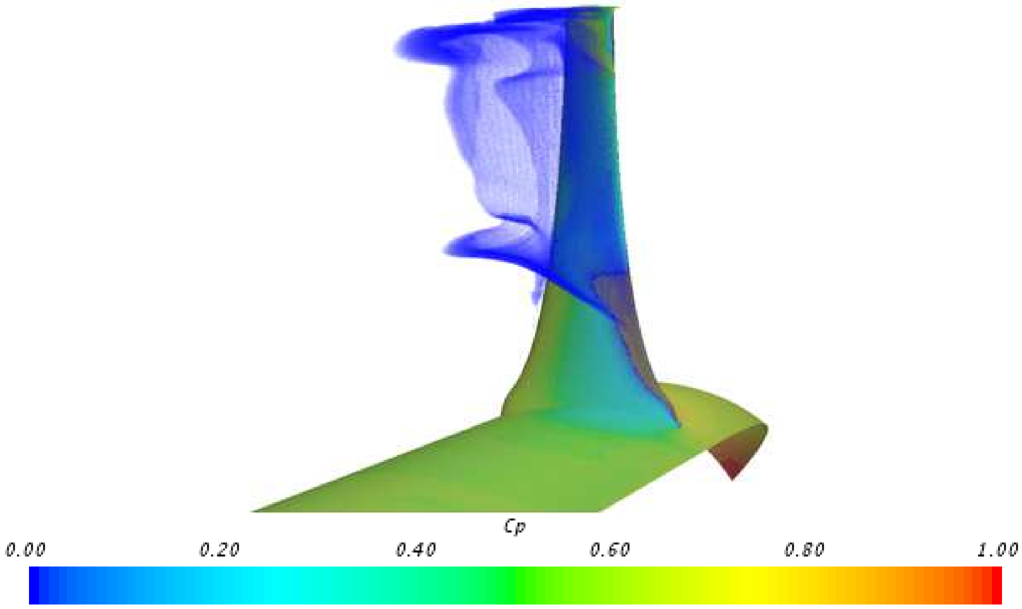

Figure 3-15: Pressure coefficient and turbulent kinetic energy (in blue) generated by D12 blade at TSR = 2.5

3.5 Structural analysis of the D12 blade

The simplified model developed enables to capture the pressure constraints applied on the turbine blades for various TSR configurations. It is of great interest for the structural analysis. Sabella asked MECA (an engineering company expert in composite materials structures) to conduct the structural analysis of the D12 tidal turbine.

After discussing with Sabella, the four cases presented hereafter are identified as reference cases for the structural design:

- 2 cases of standard operating conditions
- 1 case with the turbine parked
- 1 case of accidental operating condition

Using the developed CFD model they are run. The resulting pressure loads applied on the blade are provided to Sabella. In order to provide detailed information, the blade was divided. The decomposition carried out led to 109 surface patches over the whole blade (6 radius divisions – 9 chord divisions on both intrados & extrados + the winglet). The resulting blade is presented in Figure 3-16.The pressure load is calculated on each of these patches.

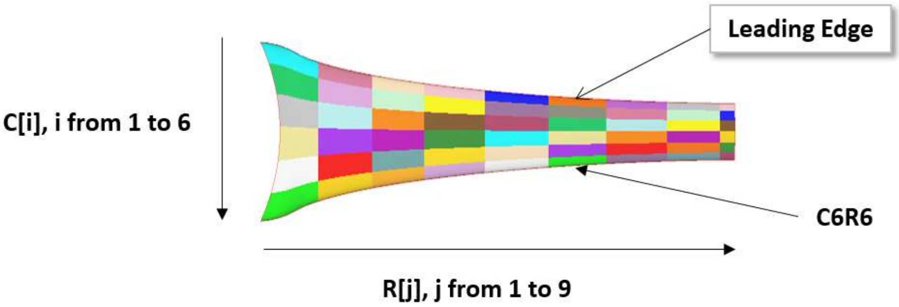

Figure 3-16: Illustration of the 108 patches division of the D12 blade

Moreover, the pressure value on each node of the mesh used in the numerical model is also provided. It make a 3D mapping of the overall pressure field on the blade available. An example of the resulting dataset is presented in Figure 3-17. Each of the sphere visible on the figure represents a node of the mesh used for the CFD calculation.

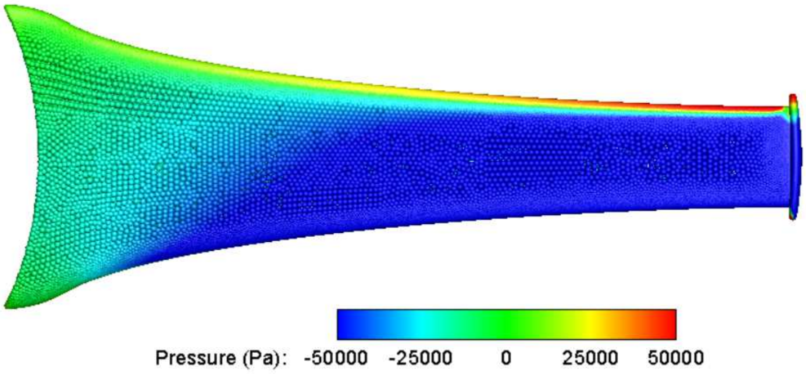

Figure 3-17: Pressure field on the D12 blade

3.6 Conclusion on the development of the model

The work carried out in this first part of the project enabled to define a useful CFD blade resolved model. It enabled to define the performance curves of the tidal turbines of interest and to provide relevant inputs for the structural analysis.

The simplification assumptions made – steady and uniform inflow, the absence of seabed and free-surface and the “slice” modelling – allowed to obtain a fine mesh on the blade with reasonable computational cost. The flow around the blade is well captured. However, this model is not usable to study the influence of realistic conditions on the turbine’s behaviour. Therefore, it is necessary to develop a more complex one enabling to do so.

The next part of the report will present the development of the more complex model enabling the integration of realistic environmental conditions. Finally, it will be used to quantify the influence of the different factors such as vertical velocity profile, structure presence, and current incidence on the turbine.

4 INTEGRATION OF REALISTIC CONDITIONS IN THE MODEL

4.1 Literature review on turbulence modelling

4.1.1 CFD models characterisation applied to turbulence

The properties of a studied flow can change drastically under the influence of turbulence. As it modifies the flow behaviour, it also impacts the flow around the tidal turbine, associated loads and resulting wake. Previous studies conducted on tidal turbines emphasize the non-negligible influence of turbulence on the wake behind tidal turbines. It is of great interest when considering possible array configurations where the wake generated by a turbine can become the inflow of another one. The impact on hydrodynamic loads seems to be less important. However, it may generates fatigue in the structure and it also need to be assess.

STAR-CCM+ is a well-known industrial fluid dynamics software. It is capable of addressing aerodynamics, hydrodynamics but also thermic and electromagnetism problems. As mentioned before, the hydrodynamic simulations realized in this project are conducted using it. It includes different turbulence models which enable to address quite accurately turbulence influence on the studied case. However, numerical modelling of flow and turbulence problems in hydrodynamics is a complex process. To adapt the numerical approach to the objective of the simulation, different resolution methods have been developed, each with its specificities. One needs to choose carefully in regard with its objectives. The most classic ones are:

- Reynolds averaged Navier-Stokes Equations (RANS)
- Large scale Eddy simulations (LES)
- Detached Eddy simulations (DES)

N.B.: One could also mention direct Navier-Stokes (DNS) simulations aiming to resolve entirely the flow without any modelling. However, due to the humongous resources and time needed to run such simulations it is completely off scope.

The main difference between these methods resides in the amount of turbulent content of the flow resolved or modelled. Different turbulent scales are present in the flow and depending on the level of detail needed, it is necessary to choose the right method to take them into account. Figure 4-1 shows the differences between the approaches mentioned above in terms of turbulent content resolution or modelling. The horizontal axis represents the size of turbulent structures – called eddies (going from big to small ones) while the vertical axis represents the amount of turbulent energy associated to these structures.

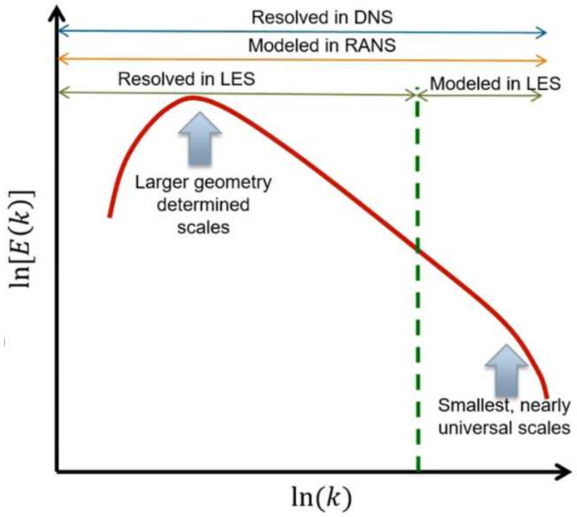

Figure 4-1: Energy characteristics of turbulent structures based on size

4.1.1.1 RANS Model

The RANS simulations are based on an averaging of the key variables considered in the Navier-Stokes (NS) equations. The global NS equations are defined as follows:

$$\rho\frac{\partial u_i}{\partial t}+\rho u_j\frac{\partial u_i}{\partial x_j}=-\frac{\partial p}{\partial x_i}+\frac{\partial}{\partial x_j}\left(2\mu s_{ij}\right)$$

With $\boldsymbol{x}$ the instantaneous time and space dependent variable. It can be decomposed between the mean value X and the associated fluctuation x.

The averaging of the NS equation give the following equation:

$$\rho\frac{\partial U_i}{\partial t}+\rho U_j\frac{\partial U_i}{\partial x_j}=-\frac{\partial P}{\partial x_i}+\frac{\partial}{\partial x_j}\left(2\mu S_{ij}-\rho\overline{u_i u_j}\right)$$

An additional and unknown term – written in red – has appeared due to the averaging of non-linear quantities. It can be interpreted as turbulent stresses – or Reynolds stresses. This new unknown does not possess a governing equation allowing resolution and closure of the newly obtained RANS equation.

Different turbulence models have been developed to close the system:

4.1.1.1.1 Reynolds Stresses model

It is probably one of the most accurate turbulence model. It aims to resolve a set of seven equations in order to close the Navier-Stokes equation instead of modelling it as most of the other turbulence models do. However, such an objective requires very high computation cost and asks for a very long calculation time. Therefore, it is almost only used for research and academic purposes. It will not be used in this project.

4.1.1.1.2 Eddy viscosity models

Except the Reynolds-Stress transport turbulence model (RSM) which intend to close the Navier-Stokes equations through the resolution of seven equations, other turbulent models use the Boussinesq approximation (1877) as closure. It relies on the observation that at molecular level momentum is diffused by viscosity. Viscous stresses appear in the Navier-Stokes governing equations as:

$$t_{ij} = \mu\left(\frac{\partial \boldsymbol{u}_i}{\partial x_j} + \frac{\partial \boldsymbol{u}_j}{\partial x_i}\right)$$

Similarly this hypothesis relates the Reynolds stresses generated by turbulent structures to the mean rate of deformation through **eddy viscosity, $\boldsymbol{\mu_t}$**:

$$\tau_{ij} = \rho\overline{u_\iota u_j} = \mu_t\left(\frac{\partial \boldsymbol{u}_i}{\partial x_j} + \frac{\partial \boldsymbol{u}_j}{\partial x_i}\right)$$

It relies on the hypothesis that normal Reynolds stresses are isotropic. These models are called Eddy viscosity models. The most classical ones are k-ε, k-ω, k-ω SST models.

4.1.1.2 **LES**

LES simulations are very effective to compute turbulence as it aims to resolve it on almost all the domain. This gives an accurate turbulent output. However, it is necessary to design a mesh of the domain sufficiently small so that turbulent structures can be identified and captured. It implies the need for a very detailed and heavy mesh leading to high computational costs. To deal with turbulent structures which may be lower than grid size, sub-grid scale models are implemented. They allow the consideration of turbulent structures having a smaller scale than grid refinement.

4.1.1.3 **DES**

The very high computational cost of LES to simulate accurately the flow and the lack of accuracy of RANS simulations due to averaging process generates the need for an intermediary method. Detached eddy simulations uses the advantages of both methods. It calculates the flow profile on the boundary layer using unsteady RANS method to avoid heavy meshes and resolves detached eddies out of the boundary layer as it is done in LES. Figure 4-2 illustrates this principle.

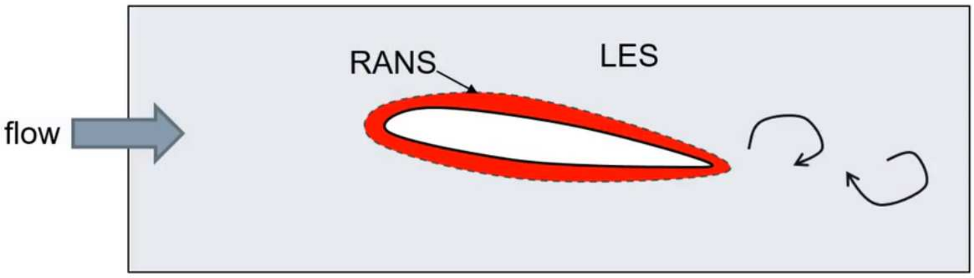

Figure 4-2: Idealized view of DES zonal repartition of calculation methods

It gives the opportunity to access LES accuracy in most of the flow with reasonable mesh and computational cost. However, some problematics arise with this method. The transition between the two methods have to be considered carefully to ensure that it is smooth. Some mismatch between the methods can occur. It creates the need for a very accurate mesh design. To counter these risks, delayed detached eddy simulations (DDES) have been developed. It aims to delay the transition from RANS to LES, ensuring a complete compatibility between the method applied and the mesh size.

4.1.2 Turbulence generation methods and related data needed for implementation

As presented before, the ambient turbulence of the flow is characterized as fluctuations of the velocity around a mean velocity profile. Therefore the flow velocity can be expressed as followed:

$$\boldsymbol{u} = \overline{\boldsymbol{u}} + \boldsymbol{u}^{turb} \quad \text{with} \quad \boldsymbol{u} = (u, v, w) = (u_i), i \in [1,3]$$

The first essential data needed to generate a turbulence flow field is obviously the mean velocity profile, mainly on the vertical axis. It is usually described by a power law profile:

$$\overline{w} = w_{@reff} \left(\frac{z}{z_{reff}} \right)^{\alpha}$$

Then comes the generation of the turbulent aspect of the velocity profile. Turbulence modelling techniques are numerous and the resulting turbulence boundary inflow generated can be quite different [4]. The turbulence data available are a strong constraint which can limit the use of some of these models. The aim of this document is to draw a preliminary list of the turbulence generation methods identified and the associated turbulence data needed to execute them. Based on the available data and BVS resources, relevant methods will be selected. At present two methods are particularly interesting in the scope of RealTide project: synthetic eddy method and discrete random flow generation based on turbulence spectra.

4.1.2.1 **Synthetic Eddy Method**

Synthetic eddy method (SEM) appears to be one of the most classical and widespread method to generate a turbulent boundary inflow. It has been developed by Jarrin & al. around 2006 [5]. STAR-CCM+ implemented this method in the pre-processing of LES and DES simulations.

It considers the turbulent flow field as a superposition of spinning turbulent structures on a mean flow profile whose main characteristics are determined using a normalized uniform distribution. It uses a correlation function to generate an approximate turbulent flow in agreement with real turbulence. The **turbulent length scales** is a mandatory input of the method. However, to describe turbulence as such, it accepts two different settings depending on the available input data:

- Turbulent length scales and Reynolds stresses tensor (RST)
- Length scales & turbulence intensity (TI)

4.1.2.2 **Discrete random flow generation based on turbulence spectra**

Another commonly used method to generate turbulent inflow conditions is based on the discretization of a turbulent power spectra using Fourier transformation. It is based on turbulence spectra established from data measurements and experimental campaigns run by IEC and NREL. The most commonly used ones are the Von Karman and the Kaimal models. It has been widely used in BEMT codes such as TurbSim developed by NREL [6] or Bladed developed by DNV GL [7]. At first, these tools were developed for wind turbines but are being updated to add tidal flow features. Wind models are used for tidal flow descriptions most of the time as data are missing to establish tidal flow models. Only TurbSim integrates a tidal spectrum based on measurements taken near Marrowstone Island in Puget Sound Washington [8].

The expression of the turbulent spectra is complex and asks for numerous data to implement the model, especially when considering 3-dimensional flows. Some of the main features needed in the Von Karman models are presented below. It is quite representative of the other models.

- Frequency range of the spectra
- Turbulent spectra
- Turbulence intensity profiles or standard deviation functions of the velocity in three directions (except for isotropic models)
- Turbulent local length scale functions
- Coherency functions and associated coherency decay number

A Fourier transformation is then used to discretise the spectrum once it has been correctly defined. It generates Fourier functions describing the evolution of the velocity profiles according to turbulence in the domain. An interesting application of this theory leading to the creation of a Matlab code was presented by H. Aboshosha, A. Elshaer & al. [9]. A complete application of the method – from the definition of the key parameters and inputs to the generation of the turbulent boundary condition – is developed in the paper.

This generation approach based on turbulence spectra analysis is very useful as it generates discretized velocity functions to describe the turbulent flow. It is adapted to BEMT codes and can also be linked to LES and DES simulations. However, it asks for a specific data on the flow to set the model correctly which are not fully available for tidal flows yet. Moreover, the measure and design of new spectra adapted to tidal flows characteristics is still in progress and very few models exist for now. Therefore, it is difficult to generalize the use of this method to turbulent tidal flow generations.

4.1.2.3 **Conclusion on the turbulent generation method**

Different methods are available to generate turbulent boundary conditions. As presented above, the requirements to operate them correctly are really different. Two methods are particularly interesting in the scope of the RealTide project:

- Synthetic eddy method
- Discrete random flow generation based on turbulence spectra

The first one is really relevant for the development of CFD turbulent realistic model [10] [11]. The two different setting options allow flexibility and adaptation capacity with regard to the available data. The second one is widely used for wind turbulence generation in CFD and particularly adapted to BEMT codes. It is a very interesting method which can be adapted to many different cases. However, at present very few data are available on tidal turbulence spectra. For now and until further measurement campaigns, the cautious use of wind models on tidal flows may be a valid option to keep using this model.

Other methods exist such as recycling-rescaling methods and database approach methods. However, they do not seem to be adapted to the scope and objective of the project and will not be investigated. A discussion with UEDIN – in charge of data acquisition [12] – enabled to define the key measurements to be realized in order to generate a realistic turbulent inflow. The next steps will be the integration of these data to STAR-CCM+ in order to create the realistic model.

Table 4-1summarizes the inputs needed to implement each of the methods presented above.

Turbulence modelling methods – Necessary inputs			
Method	**Name**	**Symbol**	**Description**
Synthetic eddy method (SEM) - RST	Turbulent length scale	$L_i \text{ with } i \in [1,3]$	Representative length scales of the turbulent structures in the flow
	Reynolds stresses tensor values	$\overline{\overline{\boldsymbol{R}}} = \begin{pmatrix} R_{uu} & R_{vu} & R_{wu} \\ R_{uv} & R_{vv} & R_{wv} \\ R_{uw} & R_{vw} & R_{ww} \end{pmatrix}$ $\text{with } R_{ij} = R_{ji}$	Tensor containing multiple information on the flow turbulence such as: • Turbulence intensity • Anisotropy • Interaction between three directions
Synthetic eddy method (SEM) - TI	Turbulent length scale	$L_i \text{ with } i \in [1,3]$	Representative length scales of the turbulent structures in the flow
	Turbulence intensity profile or mean value	$I_{turb}(x,y,z) \text{ or } I_{turb}$	Global description of the turbulence in the domain
	Anisotropy coefficients (if available)	$(\sigma_u, \sigma_v, \sigma_w)$	Precision quantifying the anisotropy of turbulence in the flow
Turbulent spectrum discretization	Turbulent power spectrum	$[S_u(f), S_v(f), S_w(f)]$	Turbulent power spectrum expression established for the turbulent model considered
	Turbulent length scales	$L_i \text{ with } i \in [1,3]$	Representative length scales of the turbulent structures in the flow
	Turbulent intensity profiles **OR** standard deviations of velocity profiles	$I_{turb,u}, I_{turb,v}, I_{turb,w}$ **OR** $(\sigma^2(u), \sigma^2(v), \sigma^2(w))$	Description of the turbulent aspect of the flow in the three directions over the domain
	Coherency functions	$Coh_{i,j} \text{ with } i,j \in [1,3]^2$	Description of the interaction with the turbulent domain depending based on the position
	Coherency decay numbers associated to the coherency functions	$c_{i,j}^{d} \text{ with } i,j \in [1,3]^2$	Characteristic coherency decay value used in coherency functions

Table 4-1: Necessary inputs for turbulence modelling method

4.2 Analysis of UEDIN data tide measurements from Orkney

A measurement campaign led by UEDIN enables to provide data characterizing turbulence in marine environment. This campaign was led at Orkney (UK) during a previous research project and was made available in the context of WP1 "*Increase reliability of tidal rotors*". Measurements were carried out at specific moments of flood tide: during the accelerating and decelerating phases. In regard with Fromveur site – deployment site of Sabella's turbine – specificities, UEDIN provided filtered data series for particular velocities of interest (from 2.2m/s to 2.8m/s).

A better understanding of these turbulent data leads to a more realistic setup of blade resolved CFD model. The analysis of UEDIN data will focus on some main turbulent parameters as turbulence intensity, turbulence length scale and velocity scale. These parameters will be used as inputs later on.

4.2.1 Description of the key turbulence parameters

4.2.1.1 Turbulence intensity

The turbulence intensity is a way to quantify the turbulence level of a flow, it depends on the current mean velocity and the fluctuations around the mean velocity. It is defined as the ratio of the root mean square (RMS) of the turbulent velocity fluctuations over the mean velocity [13].

$$\boldsymbol{I = \frac{\sqrt{1/3(std(u)^2 + std(v)^2 + std(w)^2)}}{\overline{U}}}$$

Where std stands for standard deviation. The turbulence intensity *I*, the mean velocity $\overline{U}$ and the velocity fluctuations (u, v and w) are available in UEDIN data.

4.2.1.2 Turbulence length scale

The turbulence length scale, coherence length of the large vortices, are available in UEDIN files. Its theoretical definition linked to the Reynolds average turbulence solver (k-ω SST) is based on the Kolmogorov's theory.

The Kolmogorov's theory [14] explains the energy transfer from large eddies to small ones. This energy cascade describes the division of eddy structures enabling to dissipate the turbulent energy. Blade loads and wake are mostly affected by vortices from the integral scales [15]. The integral scale theory allows to give a turbulence length scale approximation [16]:

$$\boldsymbol{Ls = {}^{\sqrt{k}}/_{\tau}}$$

The turbulence length scale depends on the turbulence time scale τ and the turbulence kinetic energy *k*. The turbulence time scale is the time of a large scale eddy turnover, it is the time scale of the flow turbulence. By definition, the turbulence kinetic energy is half of the sum of the velocity components variances.

$$\boldsymbol{k = 1/2\left(std(u)^2 + std(v)^2 + std(w)^2\right)}$$

4.2.1.3 Velocity scale

The velocity scale *Vs* is the coherent velocity of the large structures, it means the motion velocity of a large vortex (from the integral scale of turbulence) [17]. Not directly available in the UEDIN files, this parameter is defined as a function of turbulence intensity and mean velocity. This dependency leads to the expression below where the velocity scale is primarily expressed with turbulence length scale and turbulence time scale τ.

$$\boldsymbol{V_s = {}^{l_s}/_{\tau}}$$

By means of the equations presented above, the velocity scale can be expressed by the square root of the turbulent kinetic energy.

$$v_s = \sqrt{k}$$

Thanks to the Kolmogorov's theory and the turbulence model, all main turbulence parameters are defined based on data measured by UEDIN.

4.2.2 Analysis of turbulence data from UEDIN datasets

From the measurement histories provided by UEDIN it is possible to plot turbulence intensity versus the turbulence length scale. As only turbulence data in x direction are complete in UEDIN files, the subsequent analysis is only giving information on x-direction turbulence data.

Figure 4-3 represents the turbulence intensity as a function of the turbulence length scale for the first part of flood whereas Figure 4-4 concerns the second part of flood.

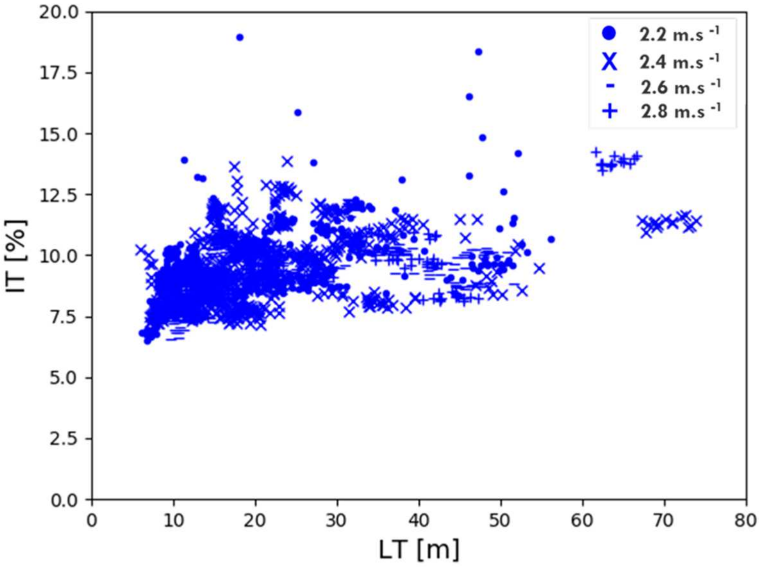

Figure 4-3 : Turbulence intensity depending on the turbulence length scale – 1st part of flood

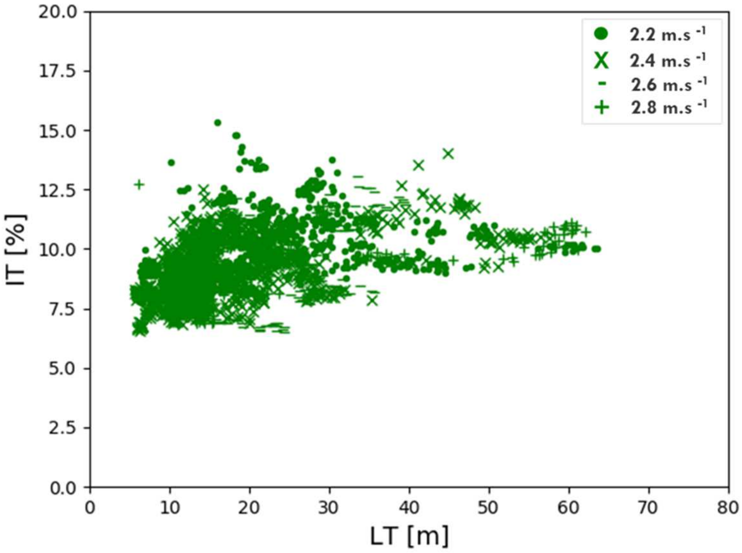

Figure 4-4 : Turbulence intensity depending on the turbulence length scale – 2nd part of flood

Range of potential turbulence parameters values in the studied marine environment is known thanks to an analysis of these scatter plots. The large range of turbulence length scale for the 1st part and 2nd part of flood are respectively [5m, 75m] and [5m, 65m]. The reference turbulence length scale chosen for those scattered data is 25m. The turbulence intensity data also has a significant range in both cases, namely [6.5%, 19%] for the 1st part and [6.5%, 15.5%] for the 2nd part. A turbulence intensity of 10% has been chosen as reference value of these ranges.

A linear regression of these data is done. Visible on Figure 4-5 and Figure 4-6, linear regressions using the least square method highlights a proportional relation between turbulence intensity and length scale. Besides part of flood does not influence turbulence intensity and length scale.

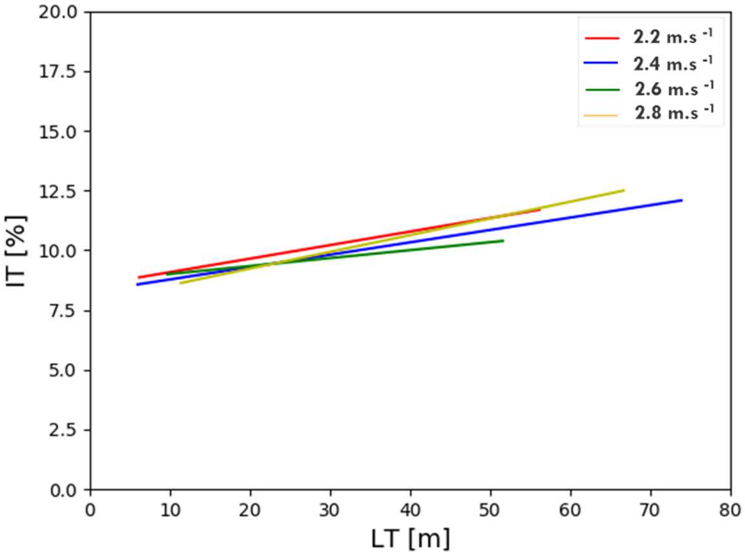

Figure 4-5 : Linear regression of turbulence intensity depending on the 1st part of flood

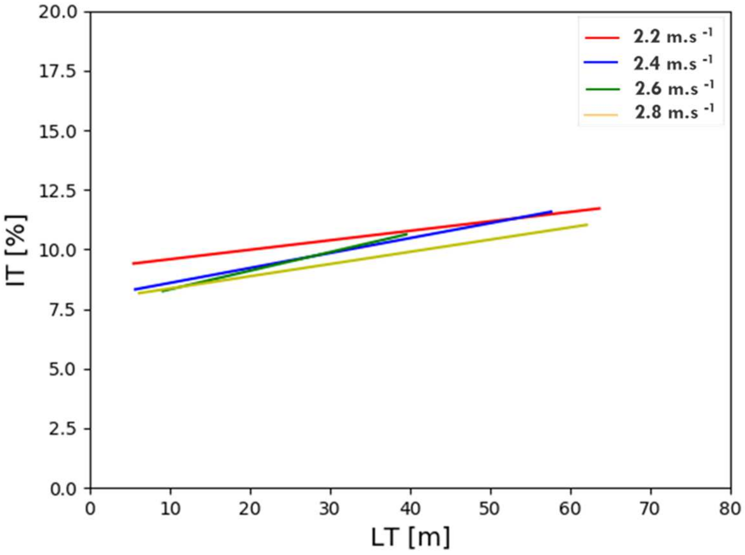

Figure 4-6 : Linear regression of turbulence intensity depending on the 2nd part of flood

The turbulent velocity scale is also post-processed and analysed from the UEDIN data. Both accelerating and decelerating phase of the tide have similar scatter plot of the velocity scale. Range of value varies from 0.2m/s to 0.5m/s. By taking into consideration only most recurrent values, a representative value for the velocity scale was identified as being 0.275m/s.

4.3 Development of a complex model integrating realistic environmental conditions

The first numerical model presented above enabled to study the tidal turbine operating in an ideal "open-water" environment. The work performed using it shows the interest of such a model. However, the operational context of tidal turbines is usually far from ideal as multiple exterior factors such as turbulence, seabed, and free surface effects are involved. It has a direct influence on the turbine performance, loads and resulting wake. Therefore, there is a strong interest into developing a model capable of integrating those realistic environmental conditions.

In order to study the influence of realistic conditions on tidal loads, a parallelepiped domain with a height equivalent to the Fromveur straight is set up. It enables to model a seabed and a realistic depth& key parameters for the velocity profile propagation. Realistic domain is characterized by a **depth of 55m and a length of 184m.** A large width is fixed to avoid blockage effects on the structure and flow. The following section presents the modification of the simplified model to this more complex model. Various modifications are required to achieve it. This is done following a step-by-step method which enables to quantify the influence of the modifications added to the model. The successive steps are presented hereafter:

- **Full modelling of the turbine and modification of the method used to implement the turbine's rotation:** The realistic model requires a parallelepiped domain shape. The simplified model is based on one-blade slice of the turbine and requires an axi-symmetry in the domain. Therefore, it is no longer applicable. The whole turbine has to be modelled. Moreover, the rotation of the turbine will be modelled by the Rigid Body Motion method (RBM method) more accurate than RFM in this context.

- **Integration of the seabed and free surface:** The integration of the seabed requires to take into account the bottom effect and the development of a viscous layer on the ground, responsible for the vertical velocity profile. A layered mesh is set up in the domain to enable a more refined mesh next to the bottom. The free-surface is implemented using symmetry plane. It enables to account for free surface effects without using multi-fluid CFD simulations. As such, it reduces the mesh size and the computational cost.

- **Integration of the turbine's structure:** The turbine is supported by a tripod structure. It does modify the flow both on the turbine and in the resulting wake. Therefore, it has to be accounted for in the model. Its integration generates the need for an appropriate mesh in order to capture the structure correctly.

The current section presents the development of the three points listed above in the new model. For each of the key step introduced above, a model is introduced. They will be used later in the report to quantify the influence of the model changes on the turbine loads, efficiency and wake.

4.3.1 Turbine fully modelled and modification of the rotation method

4.3.1.1 Presentation of the new simulation setup

As introduced above, the rotation method used in the simplified model has to be modified in perspective a domain having a parallelepiped shape. The reference frame motion (RFM) will be replaced by the rigid body motion (RBM). Two key reasons explain this need for a new rotation method:

- The implementation of vertical velocity profiles and other flow variables will generate varying loads over the turbine. The entire turbine has to be modelled to capture the phenomena clearly
- RBM is more accurate than RFM to resolve turbine's loads as it actually makes the turbine rotates while the RFM only simulates it

In this context, the RBM method is implemented and the turbine is fully modelled. The axi-symmetry is no longer used to simplify the calculations. This new rotation method implies to set up two domains:

- A domain with a cylindrical shape surrounding the rotating parts of the turbine in which the motion is imposed
- A fixed domain interfaced with the rotating domain

In order to ensure a transition with the work performed above, this first updated model will be cylindrical without taking into account seabed which will be introduced in the next point.

The rotating domain is created such as its axis is aligned with the turbine's rotation axis. It is subtracted from the main domain. The resulting model setup is presented hereafter in Figure 4-7. The boundary conditions are kept identical to simplified model with velocity inlet at the outer cylinder entrance and pressure outlet on cylinder's sides and end. Simulations settings are also identical to simplified model (cf. Table 3-1). For this model, as only the turbine's modelling has been modified, the inlet remains uniform.

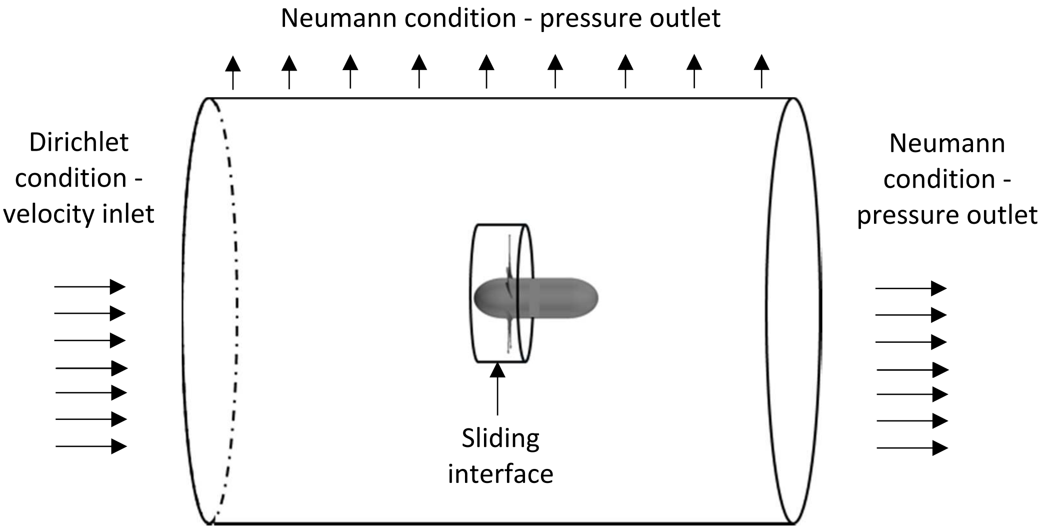
Neumann condition - pressure outlet
Dirichlet condition - velocity inlet
Neumann condition - pressure outlet
Sliding interface

Figure 4-7: Presentation of the model setup used for RBM in the cylinder

The inner and outer domains are separated and have their own mesh. An interface is set up between the two in order to ensure continuity of the flow variables when transiting from one domain to the other. The Rigid Body Motion (RBM) requires a good interpolation between the two grids. Mesh specificities ensuring it are added to the model with refinements constraints imposed to force similar cell size on at the interface.

Finally, the separation of the rotating domain and the environment domain enables to apply different mesh types in each of them. As such, the environment domain will be meshed using hexagonal cells positioned aligned with the flow direction for a good capture of the flow variables. As previously done, the rotating domain will be meshed using polyhedral cells, more flexible, which ensures good capture of the turbine geometry. However, the entire turbine is now modelled. If the mesh was kept identical to the one used in the simplified model, the resulting mesh would be over 100 million cells for a 5 bladed turbine. Therefore, to keep a reasonable CPU time, the mesh capturing the turbine have been adapted and coarsened. The resulting inner rotating domain is now composed of 15 million cells while the outer domain is composed of 5 million cells.

The resulting mesh is presented in Figure 4-8.

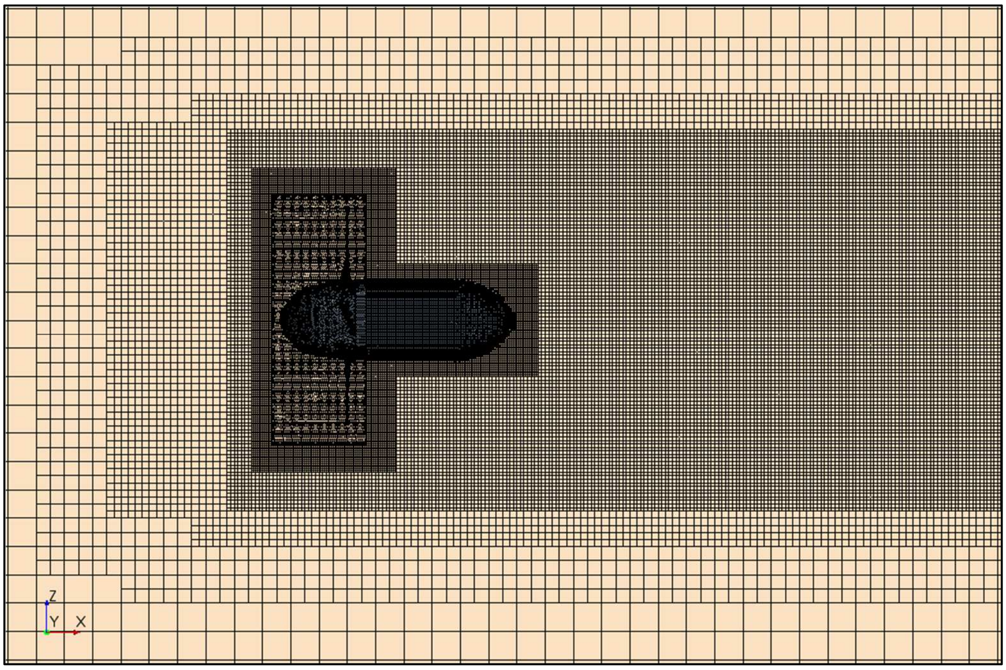

Figure 4-8: Mesh view of the RBM model applied in a cylinder domain

4.3.1.2 Definition of the reference cases

The model defined above is used to calculate the performance of the turbine on two cases:

- U = 2.75 m/s, TSR = 4.5 – It is the case of reference selected for simplified model. The results obtained on this model will help to quantify the difference of performance assessment linked to the new model setup with regard to the simplified model

- U=V0(U70), TSR = 4.5 – It corresponds to the current speed at hub height for the U70 current profile provided by Sabella (cf. 5). This case will be used as reference to study the influence of the vertical velocity profile on the turbine behaviour

The obtained results in terms of power coefficients are presented hereafter:

Model	TSR	$U_{infinity}$	Cp
Simplified	4.5	2.75	**Ref.**
RBM cylindrical		2.75	-3.88%
		V0(U70)	-4.32%

The non-negligible difference obtained between the two models for a current inflow at 2.75 m/s and a TSR value of 4.5 enables to state on the influence of the model changes. It is due to the various modifications carried out on the simulation setup from rotation method to the turbine being fully modelled along with the mesh modifications. These changes are necessary to conduct the rest of the study and develop a realistic model with reasonable computational cost. However, it also shows that direct comparison of the simplified model with the model developed hereafter are not relevant as the numerical setup and the hypothesis previously used are no longer applied here.

The results obtained on the U70 reference case is almost identical to the one obtained with an inflow of 2.75 m/s. It is expected as the TSR value used is the same. The difference is most likely only due to Reynold number effects.

4.3.2 Integration of the seabed and free surface

The cylindrical model using RBM method presented above is now being updated in order to include the seabed presence. It is necessary for taking into account more realistic environmental conditions. To do so, the cylindrical outer domain introduced above is replaced by a parallelepiped shape. As introduced, the height of the domain is chosen to be 55m with regard to the Fromveur straight depth. The length of the domain is set to 184m in order to enable sufficient distance behind the turbine for the wake to propagate with 60m in front of the turbine.

The integration of the seabed goes along with the adaptation of the mesh to add refinement layers on the ground. It will enable a more accurate capture of the viscous layer development. The resulting mesh for this new numerical model is presented in Figure 4-9 and Figure 4-10. The outer grid is composed of hexahedral cells. In STAR-CCM+®, this kind of cells is defined as trimmed cell. The trimmed grid is composed of about 15 million cells and the grid of the rotating domain is composed of 20 million cells.

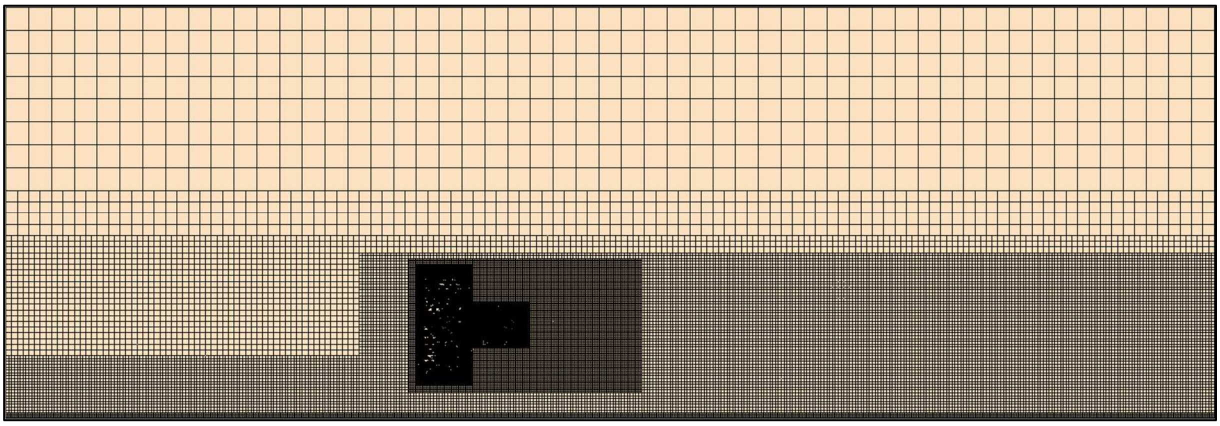

Figure 4-9: Outer grid – Stationary domain

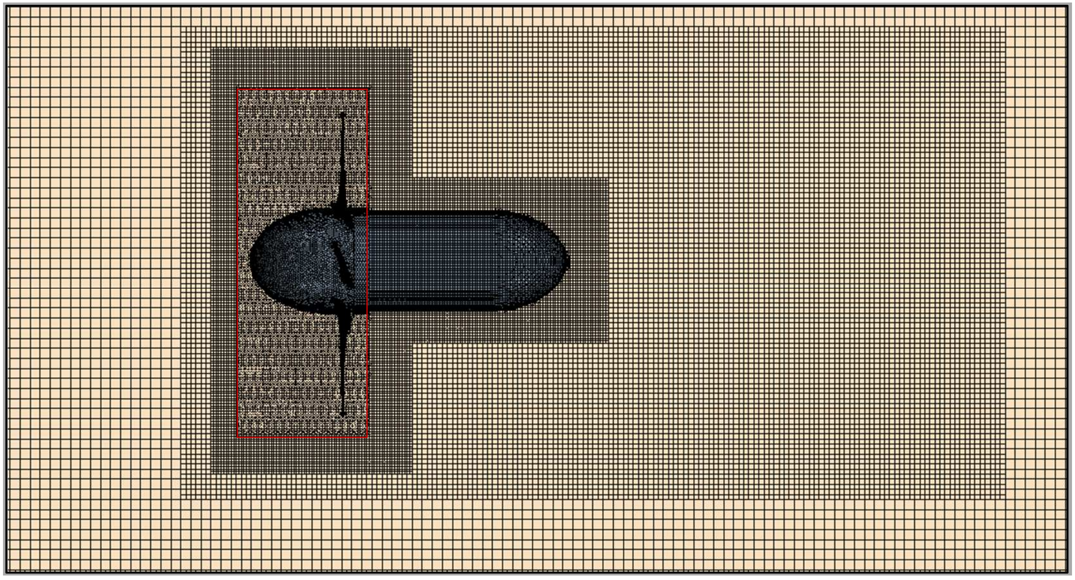

Figure 4-10: Inner grid – Rotating domain and interface with outer domain

4.3.2.1 Boundary conditions and width of the domain

The implementation of a parallelepiped domain raises the question of the conditions applied on the boundaries. The aim is to apply boundary conditions as representative of the reality as possible.

Naturally, the seabed and flow inlet boundaries are modelled by a wall and a velocity inlet respectively. The outlet of the parallelepiped is defined as a pressure outlet letting the flow free to run away without imposing any particular constraints. A simplified free surface is implemented in the model in a simplified way. The most relevant condition to simulate its presence is a symmetry plane. It enables the consideration of pressure variations encountered at the boundary.

The only surfaces on which various options exist are the domain side boundaries. As it is considered that the flow is free to propagate and evolve along the domain, the classical velocity inlet condition is no longer applicable as it would force the vertical velocity profile shape. The two remaining options are symmetry plane or pressure outlet.

This sub-section focuses on the analysis of the nature of the flow depending on the side boundary conditions. Both conditions were tested and the results compared. Key criterion is the relevance of the flow field. The Figure 4-11 presents the field velocity from an upper view for both conditions.

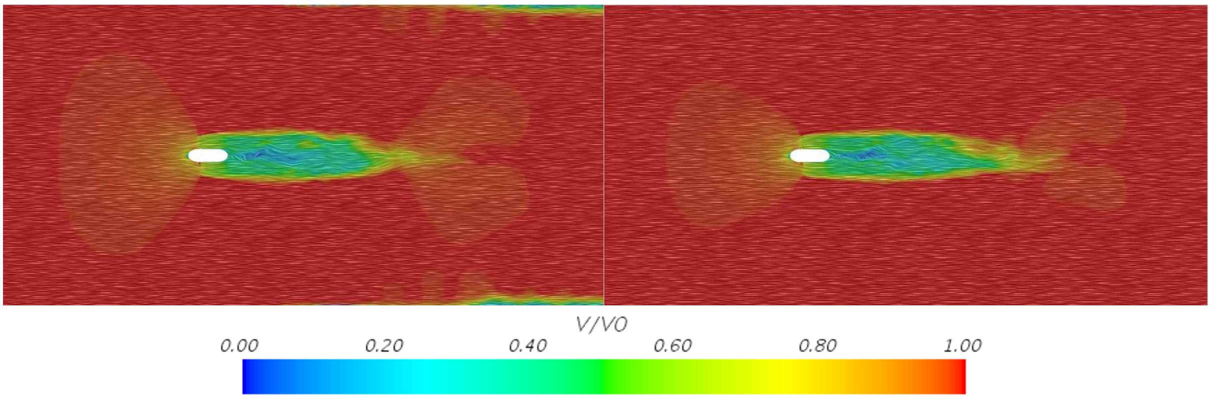

Figure 4-11: Velocity on the XZ plane (length x width) – Pressure outlet (left) vs. symmetry plane (right) applied on the sides

Comparison between models from the same upper view highlights that the change of boundary conditions on the side does not appear to influence the wake of the tidal turbine. However, a diffusion phenomenon occurs on the pressure outlet next to the end of the domain. This behaviour of the flow is unrealistic, such dead zone does not occur in the marine environment. Based on this observation, the symmetry plane type boundary is selected as it surely provide more trustworthy results.

According to the conclusions of the previous paragraph, side conditions can have an influence on the flow behaviour. The choice of the symmetry plane condition is only relevant if the calculation domain is large enough to avoid any interaction effects between the domain side limits and the flow disturbed by the turbine presence. A study is performed on the width of the domain in order to analyse the potential influence of the domain size on the turbine's performance and the flow. Two cases with different widths (92 m and 184m) are modelled. In these cases, the reference position z=0 is the turbine's rotation plane. A total of four probes are used to measure the velocity profile along the width at turbine rotation axis height, two located upstream of the tidal turbine (x=-60m (at inlet) and x=-10m) and two downstream (x=+20m and x=+30m). The resulting profiles are presented for the two domains in Figure 4-12 and Figure 4-13.

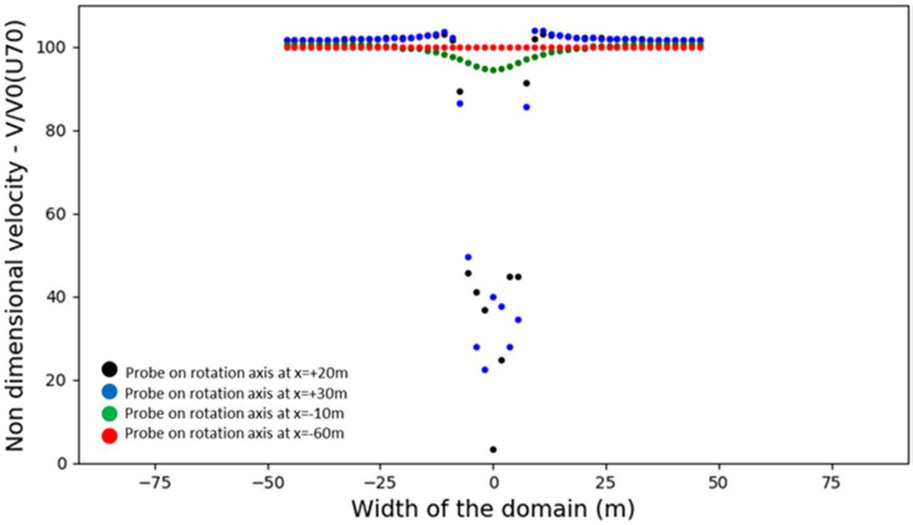

Figure 4-12: Velocity along the width of the domain – Width of 92m

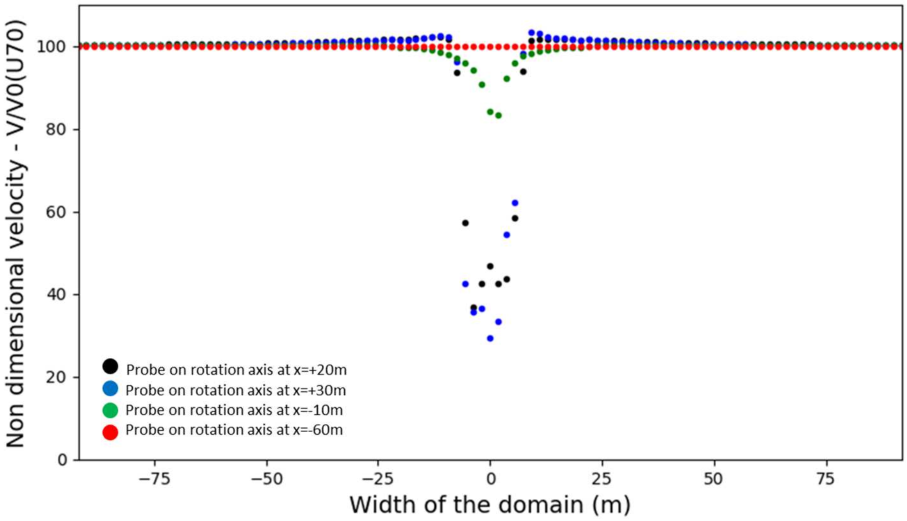

Figure 4-13: Velocity along the width of the domain – Width of 184m

The influence of the tidal turbine presence on the flow is obvious. The arriving flow is facing an obstructing effect leading to a located velocity drop – visible on the line probe x = -10m. Then, the effect of the wake generated can be seen on the line probes located downstream – x=20 and 30 m. It leads to a strong deceleration of the flow on the thirty meters width surrounding it. This effect remains visible quite far from the turbine as an important distance is necessary for this effect to disappear.

These plots enable to study influence of the dimensions on the velocity along the width. On Figure 4-12, velocity at the limits is slightly different depending on the x location. It highlights possible interaction effects at the sides. However, a converging trend is noticeable in the velocity value. It is confirmed with the Figure 4-13 illustrating the flow behaviour for the large domain of one hundred and eighty-four meters. Indeed, by setting a larger width, the distance is sufficient for the flow to reach back its far-field state at the side limits of the domain. Consequently, it will be selected rather than the domain of 92m width.

In addition to this analysis, the influence of this change of width dimensions on tidal turbine performance is studied. With identical settings on all other parameters, using a domain of 92m instead of 184m generates an error of 0.97% on the power coefficient.

4.3.2.2 Presentation of the model setup

Based on the analysis presented above, the larger domain with a width of 184 meters will be used to set up the new numerical model. The resulting domain and the associated boundary conditions are presented in Figure 4-14.

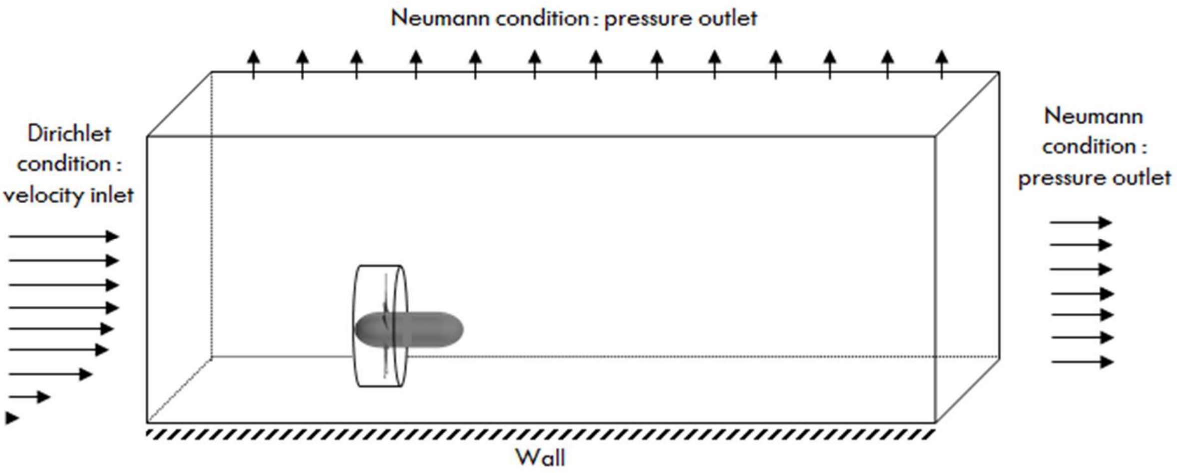
Neumann condition : pressure outlet
Dirichlet condition : velocity inlet
Neumann condition : pressure outlet
Wall

Figure 4-14: Presentation of the model using RBM method and integrating seabed

4.3.3 Integration of the turbine's structure

The last element mentioned in the introduction and still missing in the model is the turbine's structure. In reality, the turbine hub is positioned and maintained on the ground thanks to a structure stabilizing the tidal turbine. It avoids any unwanted motion due to tides or waves.

The turbine structure will influence the flow around the turbine, since it creates an obstruction close to the ground. The turbine loads and the resulting wake will therefore be modified. A new domain is created. It integrates the turbine's structure. It will be used to:

- Check the influence of the structure on the performance and flow behaviour by comparing it to the model without structure
- Run case studies later as it represents the most realistic model

The structure associated to the D12 turbine is presented at the beginning of the report in 2.3.1. The mesh of the domain has been adapted to ensure a good capture of the flow behaviour at its surroundings. It is presented in Figure 4-15 and Figure 4-16. The rest of the domain remain identical to the one presented at the end of 4.3.2.

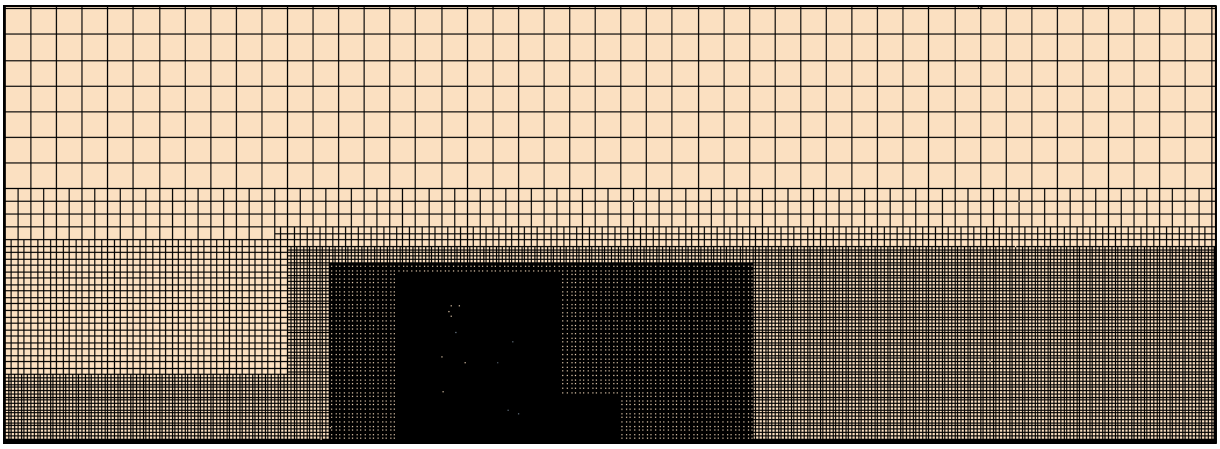

Figure 4-15: Outer grid – Domain with tripod integrated

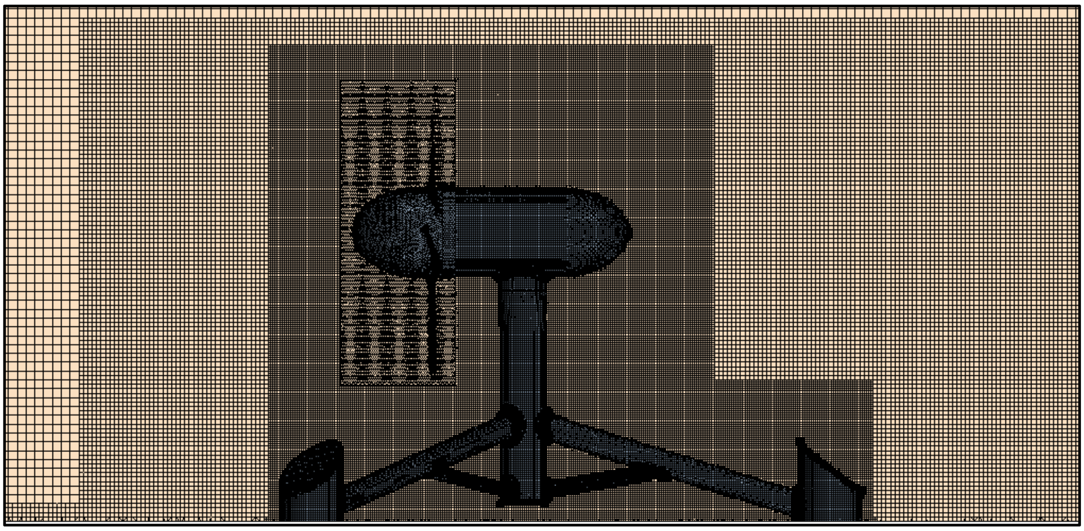

Figure 4-16: Inner grid – Domain with tripod integrated

4.4 Conclusion of the work carried out to integrate realistic conditions in the model

The work carried out in this section enabled to better understand the key numerical parameters required for a realistic model and will be of use for the case studies analysed in the next section.

The literature review increased the knowledge on the turbulence theory and modelling options. In parallel, the analysis of UEDIN data measured at Orkney helped to determine reference turbulence parameters such as turbulence length scale, velocity or intensity. These values will be used as inputs in the new model.

Finally, the iterative development of the complex model enabled to develop three models from an ideal cylinder including a full modelling of the turbine to a “Fromveur like” domain integrating both the turbine and its structure. These models will be used to quantify the influence of the different elements (vertical velocity profile, waves, structure) on the turbine behaviour and to conduct case studies on realistic environmental conditions encountered by the turbine.

5 INFLUENCE OF REALISTIC ENVIRONMENTAL CONDITIONS ON THE TIDAL TURBINE BEHAVIOUR

The work presented above enabled to develop blade resolved CFD models of the turbine based on a realistic domain. It can consider the seabed (and therefore vertical velocity profiles), reference turbulent inputs acquired by UEDIN and the turbine structure. The work presented in this section uses the three CFD models introduced above to:

- Quantify the influence of these parameters on the turbine loads and behaviour
- Analyse case studies encountered at sea by the turbine

The simulations will be carried out using D12 Sabella's turbine. It will enable a direct comparison between the results. However, it has to be noted that the models developed could be applied to any type/shape of horizontally rotating tidal turbines. The different case studies presented in this section were selected in discussion with Sabella. They are listed in Table 5-1.

Environmental conditions	Blade resolved CFD model	RANS Simulations	TSR and inflow velocity profile
Realistic current	Fromveur domain without turbine's structure	Influence of a vertical velocity profile on the turbine (with and without turbine's structure)	TSR = 4.5 U70
	Fromveur domain with turbine's structure		TSR = 4.5 U70 & U120
Waves with current	Cylindrical domain with turbine fully modelled	Influence of current oscillations on Sabella D12 tidal turbine	TSR = 4.5 U = 2.75m/s + Uwaves
	Fromveur domain with turbine's structure	Influence of current oscillations and vertical velocity profile coupled	TSR = 4.5 U = U70 + Uwaves
Critical operating condition	Fromveur domain with turbine's structure	Brutal shutdown of the turbine after freewheel rotation	TSR = 6 to TSR = 0 U120
Influence of the inflow incidence		Influence of current incidence angles on the turbine loads and performance	TSR = 4.5 U70 0°, + 10°, -10° (Ebb and flood tides)

Table 5-1: List of considered case studies

The various key parameters used in these simulations are introduced hereafter.

Warning: Due to modifications in the model setup between RBM cylindrical flume presented in 4.3.1 and the Fromveur like domain introduced in 4.3.2, a 2% uncertainty margin was estimated when comparing these models. This warning does not apply for comparisons between Fromveur models (cf. 4.3.2 or 4.3.3).

Vertical velocity profiles

The inflow velocity profiles U70 and U120 introduced in Figure 5-1 used in the simulations have been provided by Sabella. They are measured at the Fromveur straight, operating location of Sabella's turbine. These profiles represent tides with coefficients of 70 –mid-range tide – and 120 corresponding to strong tides. The velocity at the hub centre of the turbine called $V0$ for each of these profiles. V0(U70) is used as reference in this section with V0(U120) being equal to 1.43 V0(U70). The Figure 5-1 illustrates the speed profile associated these tidal coefficients reaching a maximum of 1.18 V0(U70) and 1.69 V0(U70) respectively at the surface.

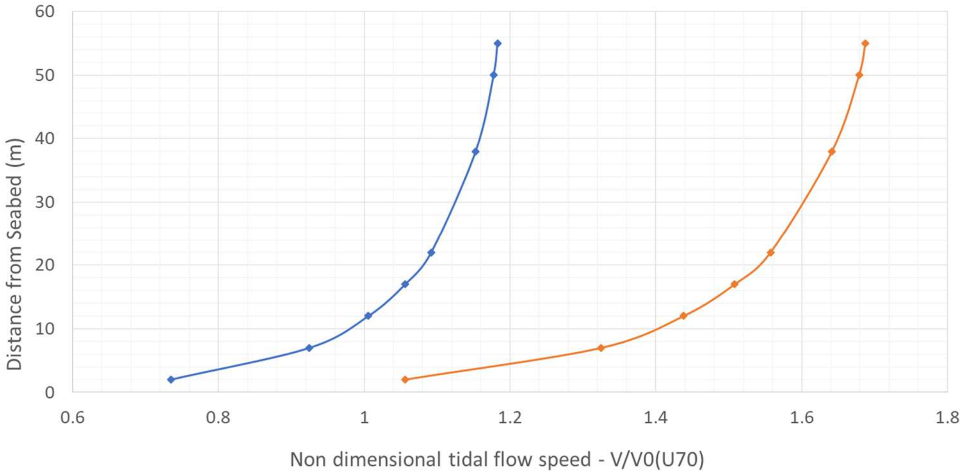

Figure 5-1: Speed profiles from different tidal coefficients

For these vertical velocity profiles, the operating point of the turbine – given by the TSR value – is calculated based on the current velocity measured at hub centre height (12.5m above seabed).

Oscillating current due to waves' influence

The consideration of waves is also important to complete the study of real flow conditions influence on the turbine. The wave condition considered in this section was discussed with Sabella. It represents a sea state corresponding to heavy weather occurring at Fromveur site with a wave height of Hs (not provided for confidentiality purposes) and a period Tp of 12.8 seconds.

The absence of free surface in the model creates the need to find an alternative method to integrate wave effects on the inflow. It is done by applying a temporal oscillation on the current imposed at the inlet. The amplitude and period of this oscillation is established by considering the horizontal component of the orbital motions of the fluid particles induced by the waves. The equations taken into account for this horizontal orbital velocity are based on the linear wave theory (Airy type) in finite depth. It is described hereafter:

$$U_{x-wave}(z,t) = \omega \left(\frac{H_S}{2}\right) \frac{\cosh(k(z+d))}{\sinh(kd)} \sin(\omega t)$$

With ω the wave circular frequency, k the wave number, d the depth and z the vertical position considered.

In the case where the cylindrical "ideal" domain is used for reference calculations, the influence of the vertical position on this formulation is neglected. It leads to the simplified equation presented below:

$$U_{x-wave}(t) = \omega \left(\frac{H_s}{2}\right) \sin(\omega t)$$

This method enables a straight forward coupling of current and waves. The oscillating horizontal orbital velocity due to wave is simply added to the current profile.

$$U_{total}(z,t) = U_{infinity}(z) + U_{x-wave}(z,t)$$

However, the drawback of this method is that neither the spatial velocity variations nor the vertical orbital velocity components of the waves are considered in the model. An improvement of this aspect could be an improvement of the model. This topic will be developed further when presenting the future work perspectives.

Turbulence parameters

The literature review carried out on turbulence and its modelling in CFD enabled to get a better understanding of the physical phenomenon involved in a turbulent flow. Various methods exist to model it with different levels of accuracy. The most relevant method would be the Detached Eddy Simulations (DES) as it offers a very good resolution of turbulence parameters. The literature review enabled to get familiar with it theory and the necessary turbulent inputs required for its use. However, it would require further development of the model which was not the direct priority. Its use will be discussed in the future work perspectives.

For the calculations carried out in this project, RANS method is used. It represents the most commonly used method and does consider the turbulence. A turbulence intensity of 10% is set for the tidal currents simulated hereafter. The other turbulence parameters needed for simulations settings are also set to their reference values, namely 25m for the turbulence length scale and 0.275m/s for the velocity scale. These values correspond to the reference values introduced by the turbulence study carried out on UEDIN datasets from Orkney (UK) presented in 4.2.

Blade sections for more refined load decomposition on the blades

This part of the work focuses on the analysis of the realistic environmental conditions influence on the turbine. A specific interest is given to the way the velocity profile influences the loads distribution along the blade. For this stake, each blade is split into different parts. Figure 5-2 illustrates the 6 sections on D12 blade.

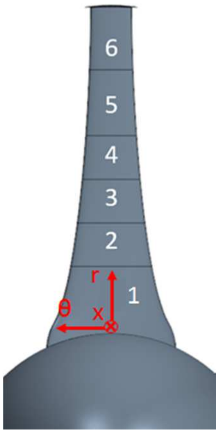

Figure 5-2: Blade sections and reference coordinate system at blade root

For each section, forces and moments are assessed from a coordinate system located at the blade root. The X-axis of the coordinate system goes in the direction of the inflow.

Non dimensional loads and performance coefficients

For confidentiality purposes, no real loads or performance coefficients values are presented in this section.

As previously introduced in the simplified model section (cf. 3.4), choice has been made for power coefficient figures to present the results as a percentage of the highest value achieved in the considered datasets.

$$Cp\ (\%) \ = \frac{Cp}{Cp\_max}$$

Similar method has been used for axial, tangential and radial load figures. However, it is important to enable a direct comparison between the three components of the load. As such, for a given case all three load components are made non-dimensional with respect to the maximum value of the axial loads.

$$Load\ (\%) \ = \frac{Load}{AxialLoad\_max}$$

The maximum value corresponds to the maximum value obtained on the considered data sample.

5.1.1 Influence of a vertical velocity profile on the turbine without structure

Using the model developed in 4.3.2, a simulation is performed with U70 vertical velocity profile imposed at the inlet. This calculation is run in order to analyse the turbine loads obtained with a realistic profile inflow. Because of the vertical velocity profile, blades are not subjected to the same inflow velocity depending on their positions during rotation.

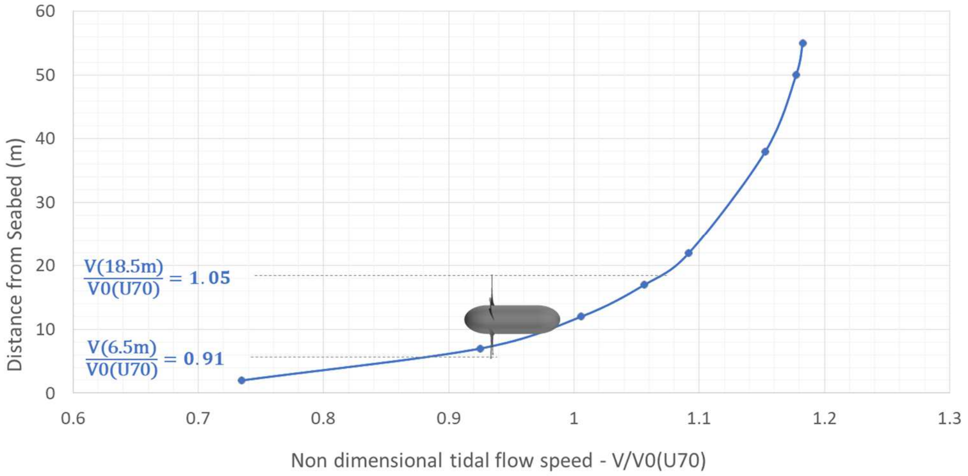

Figure 5-3: U70 inflow - Difference of velocity on the rotational plane induced by the current front

Figure 5-3 illustrates the 14% difference in inflow velocity perceived by the blade tip depending on its position. The rotation of the blade is chosen to be a constant value providing the theoretical highest rotational power (i.e. ωM_x). Based on the performance assessment of the D12 tidal turbine this is reached for a TSR of 4.5.

A simulation with a uniform inflow at velocity $V0$ of U70 profile was performed. It is presented in 4.3.1.2. It is found that the power performance of the turbine is very similar in both cases. Performance coefficient values of this case are summarized in Table 5-2.

Geometry	Inflow	Cp	Ct	Cq
Turbine alone	U70	Ref.	Ref.	Ref.

Table 5-2: U70 inflow - Turbine alone - Power coefficients

It is explained by the shape of the vertical velocity profile. The reduction of velocity at the bottom of the turbine's disk is compensated by the increase at the top. As such, the mean theoretical flow rate arriving on the turbine disk is very similar.

This first analysis tends to validate the choice of uniform simplified model to conduct preliminary assessment of turbine performance as it provides relevant results at lower computational cost.

The vertical velocity profile generates a non-constant inflow on the blades as the turbine rotates. This phenomenon has a direct influence on the angle of attack and therefore on the forces applying on the blade. It induces time varying loads on the structure depending on the blade position. The axial force is maximal when the blade is on the top of its rotation and minimal when the blade is at the bottom of its rotation. They are presented in Figure 5-4. They oscillate from about 88% to 100%. A phase shift of a fifth of the blade rotation period between the blade force curves is also noticeable. The same phase shift is observed on the tangential and radial forces presented in Figure 5-5 and Figure 5-6. These plots show the time history of the tangential and radial forces applied of the turbine blades during a turbine rotation. The sinusoidal evolution of tangential forces covers a range from 80 to 100%. As axial forces, a maximum is reached when the blade is at the top of its rotation. Value of the radial component of forces applied on the blade is an effect of the centrifugal force induced by the rotation. These forces remain negligible with regard to the tangential forces values. However, due to an overpressure created by the seabed, a slight oscillation occurs.

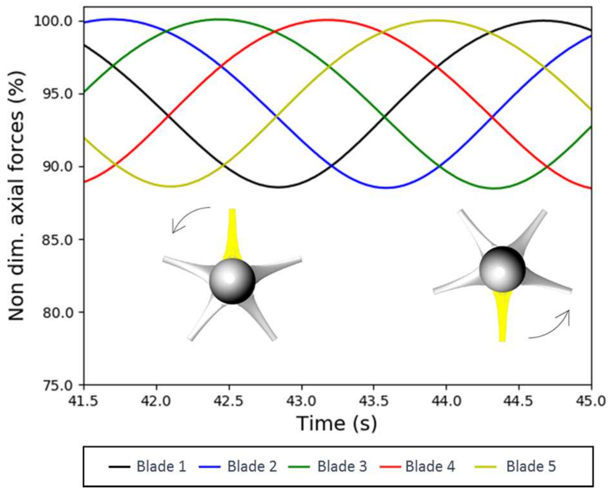

Figure 5-4: U70 inflow – Turbine alone – Axial forces acting on blades

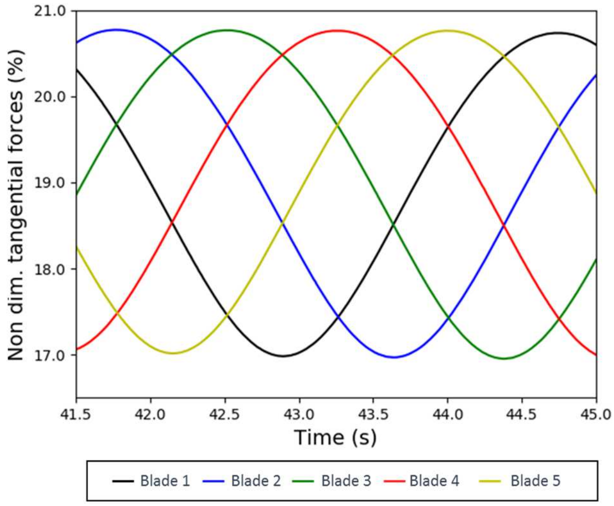

Figure 5-5: U70 inflow – Turbine alone – Tangential forces acting on the blades

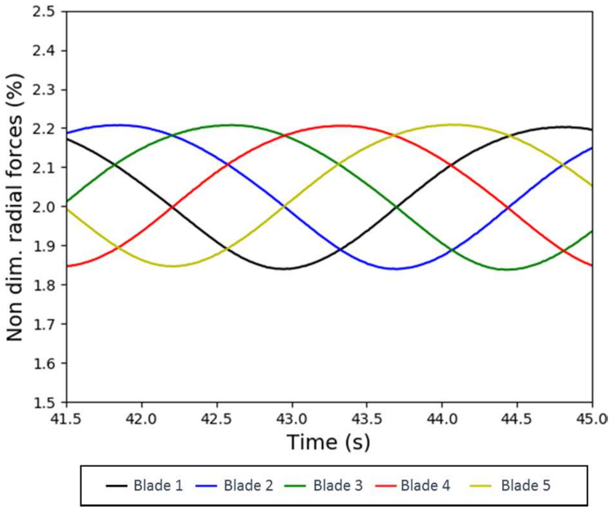

Figure 5-6: U70 inflow - Turbine alone - Radial forces acting on the blade

Main characteristics of loads acting on the tidal turbine blades are summarized in Table 5-3.

Geometry	Inflow	Load type	Mean (kN)	Max. (kN)	Min. (kN)
Turbine alone	U70	Axial	-4.90%	Ref.	-11.48%
		Tangential	-7.81%	Ref.	-20.89%
		Radial	-5.71%	Ref.	-16.19%

Table 5-3: U70 inflow - Turbine alone - Blade loads summary

In parallel, the pressure loads are also monitored for each sections of the blade (cf. Figure 5-2). Figure 5-7 shows the six corresponding curves over a period of rotation on one blade. The difference of rotation speed depending on the radius position explains the profile of the curves. It generates an increasing pressure load as the section get closer to blade tip. Oscillations are also visible on the loads. As the section get further from the rotor it is exposed to a stronger velocity variation during its rotation, it induces a higher oscillation amplitude.

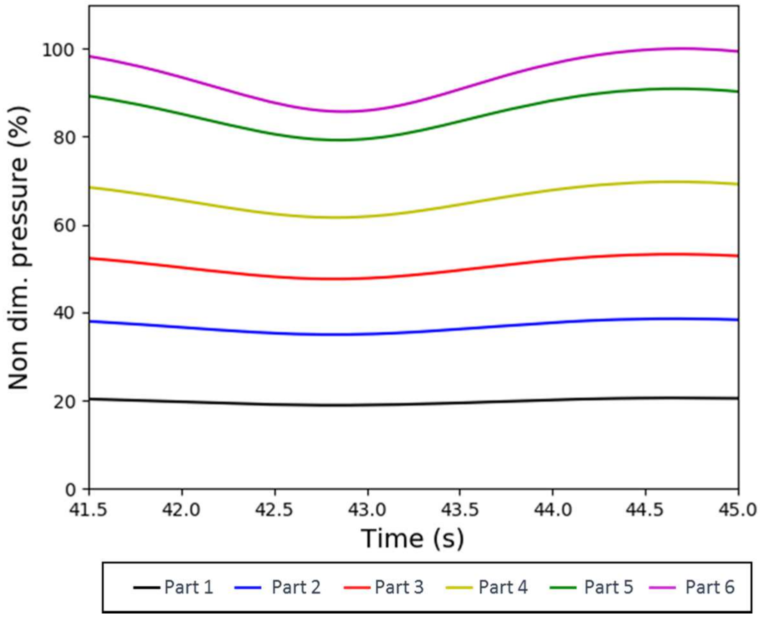

Figure 5-7: U70 inflow – Turbine alone – Pressure loads applied on the blade sections depending on the time

Speed profile implementation influences the flow behaviour around the turbine and the resulting wake. Figure 5-8 presents the velocity field through the dimensionless criterion V/V0. A significant velocity drop occurs in the wake of the turbine, these velocity drops are consequences of flow disturbance created by the structure. Moreover, part of the upstream flow runs around the turbine and is directed between the seabed and the turbine. At the end of the wake, this flow is redirected above the boundary layer generated by the seabed.

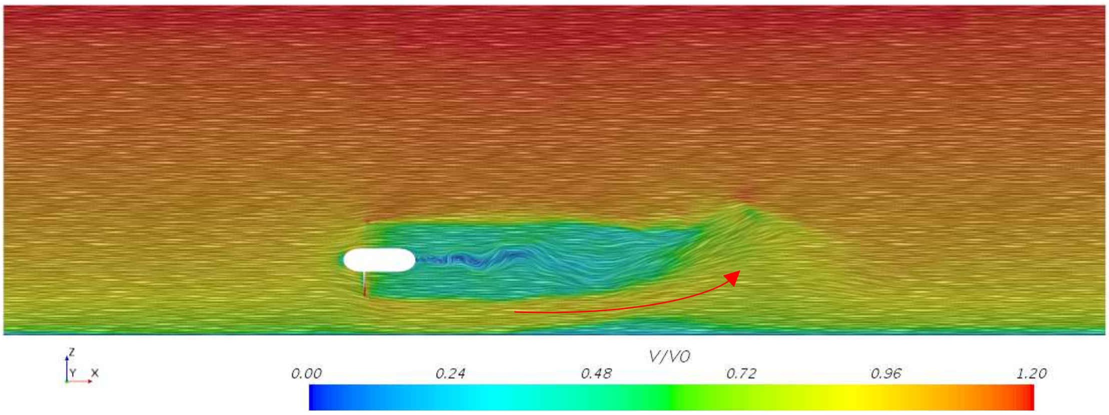

Figure 5-8: U70 inflow – Turbine inflow – Dimensionless velocity along the length of the domain

5.1.2 Influence of the turbine's structure

In real operating conditions, the Sabella D12 structure affects the flow behaviour near the turbine and have an influence on the forces applied on the turbine blades. Consequently, this influences the tidal turbine performance.

A calculation was carried out using identical simulation settings to the ones used for previous calculation except the domain which now integrates the turbine's structure. This domain was introduced in 4.3.3. The obtained results are presented hereafter. Both velocity field and turbine loads are discussed.

Figure 5-9, Figure 5-10 and Figure 5-11 present the resulting blade loads over a period of rotation. As expected, the oscillations observed on the blade loads in 5.1.1 are still noticed. However, the amplitude of these oscillations is wider (cf. Table 5-4). The shape of the oscillations is also different. It is no longer sinusoidal, and a marked decrease is visible very locally, synonym of the interaction between the turbine and its structure when the blade reaches the bottom of its course.

These differences are explained by the obstructing effect created by the turbine structure. It locally modifies the flow field in the rotating plane. Such effect has a direct consequence on the angle of attack and thus on the distribution of the efforts acting on the blades. Forces acting at the bottom of the rotating plane decrease while forces acting at the top of the rotating plane increase.

Main characteristics of loads acting on the tidal turbines blades are summarized in Table 5-4. They are compared to loads acting on turbine without structure.

Geometry	Inflow	Load type	Mean (kN)	Max. (kN)	Min. (kN)
Turbine alone	U70	Axial	Ref.	Ref.	Ref.
		Tangential	Ref.	Ref.	Ref.
		Radial	Ref.	Ref.	Ref.
Turbine with structure		Axial	+0.80%	+1.70%	-4.94%
		Tangential	+0.84%	+2.59%	-5.51%
		Radial	-1.31%	+2.82%	-14.88%

Table 5-4: U70 inflow – Turbine with structure – Blade loads summary

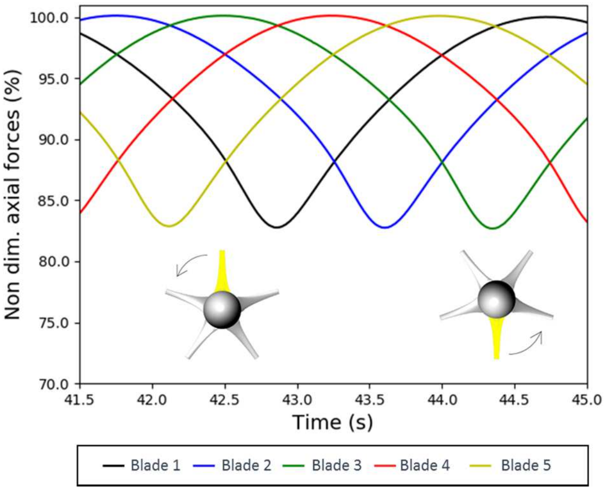

Figure 5-9: U70 inflow – Turbine with structure – Axial forces acting on the blades

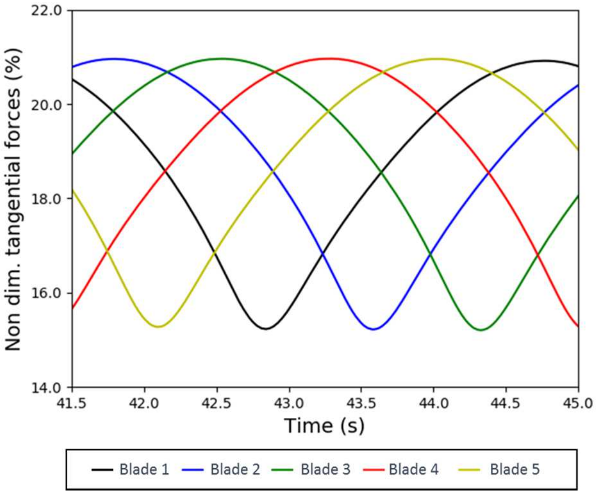

Figure 5-10: U70 inflow – Turbine with structure – Tangential forces acting on the blades

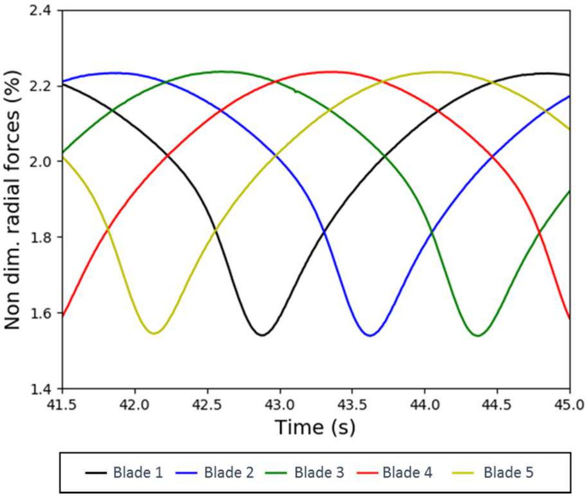

Figure 5-11: U70 inflow – Turbine with structure – Radial forces acting on the blades

The hydrodynamic phenomenon noticed has a direct influence on the power coefficient. It induces time dependent oscillations as the loads are not sinusoidal anymore. Therefore, the mean value is not constant. It is illustrated in Figure 5-12 over one turbine rotation. As observed in the load curves, the oscillation frequency corresponds to 1/5th of rotation period showing the direct link with the number of blades. Moreover, the power coefficient value reached is slightly above the one without structure. In overall, the integration of the structure leads to a 0.78% augmentation on its mean value.

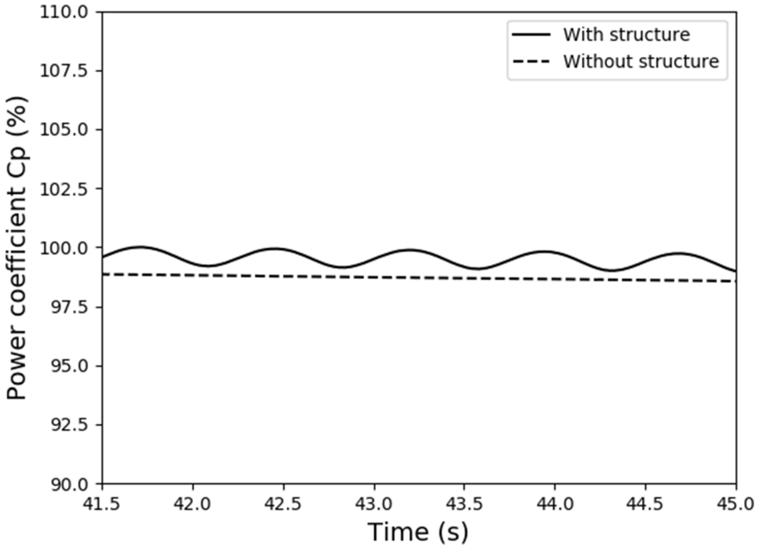

Figure 5-12: U70 inflow – Turbine with structure vs. Turbine alone – Cp over one period of rotation

Performance coefficients obtained for this case are presented in Table 5-5. They are compared to U70 results.

Geometry	Inflow	Cp	Ct	Cq
Turbine alone	U70	Ref.	Ref.	Ref.
Turbine with structure		+0.78%	+0.78%	+0.71%

Table 5-5: U70 inflow - Turbine with structure vs. turbine alone - Power coefficients

Figure 5-13 and Figure 5-14 present the velocity field around the tidal turbine through the dimensionless criterion V/V0.

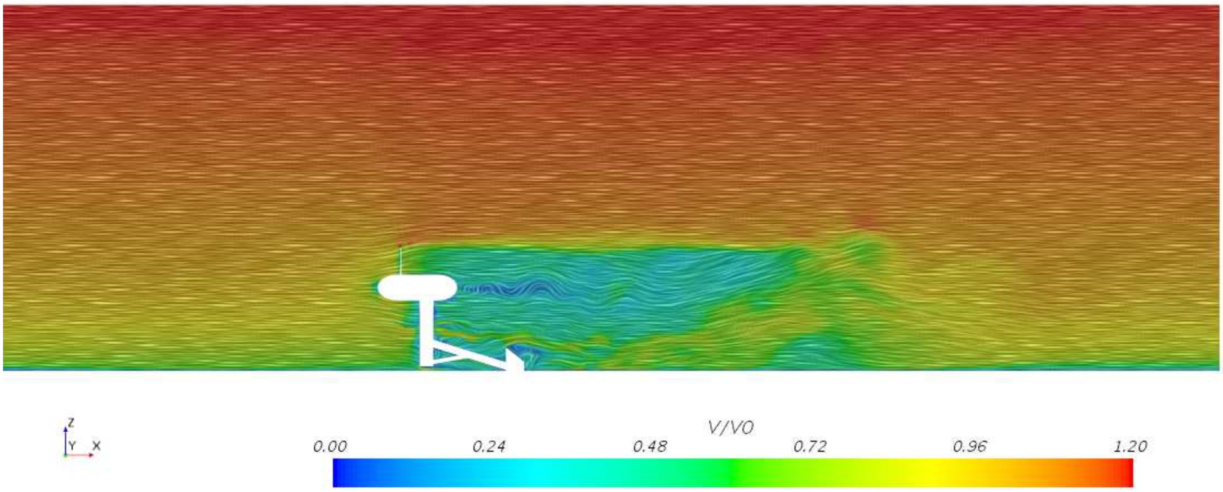

Figure 5-13: U70 inflow - Turbine with structure - Velocity field from a long distance view

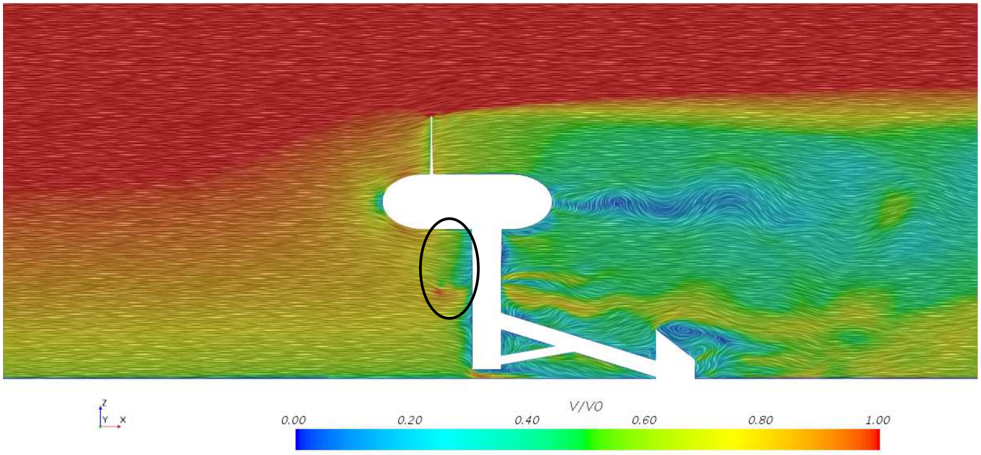

Figure 5-14: U70 inflow - Turbine with structure - Velocity field from a close view

Some strong differences with the wake generated by the turbine alone (cf. Figure 5-8) result from the integration of the structure. As introduced, Figure 5-14 displays the blockage effect induced by the mast which influences the rotating plane. Moreover, some flow separations occur downstream due to the structure especially around cylinders of tripod's legs (cf. 2.3.1) generating a blockage effect on a part of the flow next to the seabed. It generates additional wake downstream leading to a wider turbine wake in overall.

5.1.3 Comparison of influence of two speed profiles

A simulation is performed with U120 vertical velocity profile previously introduced imposed at the inlet. The calculation is run on the turbine with its structure using the Fromveur model introduced in 4.3.3. It will be of use to analyse the influence of a stronger tide current on the turbine. Figure 5-15 illustrates the differences between the two velocity profiles. The obtained results are presented hereafter. Both velocity field and turbine loads will be discussed. The U120 results are compared to U70 results.

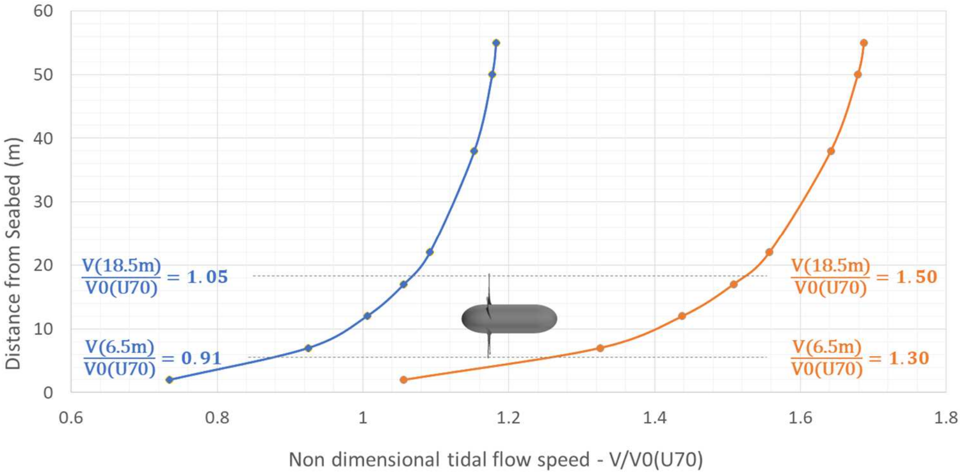

Figure 5-15: U70 vs. U120 inflow – Difference of velocity on the limits of the rotation plane

Figure 5-16, Figure 5-17 and Figure 5-18 compare axial, tangential and radial forces acting on blades during a full rotation for two different speed profiles. For each speed profile, the load oscillation and the influence of the turbine's structure is visible. As it was predictable, the forces applied on the blades are higher when facing U120 current. However, it has to be noted that these loads are higher by a factor two which is quite important with regard to the velocity difference.

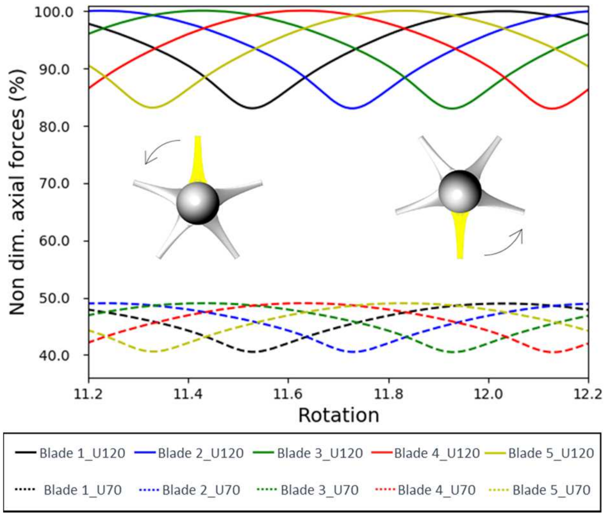

Figure 5-16: Turbine with structure – U70 vs. U120 inflow - Axial forces acting on the blades

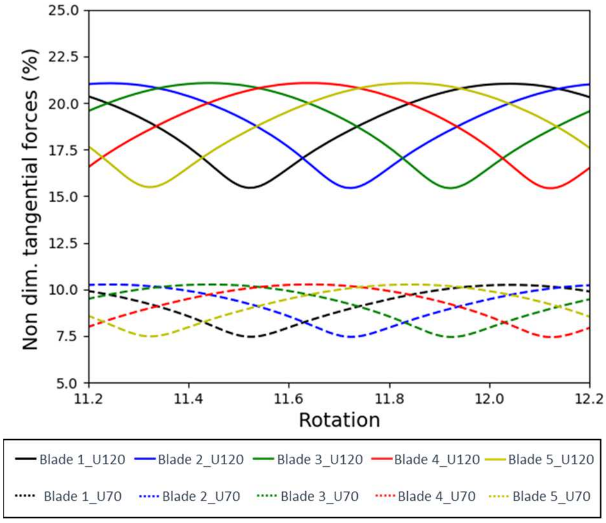

Figure 5-17: Turbine with structure – U70 vs. U120 inflow- Tangential forces acting on the blades

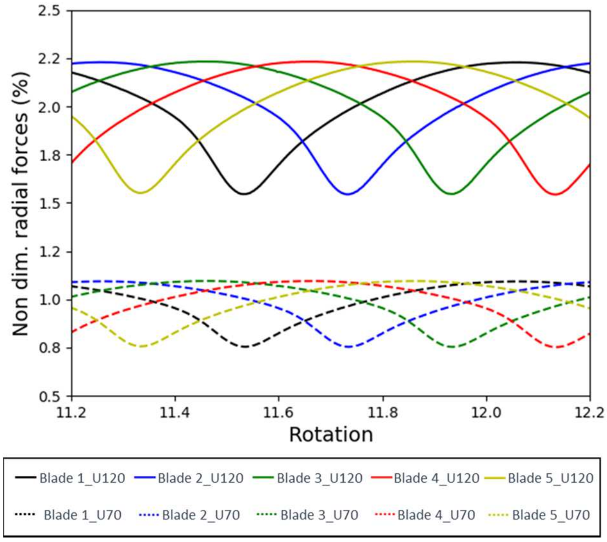

Figure 5-18: Turbine with structure – U70 vs. U120 inflow- Radial forces acting on the blades

Main characteristics of loads acting on the tidal turbine blades at different inflows are summarized in Table 5-6.

Geometry	Inflow	Load type	Mean (kN)	Max. (kN)	Min. (kN)
Turbine with structure	U70	Axial	Ref.	Ref.	Ref.
		Tangential	Ref.	Ref.	Ref.
		Radial	Ref.	Ref.	Ref.
	U120	Axial	+104.47%	+104.20%	+104.91%
		Tangential	+105.29%	+105.29%	+107.13%
		Radial	+104.25%	+103.85%	+104.90%

Table 5-6: U70 vs. U120 inflow - Turbine with structure – Loads comparison between both inflows

These load differences make the power coefficient increase by 1.08% at equal TSR value. This is most likely due to the slight difference of Reynolds number between the two cases. Comparison through performance coefficient values between the two cases is displayed in Table 5-7.

Geometry	Inflow	Cp	Ct	Cq
Turbine with structure	U70	Ref.	Ref.	Ref.
	U120	+1.08%	+0.14%	+1.08%

Table 5-7: U70 and U120 inflow - Turbine with structure – Performance coefficient comparison

A stronger tide current quite naturally influences the flow behaviour downstream the structure. Figure 5-19 highlights the disparities in the velocity fields around the turbine with the dimensionless criterion V/V0 – V0 being the theoretical current velocity at hub centre. According to these figures, the wake for a speed profile corresponding to a 120 tidal coefficient is more disturbed with a flow separation zone behind the rotor longer and stronger at the hub level.

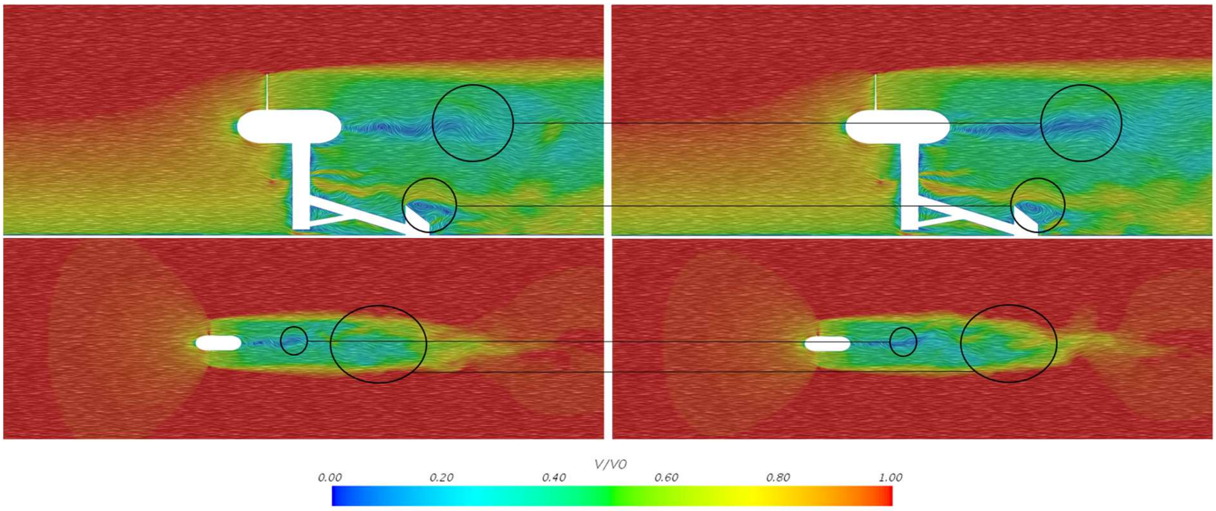

Figure 5-19: Velocity field on turbine rotation axis – U70 (left) vs. U120 (right) – Side view on top and top view at bottom

5.2 Influence of oscillating inflow due to waves

Realistic vertical velocity profile inflow was implemented. The next necessary step to get closer to environmental conditions is the integration of horizontal orbital velocity induced by waves on the current. The theory used behind the work presented here is introduced in 5.

In the first place, a preliminary study is carried out using the ideal cylinder domain introduced in 4.3.1 with a simplified oscillating inflow. It enables to get a better understanding of the physics involved. Then, the influence of vertical velocity profile coupled with horizontal orbital velocity induced by waves is studied on the turbine modelled with its structure (cf. model introduced in 4.3.3).

5.2.1 Preliminary study on ideal cylinder

The simplified domain used hereafter enables to visualize the influence of the oscillating velocity inflow. It is set to:

$$U_{total}(t) = U_{infinity} + U_{x-waves}(t) = 2.75 + \omega\left(\frac{H_s}{2}\right)\sin(\omega t)$$

The rotation speed of the turbine is defined based on a TSR value of 4.5 using the mean value of the inflow velocity at the turbine hub.

The current oscillations induce a time varying TSR value as the turbine's rotation is kept constant. It leads to an oscillation of the angle of attack, generating a time varying performance coefficient. Figure 5-20 illustrates both the variation of TSR and Cp values over time. A fall of power coefficient is observed when the TSR reaches its maximum value.

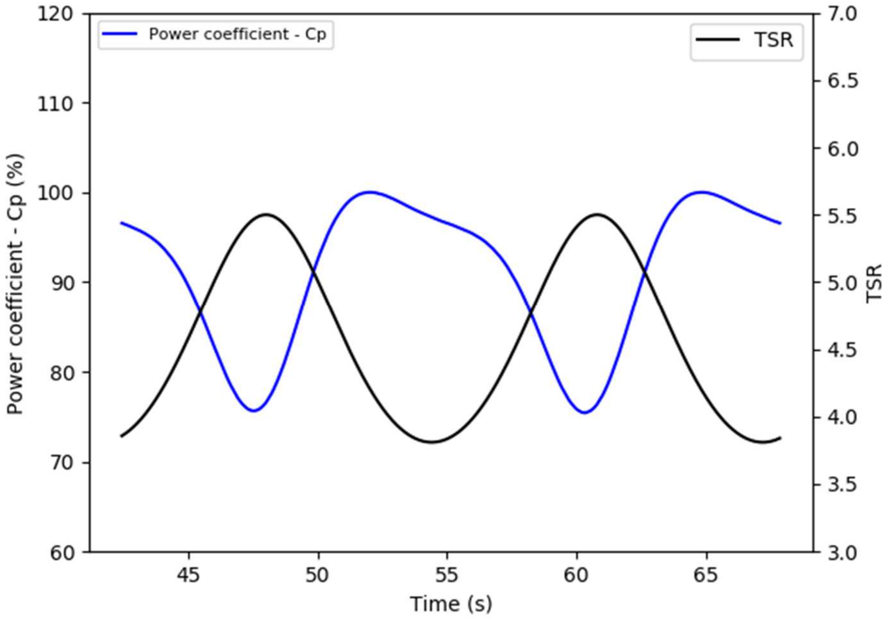

Figure 5-20: Ideal cylinder – Oscillating inflow - Temporal evolution of power coefficient and TSR

Plotting the power coefficient depending on the TSR enables to complete study of the graph above. Figure 5-21 shows the evolution of power coefficient depending on the TSR. The hysteresis cycle emphasizes the importance of flow velocity history in the relation between the power coefficient and the TSR.

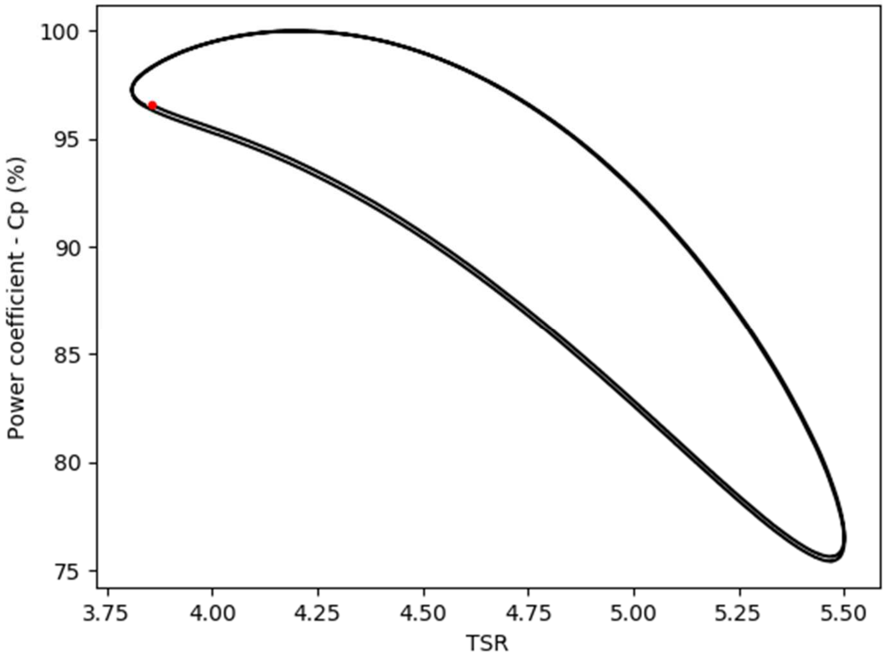

Figure 5-21: Ideal cylinder – Oscillating inflow - Power coefficient evolution depending on the TSR

At the time spotted by the red point, flow velocity is near its maximal value with a low value of TSR. At this given moment, a flow separation appears around the blade. As the inflow velocity decreases, the boundary layer separation induced by the stall phenomenon vanishes, it is the "*linkage phase*". At minimal velocity, the highest value of TSR is reached the angle of attack is small and the flow around the blade is attached. A new increase of the velocity re-induces the stall phenomenon with as the TSR decrease, it is the "*stall phase*". This sequence goes on and on.

However, the transition from one phase to the next one is not immediate as the new hydrodynamic state has reached stability. It takes additional energy to "break" it which induces a time lag between the inflow speed value and the associated hydrodynamics around the blade.

This preliminary analysis carried out with a simplified inflow enabled to better understand the hydrodynamics involved when tidal turbines are facing oscillating current due to waves. The next step is the coupling of a realistic vertical velocity profile with the oscillating horizontal orbital velocity induced by the waves.

5.2.2 Waves and U70 coupled

The study of an ideal case enabled to understand the hydrodynamics involved when a uniform time varying inflow is arriving at the turbine. The hysteresis cycle showed the importance of the flow history on the turbine's performances. The objective is now to couple the vertical velocity profile U70 with a horizontal time varying velocity component due to waves. This component is also dependent on the water depth according to the linear wave theory (Airy wave). The resulting inflow is summarized hereafter. Key wave parameters are presented in the introduction of 5

$$U_{total}(z,t) = U70(z) + U_{x-wave}(z,t)$$

$$U_{x-wave}(z,t) = \omega \begin{pmatrix} H_s \\ 2 \end{pmatrix} \frac{\cosh(k(z+d))}{\sinh(kd)} \sin(\omega t)$$

The variation of the wave horizontal velocity amplitude with the depth is illustrated in Figure 5-22. Its coupling with U70 velocity profile gives an envelope for the time varying inflow imposed at the domain inlet. It is presented in Figure 5-23 along with U70 for direct visual comparison.

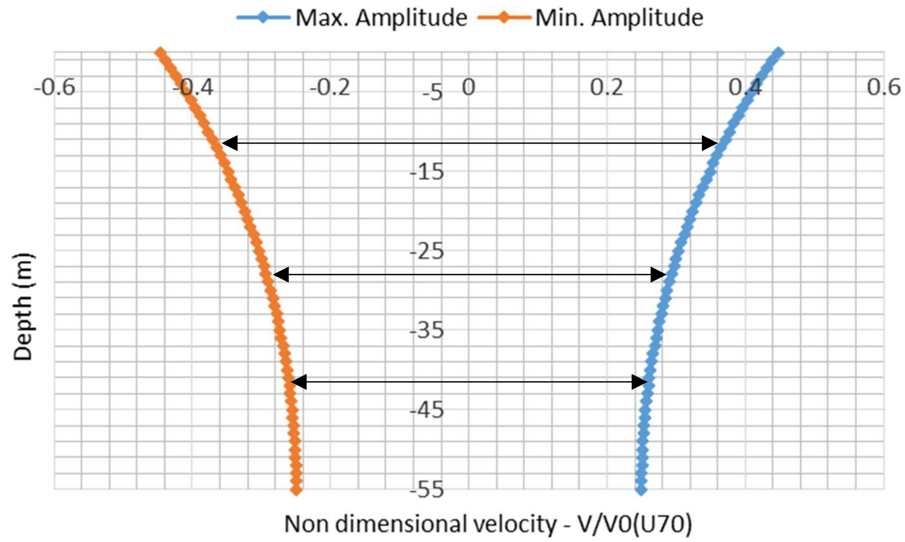

Figure 5-22: Variation of the wave horizontal velocity with the depth

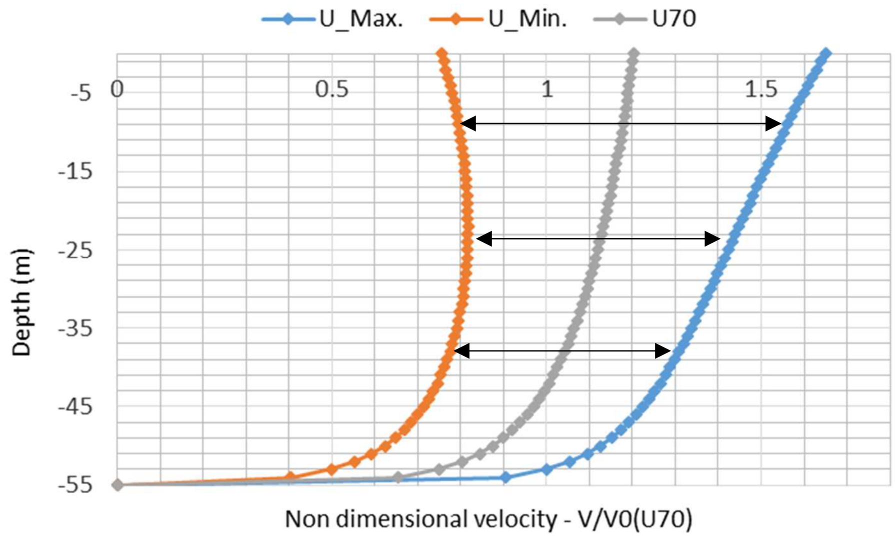

Figure 5-23: Envelope of the time varying horizontal inflow based on U70 velocity profile

The rotation speed of the turbine is defined based on a TSR value of 4.5 using the mean value of the inflow velocity at the turbine hub. It corresponds to V0 value for U70 velocity profile. It has to be noted that the velocity profiles presented above are theoretical profiles imposed at the inlet. The linear wave theory used does not account for viscous effect at the seabed. Before reaching the turbine, the inflow propagates along the domain and its shape is modified due to seabed. Therefore, the profile coming at the turbine is slightly modified compared to the theoretical inputs presented above.

The time varying reference velocity arriving at the turbine is monitored on the hub rotation axis, 20 meters ahead of the turbine. Its evolution over time is illustrated in Figure 5-24. This oscillating value V0 is used as reference velocity for TSR calculations and velocity field representations.

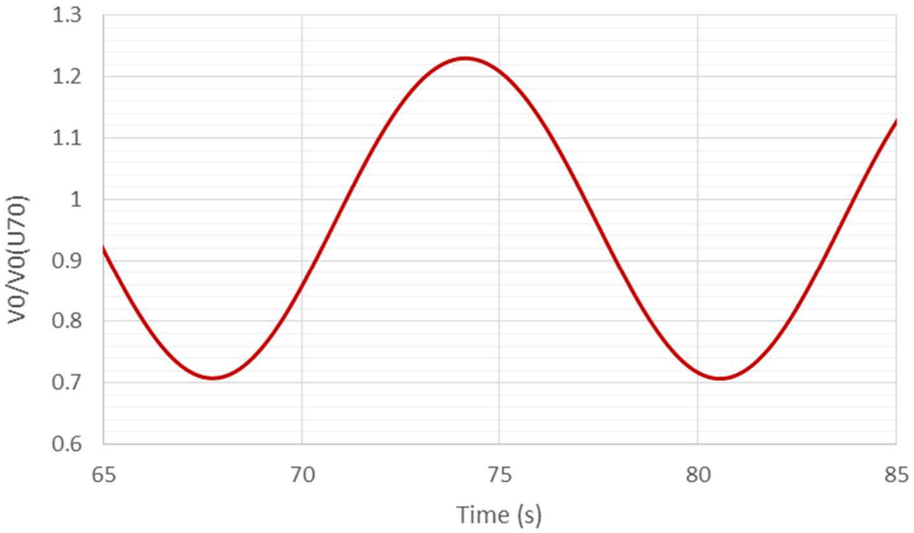

Figure 5-24: Turbine with structure – U70 oscillating inflow – V0 measured at hub level 20 m ahead of the turbine used as reference in the following analysis

The current oscillations induce a time varying TSR value as the turbine's rotation is kept constant. It leads to an oscillation of the angle of attack generating a time varying performance coefficient. Figure 5-25 illustrates both the variation of TSR and Cp values over time. A similar curve trend to what was obtained in the ideal scenario is observed.

A fall of power coefficient is observed when the TSR reaches its maximum value. In the other hand, as TSR reaches values oscillating between 3.6 and 4.8, a stable zone of high power coefficient is observed. It is highlighted in red on the figure. In this segment, oscillations induced by the coupled effect of turbine's structure and vertical velocity profile on the power coefficient are visible. It was already observed in 5.1.2. The strong variations the Cp value tend to mask them on the rest of the curve even if they are obviously still present (cf. load figures hereafter). The stability range noticed on the power coefficient is quite representative of the importance of the flow history. The variation of TSR induce modification of the hydrodynamics around the blade leading to successive apparition/vanishing of flow separations. However, energy is needed to trigger a transition from one state to the other. It leads to these "stable" segments of high power coefficient. Moreover, transition from high to low TSR values happens faster than transition from low to high TSR which tends to increase the low TSR stability zone.

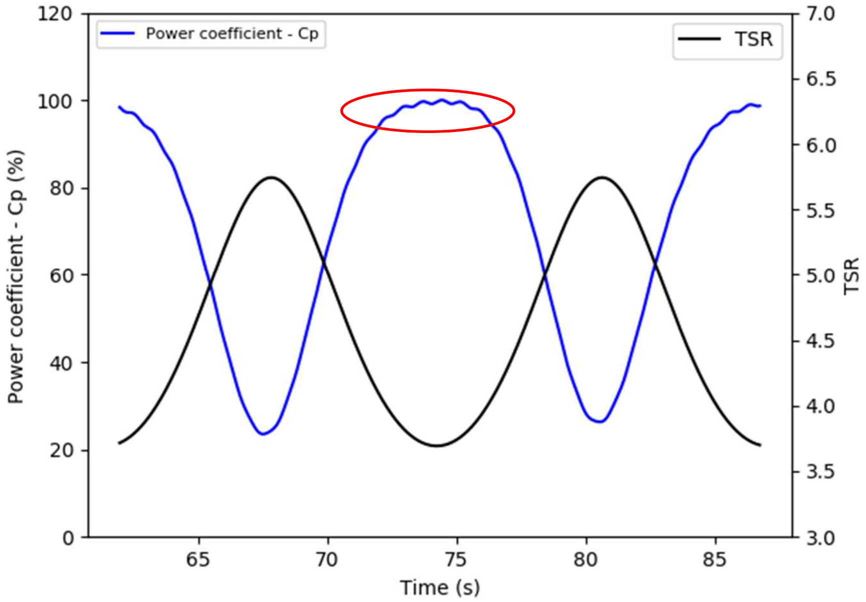

Figure 5-25: Turbine with structure – U70 oscillating inflow - Temporal evolution of power coefficient and TSR

The axial, tangential and radial loads are presented in Figure 5-26, Figure 5-27 and Figure 5-28. Two key variations are visible on the graphs. The first one was observed in the study of the turbine's structure influence. It corresponds to the oscillations due to the rotor rotation facing a vertical velocity profile and subject to the structure influence. The oscillation has a 1/5th of turbine rotation period in phase with the number of blades on the rotor. The second variations is the one of interest in this section. It corresponds to the wave influence on the turbine loads. It leads to an envelope of the loads strongly oscillating with a period corresponding to the implemented wave period. The varying inflow speed generates strong variation of the angle of attack on the blades. It induces strong load variations. Moreover, it induces a time varying pressure field in the domain. The radial loads are influenced by this pressure field. It generates a positive to negative oscillation around a mean value observed in 5.1.2. One has to keep in mind when looking at these loads that the blade surface used for calculation is open at the blade root which induces a bias in the analysis of the radial loads.

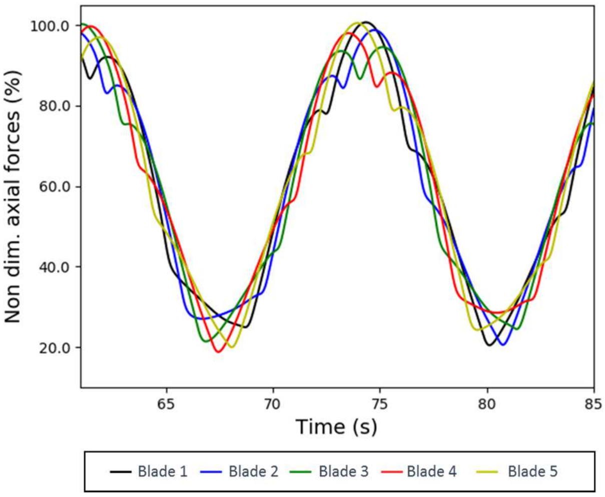

Figure 5-26: Turbine with structure – U70 oscillating inflow – Axial loads acting on the blades

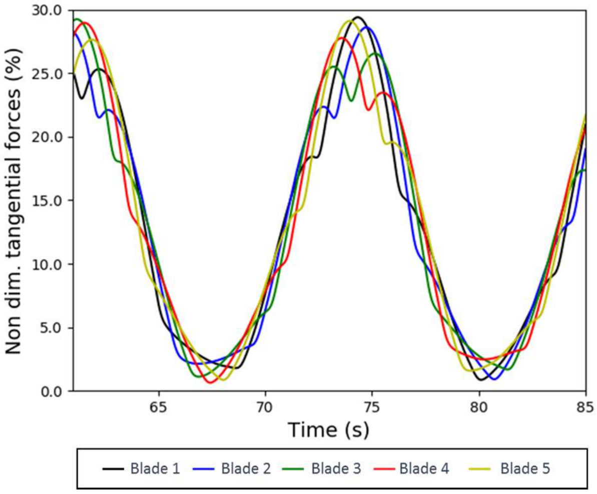

Figure 5-27: Turbine with structure – U70 oscillating inflow – Tangential loads acting on the blades

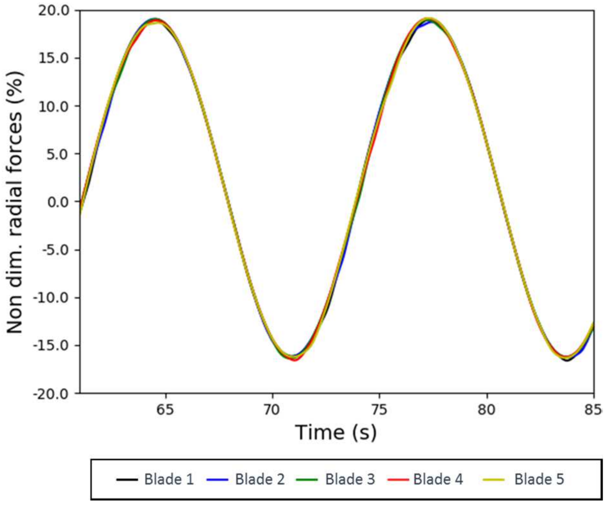

Figure 5-28: Turbine with structure – U70 oscillating inflow – Radial loads acting on the blades

The velocity field is also greatly modified over time due to the oscillating inflow. Depending on the TSR, the wake is either very smooth or can be very turbulent as it is illustrated in Figure 5-29 and Figure 5-30. It reflects the hydrodynamic behaviour of the flow around the blades. At TSR around 3.5 and 4.5

(high inflow speed) the wake is quite smooth with a well-defined shape. However, at high TSR values, the wake becomes very turbulent and an important velocity decrease is visible.

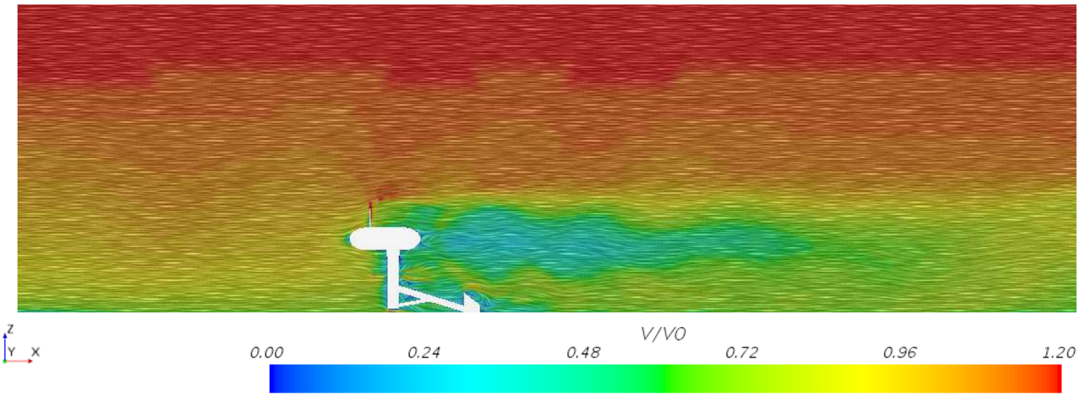

Figure 5-29: Turbine with structure – U70 oscillating inflow – Wake induced by the turbine at low TSR

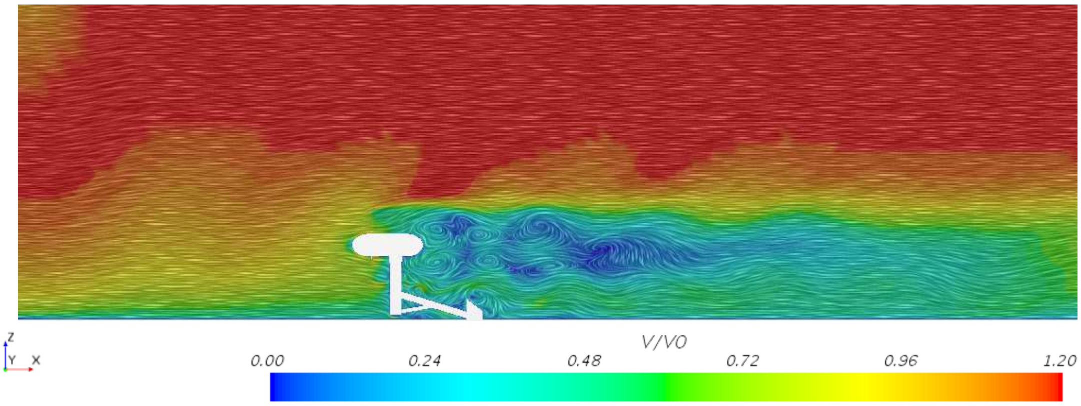

Figure 5-30: Turbine with structure – U70 oscillating inflow – Wake induced by the turbine at high TSR

This simplified method developed to include wave influence in the inflow has proven its use through this test case. It enables to quantify the influence of a time varying horizontal inflow on the turbine. It also enables to study the hydrodynamics involved with an oscillating flow coming at the turbine. However, great care has to be taken when using this approach as it is based on multiple simplifications. It only integrates time varying horizontal inflow to represent the waves, neglecting both vertical velocity and spatial oscillations. This method offers a first approach to conduct blade resolved CFD studies enabling a coupling of waves and current profile.

5.3 Critical operating condition – Forced stop after freewheel rotation

Following a mechanical failure and/or extreme flow condition, tidal turbine could race to freewheel rotation before the activation of an emergency brake to stop its rotation. This situation could lead to brutal load changes on blades. Modelling such critical operating behaviour enables to quantify the turbine loads' evolution and flow behaviour during such a case.

To perform this study, the Fromveur like model integrating the entire turbine with its structure is used. Vertical velocity profile U120 is imposed at the inlet to simulate strong tide conditions. The turbine's dysfunction is modelled with a rotor acceleration from TSR value of 4.5 to 6. Then, an emergency brake is triggered leading to complete rotor immobilization in 3 seconds. The different stages composing this critical operating behaviour are presented in Figure 5-31.

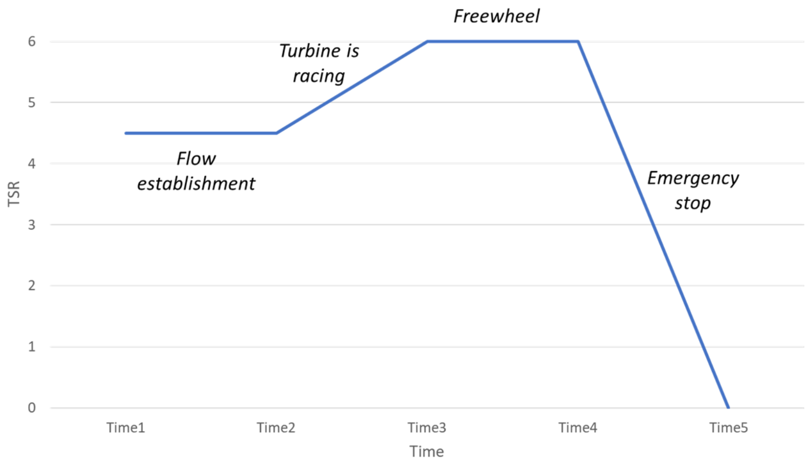

Figure 5-31: U120 inflow – Turbine with structure – Temporal evolution of the TSR during the critical operating behaviour modelling

The axial and tangential loads acting on turbine's blades are directly impacted during the different critical operating phases. It results in an evolution of the performance coefficients reflecting the various phases introduced above. These curves are presented in Figure 5-32.

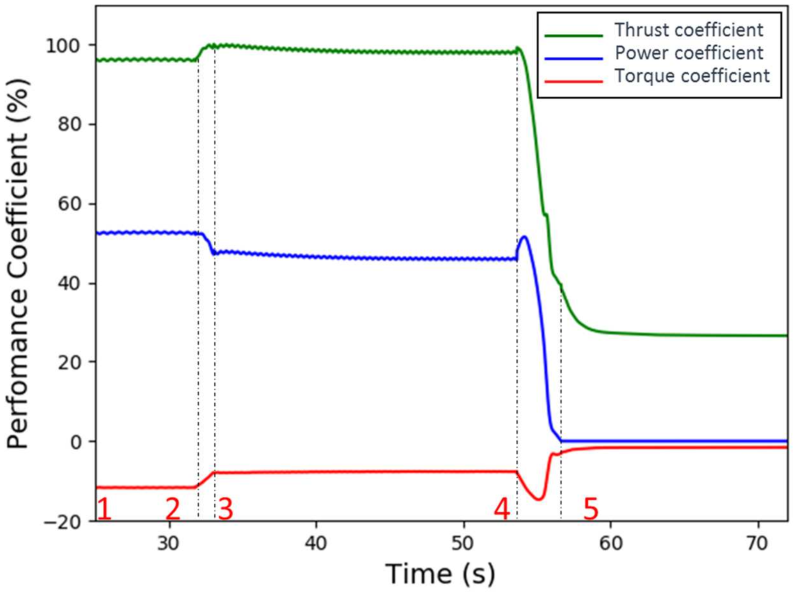

Figure 5-32: U120 inflow – Turbine with structure – Temporal evolution of performance coefficients during the critical operating behaviour modelling

The first step from the time 1 to the time 2 corresponds to the establishment phase. This phase ensures that the critical operating behaviour use a converged model. From the time 2 to time 3, the turbine rotation accelerates. It leads to a TSR change increasing thrust coefficient and reducing power and torque coefficients. After a flow establishment at the freewheel stage, an emergency brake is activated taking the turbine from TSR 6 to 0 in three seconds. This stop causes sudden coefficient changes reflecting the turbine loads evolution. Power and torque coefficient values quickly increased before converging to 0. The thrust coefficient value decreases from its established value to a residual value 73% lower due to the loads of incoming flow on the stationary turbine. It reflects the results obtained in the hydrodynamic performance analysis carried out in 3.4.1. The whole power coefficient curves are represented as the TSR goes from 6 to 0.

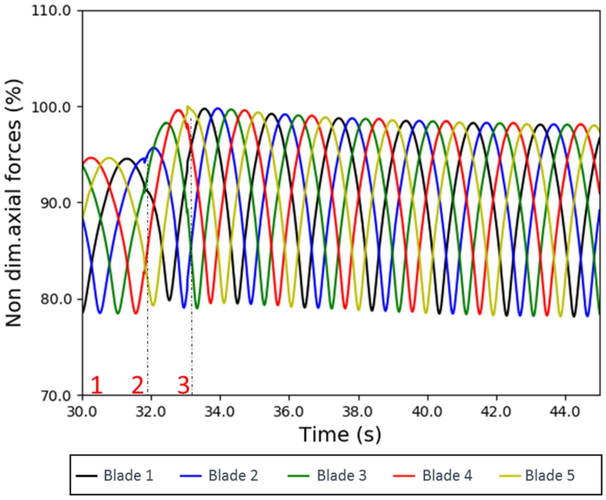

Figure 5-33: U120 inflow – Turbine with structure – Axial forces evolution during rotation rate increase

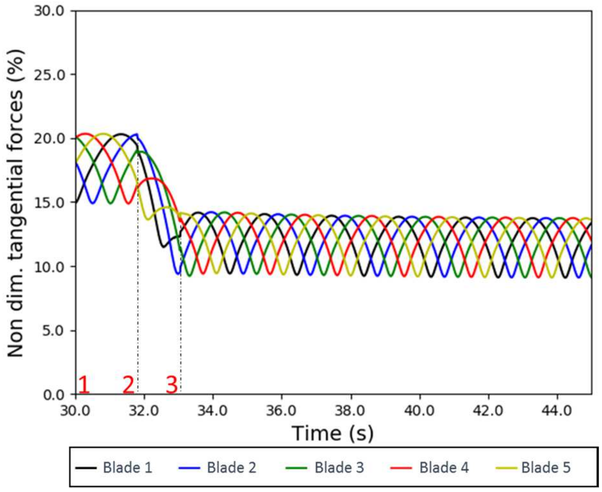

Figure 5-34: U120 inflow – Turbine with structure – Tangential forces evolution during rotation rate increase

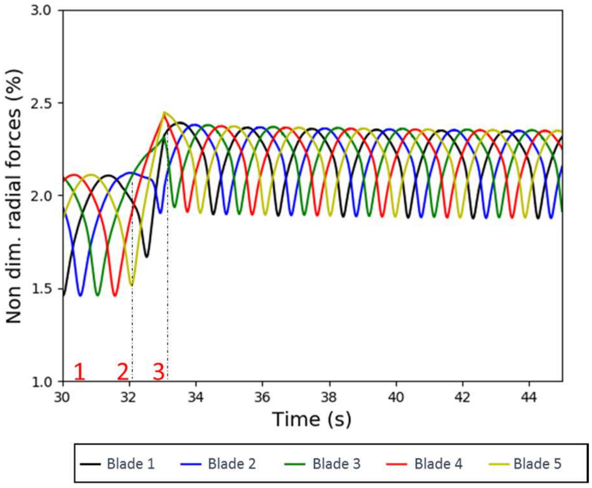

Figure 5-35: U120 inflow – Turbine with structure – Radial forces evolution during rotation rate increase

Figure 5-33, Figure 5-34 and Figure 5-35 present axial, tangential and radial loads acting on blades during the turbine acceleration. Through these plots, the change of rotation rate is highlighted with a frequency increase in the loads oscillations. Besides, TSR change leads to load value changes. Axial force amplitude is wider with higher maximum values and tangential loads are smaller. Indeed, the higher rotation rate of the turbine change the angle of attack of flow around the blade. Consequently, load distribution changes and according to Figure 3-11. The NACA profile of the blade creates less tangential forces for a TSR of 6 than a TSR of 4.5.

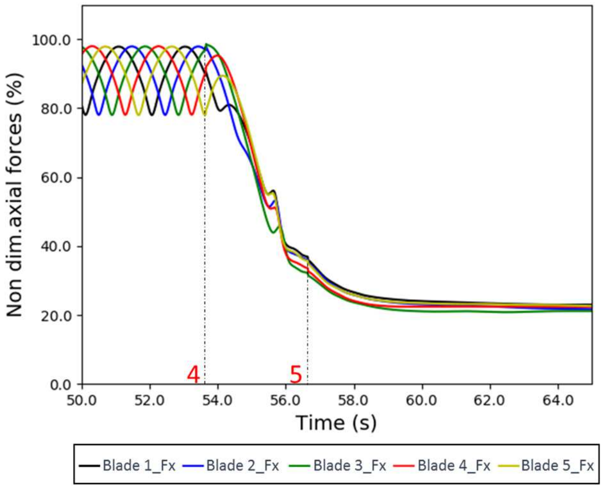

Figure 5-36: U120 inflow – Turbine with structure – Axial forces evolution during emergency stop

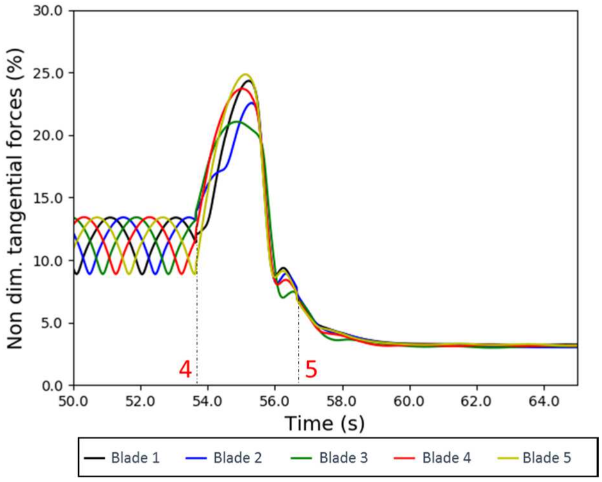

Figure 5-37: U120 inflow – Turbine with structure – Tangential forces evolution during the emergency stop

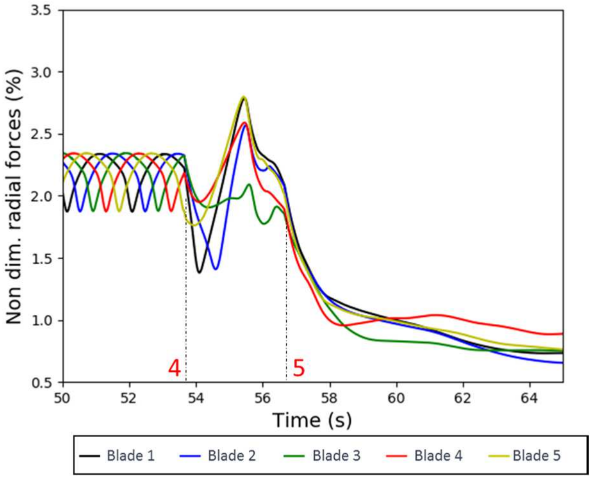

Figure 5-38: U120 inflow – Turbine with structure – Radial forces evolution during the emergency stop

Figure 5-36, Figure 5-37 and Figure 5-38 present normal and tangential loads acting on blades during the 3 seconds of emergency stop. During this phase, load oscillation vanishes because of the rotation shutdown. It leads to a strong decrease of axial loads. They converge from 100% to about 20%. For the tangential loads, this braking phase leads to a sudden increase of the loads from a mean value of 12% to 25% directly followed by a strong decrease until reaching 3-4%. The same evolution is visible on radial loads decreasing from about 2% to below 1% after a peak. This very located peak is due to the transition from TSR 6 to TSR 0. According to the performance analysis carried out in 3.4 (cf. Figure 3-11), the torque coefficient increases from a TSR of 6 to a TSR of 4.5. The constant axial and tangential loads reached at the end of the turbine stop reflect the loads applied on the turbine when fixed.

5.4 Influence of the inflow incidence

In this section, the focus is made on the influence of flow incidence on tidal turbine behaviour. Influence of the incidence angles will be studied through different criteria such as axial loads, tangential loads and power coefficients. Flow behaviour in the wake and around the structure depends of the angle of incidence. An analysis of velocity fields is also carried out to understand the flow physics.

The tide oscillates continuously between two phases: the ebb tide and the flood tide. The Sabella turbine is fixed and does not rotate to face the inflow. Therefore, the flow is coming from the rear of the turbine half of the time. This section focuses on the analysis of the influence of the tide phase on its behaviour. For clarification purposes, it has been chosen to consider a frontal inflow as flood tide and a rear inflow as ebb tide. For each phase, three cases with three different angles, namely 10°, 0° and -10° are run (cf. Figure 5-39). The model introduced in 4.3.3 is used. To simulate non-zero inflow angles, the turbine and its structure are rotated such as the domain boundaries remain identical. For all the cases considered in the following section, U70 profile is used as inflow.

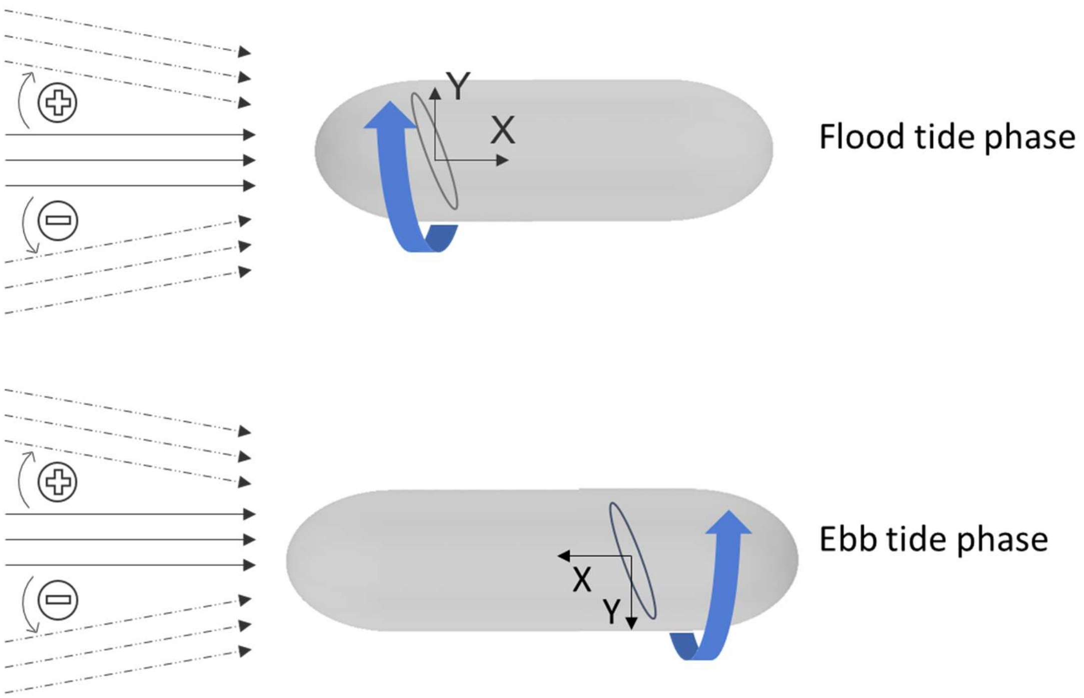

Figure 5-39: Flood and Ebb tides – Definition of the convention - Flow at different incident angle

5.4.1 Influence of inflow incidence at flood tide

In this section results obtained for the three flood tide configurations are compared. First, axial, tangential and radial forces are compared. Then, velocity fields are analysed. Finally, the power coefficients obtained for the three cases are compared.

Figure 5-40, Figure 5-41 and Figure 5-42 show the turbine axial, tangential and radial loads acting on one given blade for the three cases of interest over a period of rotation. In the case of a -10° incidence inflow, the axial forces oscillation amplitude is reduced while it is increased for the tangential forces. The opposite is visible on the case corresponding to a +10° incidence inflow. Moreover, the moment at which the maximum value is achieved is modified. It happens sooner during the rotation in the -10° case and later in the other compared to the 0 degrees inflow.

Change of inflow incidence angle has a direct influence on the blade's angle of attack. It leads to a modification of the loads applied on the blades. The differences observed between the case with a 10° inflow and the case with a -10° inflow are also explained by the rotation direction of the turbine. For one of the case, the obstructing effect of the turbine influences the ascending phase of the blade while it is the opposite in the other case.

The shape and the oscillation amplitude of the curves are influenced by the incidence angle.

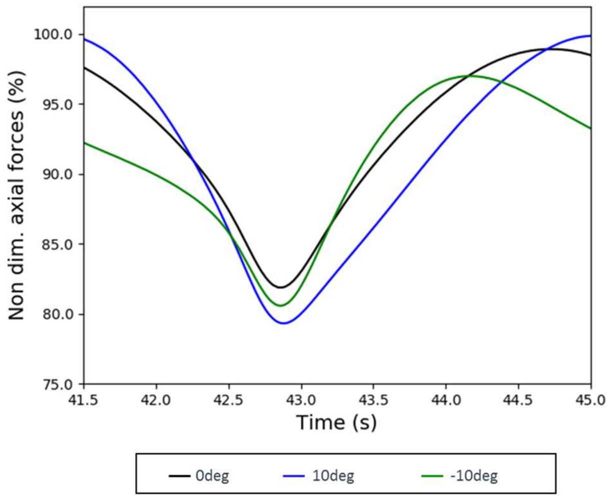

Figure 5-40 U70 inflow – Flood tide – Turbine with structure – -10° vs. 0° vs. 10° – Axial forces acting on a blade

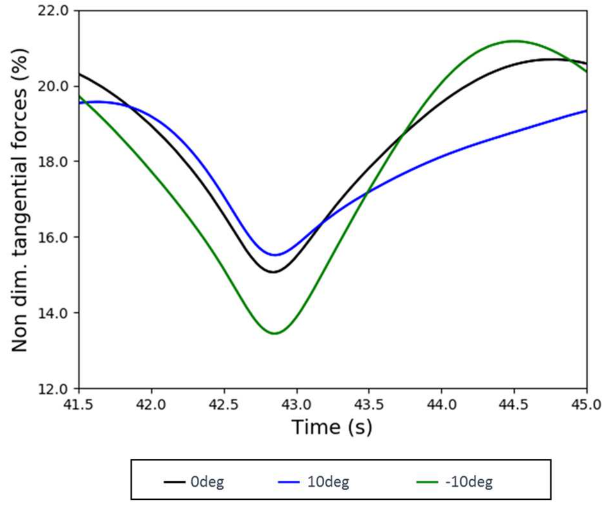

Figure 5-41: U70 inflow – Flood tide – Turbine with structure – -10° vs. 0° vs. 10° – Tangential forces acting on a blade

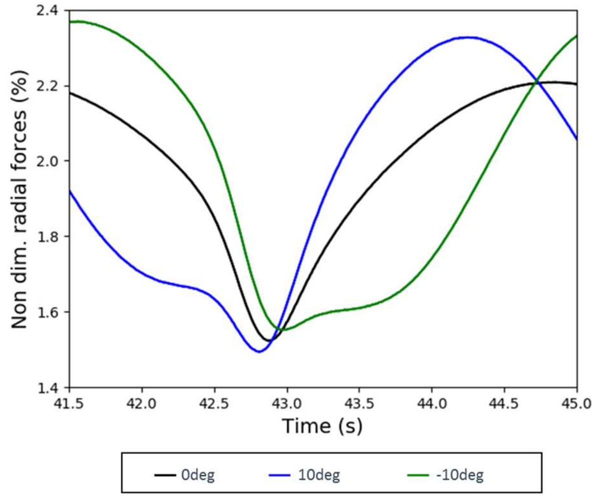

Figure 5-42: U70 inflow – Flood tide – Turbine with structure – -10° vs. 0° vs. 10° – Radial forces acting on a blade

Main characteristics of loads acting on the tidal turbines blades at different flow incidence profiles are summarized into Table 5-8.

Geometry	Inflow	Load type	Incidence	Mean (kN)	Max. (kN)	Min. (kN)
Turbine with structure	U70	Axial	10°	-1.09%	+1.09%	-3.13%
		Tangential		-3.16%	-5.43%	+1.41%
		Radial		-3.10%	+5.36%	-1.93%
		Axial	0°	Ref.	Ref.	Ref.
		Tangential		Ref.	Ref.	Ref.
		Radial		Ref.	Ref.	Ref.
		Axial	-10°	-2.43%	-1.95%	-1.58
		Tangential		-3.04%	+2.32%	-10.76%
		Radial		+0.08%	+7.28%	+1.89%

Table 5-8: U70 inflow – Flood tide – Turbine with structure – Loads comparison between different flow incidences

Analysis of velocity field in horizontal and vertical plane positioned on the turbine's rotation axis illustrates the flow behaviour around the structure and complete the analysis carried out on the loads. Figure 5-43 and Figure 5-44 present the flow behaviour behind the structure from a top view. A change of flow incidence leads to strong differences in the wake. A 10-degrees-incident flow leads to stronger disturbances and a steeper wake.

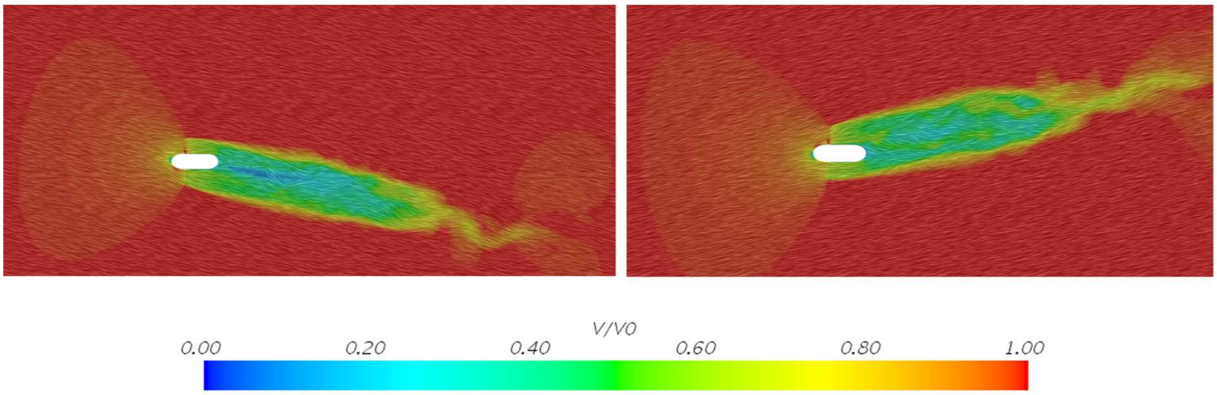

Figure 5-43: Comparison of dimensionless velocity around the structure for speed profiles for different angle of incidence – 10° (left) and -10° (right)

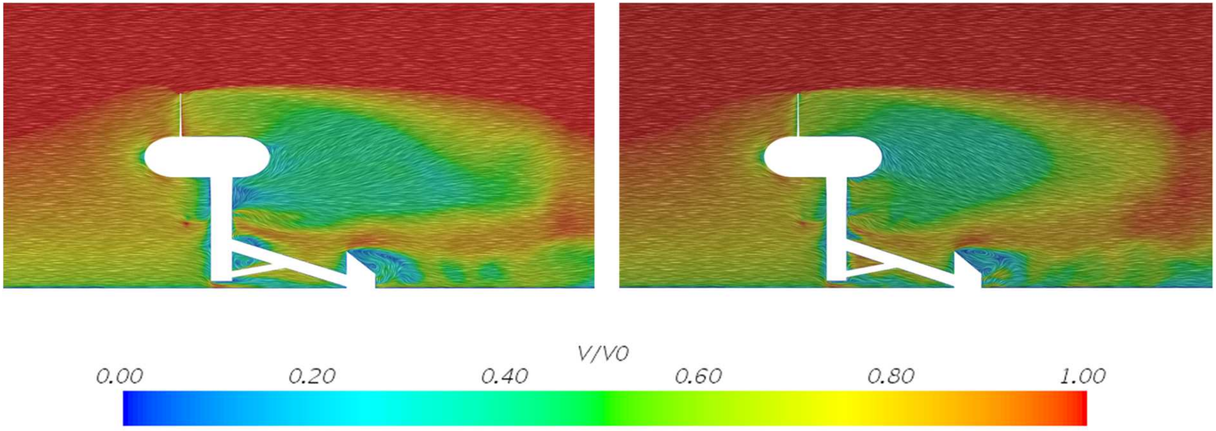

Figure 5-44: Comparison of dimensionless velocity around the structure for speed profiles for different angle of incidence – 10degrees (left) vs. -10° (right)

As observed, the change of inflow incidence creates strong variations in loads and velocity field. Consequently, the performance coefficients are influenced. Analysis of power coefficient for the three different flood tide configurations highlights a decrease of about 3% when a non-zero incident inflow is set. A comparison of the resulting power coefficient values is presented in Table 5-9.

Geometry	Inflow	Incidence	Cp	Ct	Cq
Turbine with structure	U70	10°	-3.07%	-1.74%	-3.07%
		0°	Ref.	Ref.	Ref.
		-10°	-3.04%	-2.46%	-3.04%

Table 5-9: U70 inflow – - Flood tide – Turbine with structure– Influence of the inflow incidence on the power coefficient

5.4.2 Influence of inflow incidence at ebb tide

During the ebb tide, the turbine structure and the hub are directly facing the incoming current. They create a strong disturbance of the flow just before it arrives at the turbine's rotating plan. The consequences of such an inflow on the blades are studied in the section.

As described previously, 3 simulations for 3 different incident angles (0°, 10°, -10°) are run. Results obtained for the three ebb tide configurations are compared. First, axial, tangential and radial forces are compared. Then, velocity fields are analysed. Finally, the power coefficients obtained for the three cases are compared.

Figure 5-45, Figure 5-46 and Figure 5-47 compare the axial, tangential and radial loads acting on a given blade for the three cases of interest over a period of rotation. The shape of the resulting blade loads illustrate the strong interaction between the structure presence and the rotating parts of the turbine. In these configurations, the turbine mast and the fixed part of the hub are located in front of the blades. It obstructs the flow incoming on the turbine rotation plane. It generates a wide range of the turbine rotation in which the blade loads are strongly decreased. Moreover, the modification of the angle of attack depending on the inflow angle modifies the loads applied on the blades. As previously observed, the moments at which the maximum and minimum values are achieved are also modified. It happens sooner during the rotation in the -10° case and later in the other compared to the 0 degrees inflow.

The differences observed between the case with a 10° inflow and the case with a -10° inflow are also explained by the rotation direction of the turbine rotor. For one of the case, the obstructing effect of the turbine influences the ascending phase of the blade while it is the opposite in the other case.

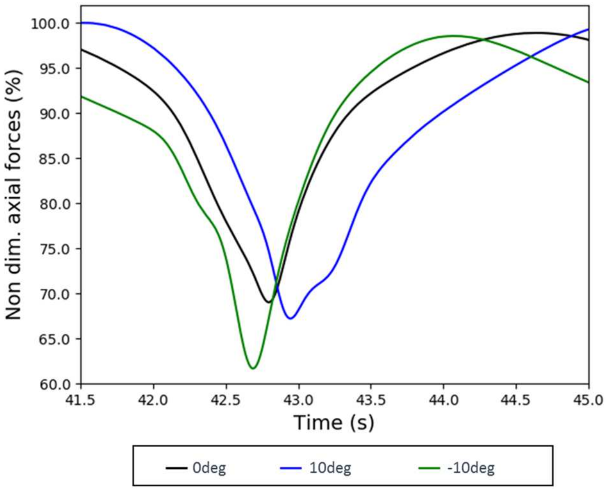

Figure 5-45: U70 inflow – Ebb tide – Turbine with structure – -10° vs. 0° vs. 10° – Axial forces acting on a blade

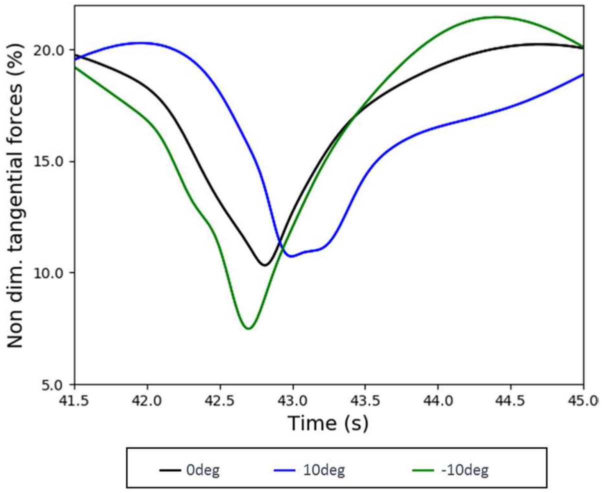

Figure 5-46: U70 inflow – Ebb tide – Turbine with structure – -10° vs. 0° vs. 10° – Tangential forces acting on a blade

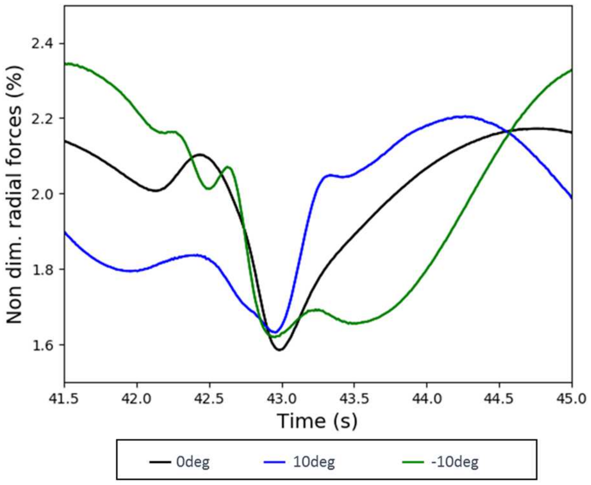

Figure 5-47: U70 inflow – Ebb tide – Turbine with structure – -10° vs. 0° vs. 10° – Radial forces acting on a blade

Main characteristics of loads acting on the tidal turbines blades at different flow incidence profiles are summarized in Table 5-10.

Geometry	Inflow	Load type	Incidence	Mean (kN)	Max. (kN)	Min. (kN)
Turbine with structure	U70	Axial	10°	-1.36%	+1.13%	-2.62%
		Tangential		-2.85%	+0.27%	+3.87%
		Radial		-3.60%	+1.50%	+2.93%
		Axial	0°	Ref.	Ref.	Ref.
		Tangential		Ref.	Ref.	Ref.
		Radial		Ref.	Ref.	Ref.
		Axial	-10°	-2.50%	-0.34%	-10.65
		Tangential		-2.06%	+6.00%	-27.52%
		Radial		+0.49%	+8.06%	+2.13%

Table 5-10: U70 inflow – Turbine with structure - Ebb tide – Loads comparison between different flow incidences

Analysis of velocity field in horizontal and vertical plane positioned on the turbine's rotation axis illustrates the flow behaviour around the structure and complete the analysis carried out on the loads. Figure 5-48 and Figure 5-49 present the flow behaviour behind the structure from a top view. A change of flow incidence leads to strong differences in the wake.

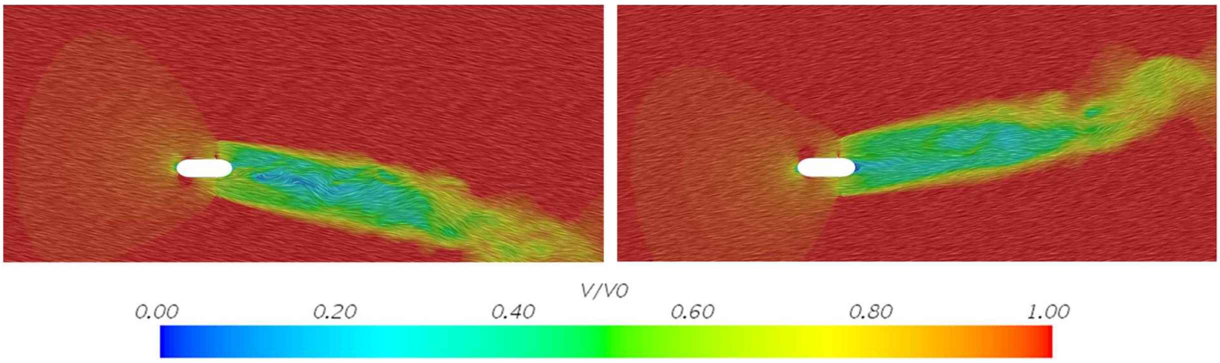

Figure 5-48: Comparison of dimensionless velocity around the structure for speed profiles for different angle of incidence – 10° (left) vs. -10° (right)

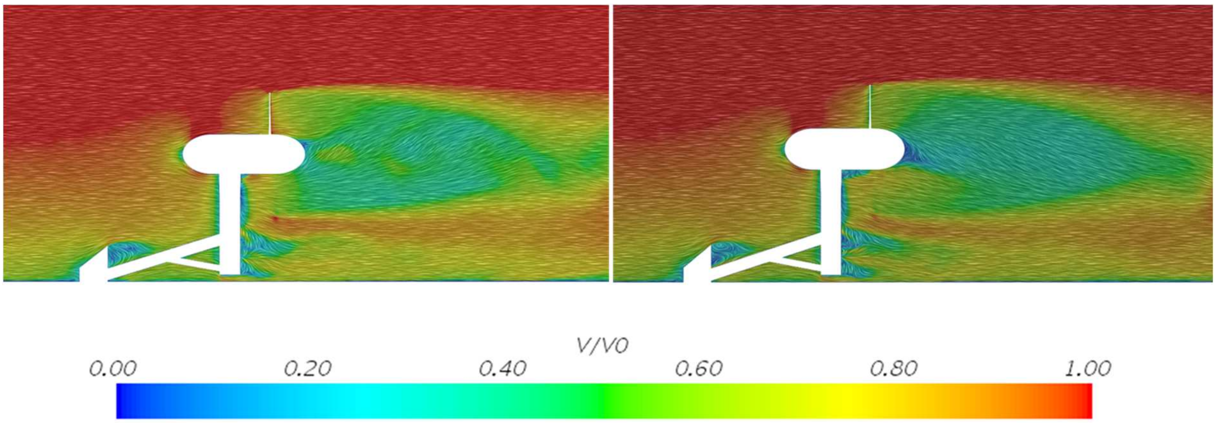

Figure 5-49: Comparison of dimensionless velocity around the structure for speed profiles for different angle of incidence – 10° (left) vs.-10° (right)

As observed, the change of inflow incidence creates strong variations in loads and velocity field. Consequently, the performance coefficients are influenced. Analysis of power coefficient for the three different ebb tide configurations highlights a decrease when a non-zero incident inflow is set. A comparison of the resulting power coefficient values is presented in Table 5-11.

Geometry	Inflow	Incidence	Cp	Ct	Cq
Turbine with structure	U70	10°	-2.75%	-2.18%	-2.75%
		0°	Ref.	Ref.	Ref.
		-10°	-2.10%	-3.42%	-2.10%

Table 5-11: U70 inflow – Turbine with structure - Ebb tide – Influence of the inflow incidence on the power coefficient

Finally, the results obtained on ebb tide are compared to the results obtained for flood tide. It enables to quantify the loss of efficiency due to the structure and hub directly obstructing the flow. The comparison is presented in Table 5-12.

	-10°	0°	10°
Cp – Flood tide	Ref.	Ref.	Ref.
Cp – Ebb tide	-4.04%	-5.07%	-4.75%

Table 5-12: U70 inflow – Turbine with structure – Ebb vs. flood tide – Comparison of power coefficient values

These results highlight the negative influence of structure directly facing the incoming current on the performance. The obstructing effect is important and generates about 4 to 5% decrease of efficiency compared to classical inflow direction.

6 CONCLUSIONS

The work carried out in WP3.2 presented in this report enabled to develop a blade-resolved CFD tool. Various configurations and model setup have been presented with different level of complexity and computational cost. The CFD simulations enabled to study the loads and performance of the turbine along with the resulting wake.

In the first phase of the project, a simplified yet blade resolved CFD model was set up. It is based on ideal uniform inflow conditions without considering the turbine's surrounding environment. Using the axi-symmetry of the turbines, quite reasonable computational time was achieved while still keeping good depiction of the hydrodynamics around the structure. It was used to conduct the performance analysis of the two turbines of interest in this project: the generic 3-bladed tidal turbine provided by UEDIN and the D12 Sabella's turbine. The obtained results are satisfying and comparison with experimental results validate the modelling choices. Finally, taking advantage of the blade resolved aspect of the model, the pressure loads applied on the turbine blades were measured in various operating conditions. They were used as input to conduct the structural analysis of the D12 turbine blade carried out in WP5.

This first approach proved its interest through the work it helped to achieve. However, the integration of realistic environmental conditions is required to go further. A more complex model is build enabling to include vertical velocity profile, reference turbulence values, along with seabed and simplified wave effects. The resulting tide current modelled is closer to reality. This was done following a step-by step approach including successively a new rotation method with full modelling of the turbine geometry, implementation of a realistic domain and finally integration of the turbine's structure. In parallel, a thorough literature review was carried out on turbulence theory and the various existing options for its numerical modelling. It enabled to acquire a good understanding of the key parameters necessary to integrate turbulence in the CFD models. An analysis of datasets measured by UEDIN – made available in T1.5 – at Orkney site (UK) provided representative values of these parameters for tide currents.

The last phase of the work presented in this report was the use of the developed models to study the influence of various realistic conditions on the turbine loads and behaviour. In discussion with Sabella, reference cases were selected based on current profiles, current directions or wave conditions encountered on the operating site of the D10 turbine. First, the integration of vertical velocity profiles as inflow was studied. It enabled to verify the appearance of oscillating blade loads on which the presence of the structure has a strong influence. In parallel, the influence of various inflow incidences for both ebb and flood tides were simulated to understand the associated hydrodynamics around the turbine and their effects on the overall performance. Then, oscillating inflow due to wave effects was analysed. The influence of an oscillating inflow direction was verified on the power coefficient with the appearance of a hysteresis cycle with regard to the time varying TSR value. Finally, a critical operating condition was considered enabling to analyse the dynamic load response applied on the turbine as it is suddenly stopped from freewheel.

The different case studies run using the developed models enabled to verify their compatibility with the objectives of the work package. The CFD modelling developed here is complementary with the other codes and models created in the context of this third RealTide work package. It enables accurate analysis of blade loads and good modelling of hydrodynamics involved in the turbine operation. However, it has a quite significant computational cost as it requires a fine mesh associated with a small time step. Its use has to be put in perspective of the objective of the study. BEMT tool and BEMT-CFD coupled model developed respectively in T3.1 and T3.3 may be more relevant in some cases. The three codes issued in WP3 will be compared in T3.4. It will help to define the advantages and limitations of each code depending on the type of calculation and check the coherence between obtained results.

7 DISCUSSION AND OPPORTUNITIES

The work presented in this report summaries the blade-resolved CFD study carried out on the 3-bladed generic and D12 Sabella's turbine. The models defined enable a good depiction of the hydrodynamics involved in the turbine operation and realistic inflow conditions are implemented. It includes seabed, vertical velocity profiles, and temporal oscillations of horizontal velocity due to waves. Multiple case studies were run to analyse the effect of flow environmental flow conditions on the turbine loads and performance.

The work carried out provides an interesting model for industrial use. The detailed turbine loads are available through this model. It could be of great interest for different applications such as tidal turbine design phases or verification of experimental results.

The inclusion of the tide-to-wire model developed in Task 3.1 was not handled as it was initially planned. This was discussed with UEDIN and BV teams. The realistic blade resolved CFD developed generate simulations with a very high computational cost. As such, it was decided to focus its use on the calculation of detailed turbine loads for a given environmental conditions rather than a tide to wire model providing rotation speeds outputs. It would have required too much work and excessively long simulations. This point emphasizes the complementary aspects of the different models developed in the context of WP3. Depending on the objectives of the calculation, a wise choice of the tool must be made.

When considering future work perspectives, the following points are of interest:

- Integration of free-surface and wave modelling: The choice was made not to include free surface and waves modelling directly into the model. It enabled to reduce the mesh size and keep a reasonable calculation time. As such, the current model does not integrate the spatial or vertical velocity oscillations induced by waves. It would be interesting to integrate it as it would provide a model closer to reality and enable the consideration of various wave fields.

- Turbulence resolution using DES method: All calculations presented in this report were carried out using RANS method. The DES method was not implemented in the blade resolved CFD model. Its integration in the model would lead to a more accurate turbulence integration and resolution. The literature review carried out enabled to understand all the necessary physics and key inputs to do so.

The inclusion of the points presented above could provide useful enhancements of the blade resolved CFD model. It could be very useful for further work on novel turbine blade design research as part of WP5. However, wave and current coupling goes along with multiple difficulties as it requires the adaptation of the domain mesh and simulation time to ensure good wave propagation. Similarly, DES method generates the need for a very well defined mesh adapted to the turbulence structures considered. It will induce a complexity increase of the model which may generate very important computation time. Therefore, these opportunities must be considered with regard to the potential added value it will generate for RealTide project. This will be discussed during the next general assembly meeting with other partners.

APPENDIX – STAR-CCM+ SOFTWARE PRESENTATION

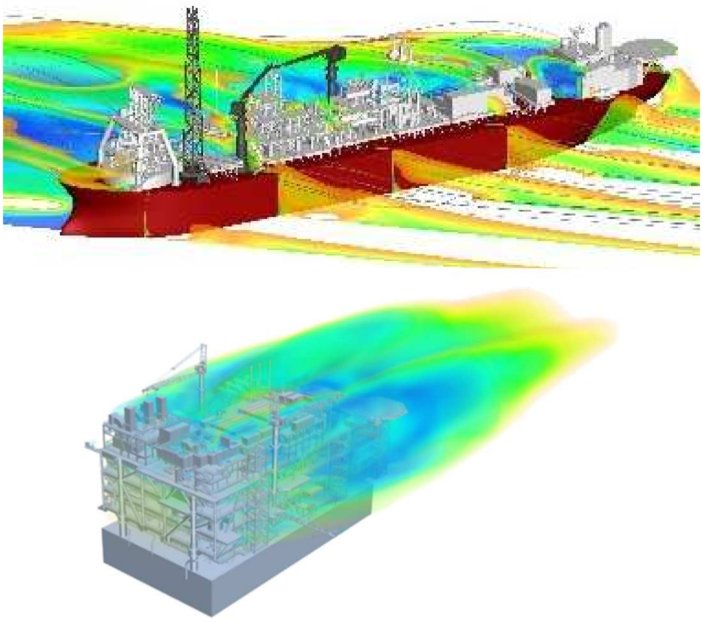

STAR-CCM+ output views extracted from aero and hydrodynamic simulations

STAR-CCM+ is used in this study as a mesher and solver. This software has the particularity to be used for many applications: aerodynamics, hydrodynamics, thermics, etc. In particular, BV Solutions M&O has developed a high expertise to simulate complex aerodynamic applications using this software.

Characteristics of STAR-CCM+ meshing

- The meshing can be structured or unstructured
- Isotropic mesh
- Advanced boundary layer integration
- Wrapping module that allows the meshing of very complex CAD

The solver can be set to RANS (Reynolds Averaged Navier-Stokes Equations) solver but also to DES (Detached eddy simulation) solver. Several turbulence models are available, such as k-ω SST or k-ε. The Finite Volume method is used for spatial discretization. Depending on the application, steady or unsteady calculations can be performed. The main advantage of this solver is the large panel of models. A non-exhaustive list of available applications are listed below.

Characteristics of STAR-CCM+ Solver

- 6 DOF motion
- Incident regular or irregular waves
- Manoeuvring capabilities of hulls and appendages
- Propulsion with actuator disk or with rotating propeller
- Free surface capturing method using VOF approach
- Loads fluctuations analysis

For this study, all simulations but one are carried out using RANS solver and k-ω SST turbulence model. One simulation on reference case is carried out using DES solver and k-ω SST turbulence. All simulations are unsteady and convergence is checked after each run. Details of simulations parameters are presented in the report.